

Improved interpolating fields in the Schrödinger Functional

D I S S E R T A T I O N

zur Erlangung des akademischen Grades
doctor rerum naturalium
(Dr. rer. nat.)
im Fach Physik

eingereicht an der
Mathematisch–Naturwissenschaftlichen Fakultät I
Humboldt–Universität zu Berlin

von
Herrn Dipl.–Phys. Heiko Molke
geboren am 01.02.1976 in Frankfurt/Oder

Präsident der Humboldt-Universität zu Berlin:
Prof. Dr. Jürgen Mlynek

Dekan der Mathematisch–Naturwissenschaftlichen Fakultät I:
Prof. Dr. Michael Linscheid

Gutachter:

1. Prof. Dr. U. Wolff
2. Dr. R. Sommer
3. Dr. H. Wittig

eingereicht am: 16.01.2004
Tag der mündlichen Prüfung: 26.04.2004

Abstract

The general aim of this thesis is to probe several methods to extract low-energy quantities (masses, decay constants, ...) more reliably in lattice gauge theory. We will investigate how to suppress contributions to correlation functions from the first excited meson state. We will show how to construct so-called improved meson interpolating fields, as they have only small contributions from the first excited meson state, from a basis of interpolating fields at the Schrödinger functional boundaries.

The variational principle is applied to correlation matrices that are built up from boundary-to-boundary correlation functions. It will deliver information about the lowest-lying meson states in the considered channel.

We also investigate the possibility to cancel the first excited state contribution by means of an alternative method. Moreover, an alternative way to extract the mass gap between the ground and the first excited state will be presented.

Monte-Carlo simulations at several lattice spacings are performed in the 'quenched approximation'. Spectral properties of light-light and static-light pseudoscalar mesons are investigated.

The first type is realised by two mass-degenerate quarks at about the strange quark mass, the second type by a light quark with the mass of the strange quark and an infinitely heavy b -quark. The light-light channel describes unphysically heavy pions and the static-light one is an approximation for the B_s -meson.

The investigation of the latter case is particularly interesting since so-called B-factories, such as BaBar and Belle, are gathering physical information about masses, decay modes and CP-violating effects in the B-meson system.

Keywords:

Lattice gauge theory, Lattice QCD, weak matrix elements, B-physics, HQET, variational principle, Schrödinger Functional

Zusammenfassung

Diese Arbeit befasst sich mit der Konstruktion verbesserter interpolierender Mesonenfelder in der Gitter-QCD. Sie hat das primäre Ziel, Korrelationsfunktionen mit einem deutlich reduzierten Beitrag des ersten angeregten Mesonenzustandes zu erhalten, um eine sicherere Bestimmung von Massen und Zerfallskonstanten der Mesonen zu ermöglichen. Eine Basis solcher interpolierender Mesonen-Randfelder wird im Schrödinger Funktional in der gequenchten Approximation benutzt.

Verbesserte interpolierende Felder zur Bestimmung spektraler Eigenschaften leichter pseudoskalarer Mesonen sowie des B-Mesonensystems (letzteres wird in führender Ordnung der HQET behandelt) werden auf mehreren Wegen gewonnen.

Ein Hilfsmittel, verbesserte Felder zu konstruieren, ist das Variationsprinzip. Es wird auf Matrizen von Rand-Rand-Korrelationsfunktionen angewandt. Darüber hinaus werden alternative Analysemethoden vorgestellt. Sie erlauben sowohl die Abschätzung der Grundzustandsenergie als auch der Energielücke zum ersten radial angeregten Zustand.

Die Untersuchung des B-Mesonensystems ist in vielfacher Hinsicht interessant. Zum einen werden sie in sogenannten B-Fabriken, wie z. B. im BaBar- und Belle-Experiment, in grosser Zahl erzeugt, um ihre charakteristischen Eigenschaften (Masse, Zerfallsbreiten, CP-Symmetrie verletzende Zerfälle usw.) genau zu messen. Zum anderen müssen die von der Theorie vorhergesagten auftretenden Phänomene, wie z. B. die CP-Verletzung, auch verstanden werden. Die Methoden der Gittereichtheorie können unter anderem dabei helfen, bestehende Unsicherheiten in CKM-Matrixelementen durch nicht-perturbative Bestimmungen hadronischer Massen, Zerfallskonstanten usw. zu reduzieren.

Schlagwörter:

Gitter-Eichtheorie, Gitter-QCD, Matrixelemente, B-Physik, HQET, Variationsprinzip, Schrödinger-Funktional

Contents

1	Basics of Lattice Gauge Theory	3
1.1	Discretisation of the continuum	
	SU(N) Yang–Mills Action	4
1.2	The Wilson-Dirac Fermion Action	5
1.3	The Symanzik Improvement Programme	7
2	The Schrödinger Functional	9
2.1	Model	9
2.1.1	Motivation	9
2.1.2	Formal Definition – Pure Gauge Theory	10
2.1.3	Formulation with Fermions	13
2.1.4	Lattice Formulation	15
2.1.5	The Renormalised Coupling $\bar{g}(L)$	17
2.2	O(a) Improvement Programme	18
2.2.1	Gauge Action	18
2.2.2	Fermion Action	19
2.3	The Correlation Functions f_A, f_P and f_1	20
2.4	Spectral Representations of Correlation Functions	23
2.4.1	The QCD Transfer Matrix Formalism in the Schrödinger Functional	23
2.4.2	Spectral Decomposition of Correlators	25
2.5	Pseudoscalar Masses and Decay Constants	28
2.5.1	The Pseudoscalar Mass m_{PS} of the Ground State	28
2.5.2	The Pseudoscalar Decay Constant F_{PS} of the Ground State	29
2.6	The PCAC Relation on the Lattice	31

3	The b-quark on the Lattice	35
3.1	Introduction	35
3.2	The Static Approximation	36
3.3	The Static b -quark in the Schrödinger Functional	38
3.3.1	The Action	38
3.3.2	Correlation Functions	39
3.3.3	The Static Decay Constant	41
4	Wave Functions	43
4.1	Motivation	43
4.2	The Variational Principle	44
4.3	The Variational Principle in Practice	47
4.4	The Program Implementation	48
4.4.1	General Remarks	49
4.4.2	Propagators and Correlation Functions	49
4.4.3	Details of used Wave Functions	53
4.4.4	Program Tests	54
4.4.5	Performance and Scaling	54
4.4.6	A brief Remark on the Static Approximation	58
5	Alternative Extraction Techniques	61
5.1	Ground State Masses and Decay Constants	61
5.2	The First Excited State	64
5.3	The Mass of the 0^{++} -Glueball	65
6	Numerical Results	67
6.1	The Choice of the light Quark Mass	68
6.2	The Variational Principle	68
6.2.1	The Relativistic Case	69
6.2.2	The Static Case	75
6.3	Extraction of Masses with optimal Wave Functions	78
6.3.1	The Relativistic Case	78
6.3.2	The Static Case	79
6.3.3	An Alternative Way without applying the Variational Principle	84
6.4	Alternative Extraction of the Pseudoscalar Mass Gap	88
6.4.1	The Relativistic Case	88

6.4.2	The Static Case	90
6.5	Decay Constants	91
6.5.1	The Relativistic Case	91
6.5.2	The Static Case	93
6.6	The Mass of the 0^{++} –Glueball	96
6.7	Summary and Discussion of the Results	98
6.7.1	The Relativistic Case	98
6.7.2	The Static Case	99
7	Conclusions and Outlook	101
	Appendix	103
A	Notation	103
B	Program Implementation and related Issues	105
B.1	The Quark Propagator	105
B.2	The Fermionic Generating Functional	106
B.3	Quark Two-Point Functions	108
B.4	Correlation Functions in terms of Two-point Functions	108
B.4.1	The Correlator f_A	108
B.4.2	The Correlator f_1	110
C	Numerical Results	111
C.1	Simulation Parameters	111
C.1.1	Wave functions	111
C.1.2	Data sets	111
C.2	The Variational Principle	113
C.2.1	The Relativistic Case	113
C.2.2	The Static Case	120
C.3	Alternative Extraction of the Ground State Mass	122
C.3.1	Relativistic case, $\beta = 6.2$	122
C.3.2	Static Case, $\beta = 6.45$	123

List of Figures

1.1	The plaquette is the smallest closed and gauge-invariant path.	5
2.1	Visualisation of the Schrödinger functional as a four-dimensional cylinder.	14
2.2	Visualisation of the contribution $Q_{\mu\nu}(x)$ in the SW clover term.	20
2.3	Visualisation of the correlators f_A and f_P , respectively. Currents A_0 or P are inserted in the interior.	21
2.4	The boundary-boundary correlator f_1	22
3.1	Visualisation of the correlators f_A^{stat} (left) and f_1^{stat} (right). The static quark is drawn with a double line. The current A_0^{stat} is inserted in the interior of the left figure.	40
4.1	An effective energy plot from the static axial current on a $24^3 \times 36$ lattice at $\beta = 6.2$, $\theta = 0$ and $\kappa \approx \kappa_s$. Symbols are displaced horizontally for clarity. The static quark is either smeared (red plusses) or not (blue stars). Due to symmetry relations, the same average is expected. Obviously, this fact does not need to hold for statistical errors.	60
6.1	Effective pseudoscalar ground state mass from the variational principle, relativistic case, $\beta = 6.0$, $\kappa = \kappa_s$, in comparison to the extracted mass $m_{\text{PS}}(f_A^I)a = 0.340(3)$ (dotted lines).	70
6.2	Effective mass of the pseudoscalar ground state from the variational principle, relativistic case, $\beta = 6.2$, $\kappa \approx \kappa_s$, in comparison to the extracted mass $m_{\text{PS}}(f_A^I)a = 0.250(5)$ (dotted lines).	71

6.3	Effective mass of the first excited pseudoscalar state from the variational principle, relativistic case, $\beta = 6.0$, $\kappa = \kappa_s$, in comparison to the result $m_{\text{PS}}^* a = 0.83(5)$ from f_{A}^{I} or f_{P} (dotted lines).	72
6.4	Effective pseudoscalar mass gap from the variational principle, relativistic case, $\beta = 6.0$, $\kappa = \kappa_s$. Error bands: $a\Delta = 0.55(5)$ (text).	74
6.5	Effective pseudoscalar mass gap from the variational principle, relativistic case, $\beta = 6.2$, $\kappa \approx \kappa_s$. Error bands: $a\Delta = 0.41(5)$ (text).	74
6.6	Effective ground state binding energy from the variational principle, static case, $\beta = 6.0$, $\kappa = \kappa_s$.	76
6.7	Effective binding energy of the first excited state, obtained from the variational principle, static case, $\beta = 6.0$, $\kappa = \kappa_s$.	76
6.8	Effective energy gap from the variational principle, static case, $\beta = 6.0$, $\kappa = \kappa_s$.	77
6.9	Effective ground and first excited state mass, $\beta = 6.0$, $\kappa = \kappa_s$, relativistic case.	80
6.10	Scaling of effective ground and first excited state masses, $\beta = 6.0$ and 6.2 for the relativistic case. Symbols are as in figure 6.9.	80
6.11	Smearing is essential in the static case: Effective energy plot of the static axial current correlator with(out) smearing, $\beta = 6.0$, $\kappa = \kappa_s$.	81
6.12	Effective energy plot of the static axial current corr., $\beta = 6.0$.	82
6.13	Scaling of $r_0(E - \Gamma^{\text{stat}})$ using vectors $v^{(0)}$, $v^{(1) \prime}$ at all β 's.	82
6.14	Effective mass plot using f_{A}^{I} and various values of R_{ij} , $\beta = 6.2$, $\kappa \approx \kappa_s$, relativistic case. Values for R_{ij} are taken from table C.14.	85
6.15	Effective mass plot using f_{A}^{I} for the original basis and an improved case with R from eq. (5.10), at $\beta = 6.2$, $\kappa \approx \kappa_s$, relativistic case.	86
6.16	Effective energy plot from the static axial correlator, for two R_{ij} -values, $\beta = 6.45$, $\kappa = \kappa_s$.	87
6.17	Effective pseudoscalar mass gap, $\beta = 6.0$, $\kappa = \kappa_s$, relativistic case. Effective masses from f_{P} and several pairs of wave functions are used.	89
6.18	Scaling of the eff. pseudoscalar gap, relativistic case, $\kappa \approx \kappa_s$.	89

6.19	Scaling of the effective energy gap (upper plot) and the continuum extrapolation for $x_0 \approx r_0$ (lower plot), static case, $\kappa = \kappa_s$	90
6.20	Change of the effective bare pseudoscalar decay constant (ground state) for several time extents T , a suitable ω_{opt} (given in the text), $\beta = 6.0$ and 6.2 , $\kappa \approx \kappa_s$, relativistic case.	92
6.21	Change of $r_0^{3/2} \Phi_{\text{RGI}}$ for several time extents T' and ω'_{opt} at $\beta = 6.0$, $\kappa = \kappa_s$	95
6.22	Quark mass dependence of m_G (from eq. (5.16)) at $\beta = 6.2$. . .	97
6.23	Plot of $m_G - m_{\text{PS}}$ for various quark masses and β -values. . .	97

List of Tables

4.1	Comparison of the statistical errors for different estimators. . .	55
4.2	Comparison of the statistical error with/out translational invariance. The same set of parameters is used.	56
4.3	Scaling of the time [secs] to solve the Dirac equation on a $(L/a)^4$ lattice on a board, quenched case.	57
4.4	Total time in seconds to build up a 2×2 correlation matrix (as given in column 2 & 3) as a function of L/a on a board, quenched case.	57
4.5	Total time in seconds to build up the correlation matrix as a function of N_ω for $L/a = 12$ on a board.	58
6.1	Pseudoscalar masses for the light-light case taken at $x_0 \approx 2r_0$ (ground state) and at $x_0 \approx r_0$ for the first excited one.	79
6.2	Results for the static-light case, eq. (6.11), taken at $x_0 \approx 1.3r_0$ (resp. $x_0 \approx 1.8r_0$), $\Gamma^{\text{stat}}(L_2) = 0.410024 - 0.131595(\beta - 6)$ for $6.0 \leq \beta \leq 6.45$	83
6.3	Energy gap for the static-light case taken at $x_0 \approx r_0$	90
6.4	Systematic shift of the plateau level for aF_{PS} (bare case) as a function of $T' \leq T$, relativistic case. The value for $T = 3L/2$ has been fixed.	93
6.5	Renormalisation constants to compute Φ_{RGI} from available data. 94	
6.6	The quantity $r_0^{3/2}\Phi_{\text{RGI}}$ at $\beta = 6.0$, $L = 16a$, $T = 24a$ fixed and various $T' < T$. The optimal wave functions are given in the text. Quoted plateau values are taken at $x_0 \approx 2r_0$	95
6.7	Summary of pseudoscalar masses in the relativistic case, $\kappa \approx \kappa_s$. 99	
6.8	Summary of the results in the static case, $\kappa = \kappa_s$	100
C.1	The set of 4 hydrogen-like trial wave functions.	111

C.2	Relativistic case: List of several time extents of the Schrödinger functional box.	112
C.3	Static case: List of several time extents of the Schrödinger functional box.	112
C.4	Effective masses directly from the Variational Principle, eq. (4.9), or à la Lüscher-Wolff, eq. (4.10), for the relativistic case, at $\beta = 6.0$ and $\kappa = 0.133901$	113
C.5	Continuation of table C.4	114
C.6	Continuation of table C.4	115
C.7	Basis vectors b_i and state vectors $v^{(n)}$ in that basis, from the Variational Principle for the relativistic case, $\beta = 6.0, \kappa = 0.133901$	116
C.8	Continuation of table C.7	117
C.9	Continuation of table C.7	118
C.10	Effective masses directly from the Variational Principle, eq. (4.9), or à la Lüscher-Wolff, eq. (4.10), for the relativistic case, at $\beta = 6.2$ and $\kappa = 0.13485$	118
C.11	Basis vectors b_i and state vectors $v^{(n)}$ in that basis, from the Variational Principle for the relativistic case, at $\beta = 6.2$ and $\kappa = 0.13485$	119
C.12	Effective energies directly from the Variational Principle, eq. (4.9), or à la Lüscher-Wolff, eq. (4.10), for the static case, at $\beta = 6.0$ and $\kappa = 0.133901$	120
C.13	Basis vectors b_i and state vectors $v^{(n)}$ in that basis, from the Variational Principle in the static approximation, $\beta = 6.0, \kappa = 0.133901$	121
C.14	Various determinations of R_{ij} to build up ω_{opt} from a linear combination of trial WFs ω_i and ω_j , $\beta = 6.2$, relativistic case.	122
C.15	Values for $R_{f_{\text{A}}^{\text{I}} f_{\text{P}}}$ to build up f_{A}^{I} with an absent first excited pseudoscalar state, $\beta = 6.2$, $\kappa = 0.13485$, relativistic case.	123
C.16	Some more extracted R -values for the application of eq. (5.10).	123
C.17	Table of weights R_{ij} (E_{eff} and $d_0(\omega_i)/d_0(\omega_j)$ are extracted from $\text{O}(a)$ -improved $f_{\text{A}}^{\text{stat}}$) to build up ω_{opt} from ω_i and ω_j , $\beta = 6.45$, static case.	123

Introduction

To gain a better understanding of nature, particle physicists have been exploring the fundamental forces down to distance scales of roughly 10^{-18} m for some decades. Usually, this is done in high-energy collision experiments, such as in a ring collider at CERN or in a linear collider at SLAC. The experimental observations may be accurately described and predicted by a theoretical framework that is known as the Standard Model of elementary particles. It unifies the description of the electromagnetic, weak as well as strong force and is based on a local gauge principle [1] of the group

$$G_{\text{loc}} = \text{SU}(3)_c \otimes \text{SU}(2)_L \otimes \text{U}(1)_Y. \quad (1)$$

It is essentially determined once the matter fields and their transformation laws under G_{loc} are specified.

The electroweak sector is described by the product group $\text{SU}(2)_L \otimes \text{U}(1)_Y$ [2, 3, 4] with self-coupling gauge fields W_μ^a for the former and an Abelian field B_μ for the latter factor. They carry the quantum numbers of the weak isospin T_3 respectively the weak hypercharge Y . Mixing of these gauge fields produces the observable photon (γ) for QED and the triplet (W^+, W^-, Z^0) that mediates the weak force. Left-handed matter fields are grouped into doublets, right-handed ones are singlets. This undemocratic treatment is due to maximal parity (P-) violation. Also CP-violation is known from experimental observations in the kaon- [5, 6] and recently in the B-meson system [7, 8, 9]. The gauge group of the electroweak sector is spontaneously broken through a Higgs mechanism [10] to $\text{U}(1)_{\text{em}}$, and particle fields acquire masses according to their coupling strength to the Higgs boson.

The unbroken subgroup $\text{SU}(3)$ of G_{loc} is the non-Abelian gauge group of the strong interaction (QCD) [11]. Its 8 spin-1 gauge bosons, the gluons, are massless and carry a colour charge. In contrast to the more familiar photons of QED, self-interactions are here admitted due to the non-Abelian nature of

QCD. Coloured quarks [12, 13] couple to them but cannot occur as free particles in nature. Their confinement at low energies allows only colour-singlet realisations, the hadrons, as observable states. They form a rich spectrum with a multiplet structure. In the regime of high energies, the strong coupling α_s is small and hence perturbative techniques may be applied. Quarks are asymptotically free there [14, 15], as deep-inelastic scattering experiments at high energies have revealed. In the low-energy region, however, α_s is too large for perturbation theory to give reasonable results. Non-perturbative methods or effective theories are needed to describe QCD there.

In 1974, Wilson proposed to formulate gauge field theories on a discretised Euclidean space-time, the lattice, and showed in conjunction with a strong coupling expansion that pure SU(3) lattice gauge theory may exhibit colour confinement. The inverse lattice spacing a^{-1} serves as ultraviolet cutoff that has to be removed at the end by sending a to zero. The lattice formulation is the only known non-perturbative regularisation of quantum field theories and allows the treatment as a classical statistical system.

Typical tasks are the computation of running couplings at any given scale, hadron and glueball masses as well as weak matrix elements. If the latter involve hadronic states, they will contain a QCD part that is parametrised by QCD matrix elements. They had to be computed non-perturbatively and some of them are investigated in this work. Free parameters are fixed by experimental low-energy observables such as hadron masses.

The thesis is divided as follows: an introduction to the basics of lattice gauge theory is given in chapter 1. As the working ground, the Schrödinger Functional (SF) is explained in chapter 2, where furthermore a running coupling \bar{g} and fermionic correlation functions are defined. In view of recent experiments in B-physics, such as BaBar and Belle, chapter 3 explains how heavy meson systems may be treated on the lattice and which problems arise. Improved meson interpolating fields at the boundaries are used to accelerate the approach to ground state dominance in correlators. This issue is discussed in chapter 4 together with their determination through the variational principle and details to their implementation in the program. The variational principle is not the only tool to extract information about the meson ground state and its lowest excitations. Others are introduced in chapter 5.

Data analysis and results are discussed in chapter 6, and final conclusions are drawn in chapter 7.

Chapter 1

Basics of Lattice Gauge Theory

Lattice QCD is a non-perturbative implementation of field theory from first principles using the Feynman path integral approach. The lattice Λ discretises four-dimensional continuum space-time by a finite lattice spacing a ,

$$\Lambda = a\mathbb{Z}^4 = \{x|x_\mu/a \in \mathbb{Z}\}, \quad \mu = 0, 1, 2, 3. \quad (1.1)$$

Fourier transforms of functions defined on the lattice can be restricted to the first Brillouin zone, $p \in [-\frac{\pi}{a}, \frac{\pi}{a})$. So there is an intrinsic ultraviolet cutoff π/a of lattice momenta.

By changing from Minkowskian to Euclidean space, $x_0 = -ix_4$, one may relate field theory to statistical mechanics [16]. A vast amount of degrees of freedom are to be integrated over in the path integral. As this is numerically impossible within a reasonable time, one has to employ a stochastic integration. So one may non-perturbatively compute quantities \mathcal{O} of interest, such as running couplings, hadron masses and decay constants as well as moments of structure functions, by means of Monte-Carlo techniques. The expectation value is given by a sum,

$$\langle \mathcal{O} \rangle = \frac{1}{n} \sum_{i=1}^n \mathcal{O}_i + \mathcal{O}(n^{-1/2}), \quad (1.2)$$

over $n \gg 1$ gauge configurations of a statistical ensemble which is given by the action. This formula turns out to be asymptotically exact, because the error term is a purely statistical one and can in principle be made arbitrarily small. Once quantities have been computed non-perturbatively on the lattice, they have to be related to the continuum. In practice, this 'continuum

limit' is realised by first computing the same quantity on lattices at different lattice spacings a and then by extrapolating the quantity to $a = 0$.

This chapter continues with a brief introduction which action has been used and how one can improve the approach of lattice results to the continuum. More detailed reviews on the subject are for instance [17, 18, 19] and [20].

1.1 Discretisation of the continuum SU(N) Yang–Mills Action

In this section, the discretised gauge part of the action is introduced. Starting with the general case, that is the Euclidean SU(N) Yang–Mills action in the continuum,

$$S_G = \frac{1}{4} \int d^4x F_{\mu\nu}^a F_{\mu\nu}^a = -\frac{1}{2g_0^2} \int d^4x \operatorname{tr} (F_{\mu\nu} F_{\mu\nu}), \quad (1.3)$$

one has to find a suitable discretised version.¹ The trace is taken over the generators T^a of the gauge group SU(N). The vector potential $A_\mu(x) = A_\mu^a(x)T^a$, $a = 1 \dots N^2 - 1$ is in the adjoint representation. The field strength tensor $F_{\mu\nu}(x) = F_{\mu\nu}^a(x)T^a$ is defined through

$$F_{\mu\nu}^a(x) = \partial_\mu A_\nu^a(x) - \partial_\nu A_\mu^a(x) + f_{abc}A_\mu^b(x)A_\nu^c(x). \quad (1.4)$$

The symbol f_{abc} shall denote the structure constant for the SU(N) Lie algebra and g_0 is the bare coupling.

On the lattice, it is more convenient to replace the SU(N) Lie algebra valued gauge field $A_\mu(x)$ by an SU(N) group element $U(x, \mu)$, $\mu = 0, 1, 2, 3$ represented by a unitary $N \times N$ matrix. This 'link variable' may be considered a transporter of colour charge between the sites x and $x + a\hat{\mu}$. Formally, the relation to $A_\mu(x)$ in the continuum is

$$U(x, \mu) = U(x, x + a\hat{\mu}) = \exp(aA_\mu(x)) = 1 + aA_\mu(x) + O(a^2), \quad (1.5)$$

where the exponential has been expanded up to the term linear in the lattice spacing a . Links are covariant under local SU(N) gauge transformations $\Lambda(x)$,

$$U(x, \mu) \rightarrow \Lambda(x)U(x, \mu)\Lambda(x + a\hat{\mu})^\dagger. \quad (1.6)$$

¹The case $N = 3$ is of particular interest since SU(3)_c is the local gauge group of QCD.

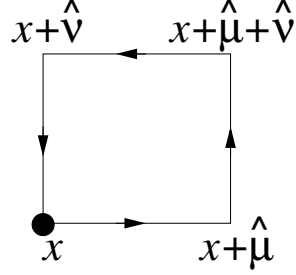


Figure 1.1: The plaquette is the smallest closed and gauge-invariant path.

The smallest gauge-invariant loop on the lattice, as shown in figure 1.1, is referred to as plaquette,

$$U(p) = U(x, \mu)U(x + a\hat{\mu}, \nu)U(x + a\hat{\nu}, \mu)^{-1}U(x, \nu)^{-1}. \quad (1.7)$$

It may be used to construct gauge-invariant quantities, such as the Yang-Mills lattice action [21],

$$S_G = \frac{\beta}{2N} \sum_p \text{tr} (1 - U(p)), \quad g_0^2 = \frac{2N}{\beta}, \quad (1.8)$$

where the sum has to be taken over all oriented plaquettes. It can be shown that Wilson's plaquette action is a lattice version of eq. (1.3) that has $O(a^2)$ lattice artefacts.

1.2 The Wilson-Dirac Fermion Action

Since QCD includes fermions, the quarks, one has to discretise the Euclidean continuum fermion action,

$$S_F = \int d^4x \bar{\psi}(x)(\gamma_\mu D_\mu + m_0)\psi(x), \quad (1.9)$$

for quarks with mass m_0 in the fundamental representation of $SU(3)$.² In the continuum, chiral symmetry is only broken by non-zero quark masses.

²Accordingly, anti-fermions are in the $SU(3)^*$.

In general, a Dirac field $\psi(x)$ at the lattice site x carries colour (α), Dirac (A) and flavour (i) indices,

$$(\psi_i(x))_{\alpha A}, \quad i = 1 \dots N_f, \alpha = 1 \dots 3, A = 1 \dots 4. \quad (1.10)$$

From now on, colour and Dirac indices are suppressed, and flavour indices are written down where appropriate.

QCD interactions are realised through the concept of minimal coupling. The symbol $D_\mu = \partial_\mu + A_\mu$ denotes the covariant derivative, and the γ_μ are the Euclidean Dirac matrices listed in appendix A. As a discretised version of $\gamma_\mu D_\mu$, one may use the Wilson-Dirac operator

$$D = \frac{1}{2} \sum_{\mu=0}^3 \left(\gamma_\mu (\nabla_\mu^* + \nabla_\mu) - ar \nabla_\mu^* \nabla_\mu \right). \quad (1.11)$$

The symbol r is the Wilson parameter and ∇_μ, ∇_μ^* are the covariant lattice forward/backward derivatives,

$$\begin{aligned} \nabla_\mu \psi(x) &= \frac{1}{a} [U(x, \mu) \psi(x + a\hat{\mu}) - \psi(x)], \\ \nabla_\mu^* \psi(x) &= \frac{1}{a} [\psi(x) - U(x - a\hat{\mu}, \mu)^{-1} \psi(x - a\hat{\mu})]. \end{aligned} \quad (1.12)$$

Wilson proposed to write the fermionic lattice action as

$$S_F[U, \bar{\psi}, \psi] = a^4 \sum_x \bar{\psi}(x) (D + m_0) \psi(x). \quad (1.13)$$

It converges with a rate proportional to a to its continuum version.

Through the naive discretisation, $r = 0$, of $\gamma_\mu D_\mu$ the fermion propagator has $2^d - 1$ additional zeros for $p_\mu \neq 0$ in the Brillouin zone. Due to the extra term $a \nabla_\mu^* \nabla_\mu$, they get a mass $\propto a^{-1}$, freeze out in the continuum limit and thus disappear from the physical spectrum. Throughout this work, r has been set to one.

A serious disadvantage of Wilson fermions is that even in the massless case, $m_0 = 0$, they explicitly break chiral symmetry.

Nielsen and Ninomiya [22] pointed out that if one uses an action which

- is translation invariant,
- has continuum lattice momenta in the range of $[-\pi, \pi)$ for $L \rightarrow \infty$,

- has only local interactions,
- gives the correct continuum properties in the continuum limit,
- and preserves chiral symmetry, $\{D, \gamma_5\} = 0$, at finite lattice spacing a ,

then the theory will have doublers. To avoid fermion doubling, one has to give up at least one of these properties. Points one to four are usually kept and therefore point five is violated. The absence of doublers is at the cost of a broken chiral symmetry, even for $m_0 = 0$.

A recent development are so-called Ginsparg-Wilson (GW-) fermions. They preserve chiral symmetry in the form of a modified infinitesimal chiral transformation. To order ϵ , the action is invariant under

$$\psi \rightarrow \psi + \epsilon \gamma_5 (1 - a \hat{D}) \psi, \quad \bar{\psi} \rightarrow \bar{\psi} + \epsilon \bar{\psi} \gamma_5.$$

The lattice Dirac operator \hat{D} satisfies the Ginsparg-Wilson relation [23],

$$\{\hat{D}, \gamma_5\} = a \hat{D} \gamma_5 \hat{D}, \quad (1.14)$$

as well as γ_5 -hermiticity. Simulations using this formulation are numerically very expensive. But the computational power is growing and algorithms are improving. In view of nowadays computing power (and the purpose of this work), Wilson fermions are still the more favourable choice.

1.3 The Symanzik Improvement Programme

To accelerate the approach to the continuum, Symanzik studied an effective continuum theory where the lattice spacing a is made explicit [24, 25]. Close to the continuum, lattice theory may be described by an effective action

$$S_{\text{eff}} = S_0 + a S_1 + a^2 S_2 + \cdots, \quad S_k = \int d^4x \mathcal{L}_k, \quad (1.15)$$

with the QCD continuum Lagrangian \mathcal{L}_0 and linear combinations of dimension $4 + k$, $k \geq 1$ local operators in \mathcal{L}_k . The dimensional counting here includes (non-negative) powers of the quark mass m_0 by which some of the fields may be multiplied. The presence of operators in eq. (1.15) is restricted to those that are invariant under the symmetries of the lattice theory. Their

number can be further reduced by partial integration.

As a concrete example, ref. [26] give terms that may occur in an order a effective Lagrangian \mathcal{L}_1 .

Cutoff effects do not only originate in the action, but may also be involved in local composite fields $\phi(x)$. In many cases, they need to be improved as well. In the effective continuum theory, renormalised lattice fields are represented through effective fields of the form

$$\phi_{\text{eff}} = \phi_0 + a\phi_1 + a^2\phi_2 + \dots \quad (1.16)$$

The fields ϕ_k are linear combinations of local fields with appropriate dimension. They have to transform under the lattice symmetries in the same way as the lattice field to be represented. To order a , the lattice correlation functions are given by

$$\begin{aligned} G_n(x_1, \dots, x_n) &= \langle \phi_0(x_1) \dots \phi_0(x_n) \rangle_{\text{con}} \\ &\quad - a \int d^4y \langle \phi_0(x_1) \dots \phi_0(x_n) \mathcal{L}_1(y) \rangle_{\text{con}} \\ &\quad + a \sum_{k=1}^n \langle \phi_0(x_1) \dots \phi_1(x_k) \dots \phi_0(x_n) \rangle_{\text{con}} + O(a^2), \end{aligned} \quad (1.17)$$

where the label 'con' on the correlation functions means their connected form. The expectation values on the right-hand side are with respect to the continuum action S_0 . The second term is a contribution of the $O(a)$ correction in the effective action. When y gets close to any $x_i, i = 1 \dots n$, divergences may arise and hence subtraction prescriptions have to be employed. This amounts to a redefinition of the field $\phi_1(x)$. A further reduction of the operator basis may be achieved through the equations of motion. Because they are only valid up to contact terms, their application is restricted to position space correlation functions at non-zero physical distance. But this restriction is not severe since most on-shell quantities, such as hadron masses and decay constants, can be extracted from such correlation functions.

Chapter 2

The Schrödinger Functional

2.1 Model

The Schrödinger functional is the propagation kernel for the transition from some field configuration at time $x_0 = 0$ to some other configuration at $x_0 = T$. In Euclidean space-time it can be written as a functional integral over all fields with the specified initial and final values [27, 28, 29].

In section 2.1.1 the model is motivated in view of lattice simulations, and it is introduced for $SU(N)$ Yang-Mills theory for continuum space-time in section 2.1.2. The Schrödinger functional turns out to be renormalisable [27]. For the Yang-Mills case, only standard counterterms for the action are required. A running coupling, that only depends on one scale, is introduced in section 2.1.5. The extension to QCD [29] is shortly mentioned in section 2.1.3, and section 2.1.4 introduces the reader to the formulation of the Schrödinger functional on the lattice.

Good reviews on the topic can be found in [30, 18].

2.1.1 Motivation

QCD is a theory in which totally complementary physics takes place. At low scales, $q \sim 1 \text{ GeV}$, the mass of the proton, there is quark confinement – a non-perturbative phenomenon, whereas at very large scales, say $q \sim 100 \text{ GeV}$, quarks behave like free particles. This is the domain of jet physics, where perturbative techniques are applicable. The two scales differ by two orders of magnitude. If one is interested in a non-perturbative computation of the running strong coupling α_s or the renormalisation group invariant (RGI-)

quark mass M in a lattice simulation, one has to relate both disparate scales to each other. This is because in the lattice regularisation QCD is naturally renormalised through the hadron spectrum.

By means of perturbation theory, one is able to evolve α_s and the running quark mass \bar{m} from infinite energy down to scales of $q \sim 10 \text{ GeV}$ with controlled perturbative errors. But to reach the low-energy regime of hadron physics for renormalisation, at least one order of magnitude in the energy scale q still remains to be overcome. To avoid large discretisation effects on the lattice and to be able to take the continuum limit, one should keep q away from the cutoff a^{-1} as well. Large physical box lengths L compared to the confinement scale are needed to keep finite-size effects small.¹ These conditions are summarised by

$$L \gg \frac{1}{0.4 \text{ GeV}} \gg \frac{1}{q} \sim \frac{1}{10 \text{ GeV}} \gg a. \quad (2.1)$$

Thus, to fulfil all requirements on a single lattice, one needs very fine lattices, $N = L/a \gg 25$. But this is still too demanding for present computers.

A solution to this problem has been pointed out by Lüscher, Weisz and Wolff [31]. By identifying the two physical scales

$$q = 1/L, \quad (2.2)$$

one may take a finite-size effect as a physical observable. The running coupling may then be computed recursively in several steps, where q is changed by a factor s in each step. In this way, no large scale ratios appear and discretisation errors are small for $L/a \gg 1$ in each step.

2.1.2 Formal Definition – Pure Gauge Theory

One starts in the Hamiltonian theory in the temporal gauge [28]. The Schrödinger functional is defined by the Hamiltonian evolution of the gauge fields. The Hamiltonian has to be written down, for instance at $x_0 = 0$, by assuming commutation relations among the basic fields.

Because the Schrödinger functional will be used to study scaling properties of the theory in finite volume, space is taken to be an $L \times L \times L$ box with periodic boundary conditions. $SU(N)$ gauge fields are accordingly represented

¹The confinement scale, $q \sim 0.4 \text{ GeV}$, is given by the square root of the string tension.

by periodic vector potentials² $A_k(\mathbf{x})$ on \mathbb{R}^3 in the Lie algebra of $SU(N)$. The index $k = 1, 2, 3$ labels the direction, the symbol \hat{k} shall denote the unit vector in k -direction. Periodicity under gauge transformations

$$\begin{aligned} A_k(\mathbf{x}) &\rightarrow A_k^\Lambda(\mathbf{x}) = \Lambda(\mathbf{x})A_k(\mathbf{x})\Lambda(\mathbf{x})^{-1} + \Lambda(\mathbf{x})\partial_k\Lambda(\mathbf{x})^{-1}, \\ A_k(\mathbf{x} + \hat{k}L) &= A_k(\mathbf{x}), \quad \Lambda(\mathbf{x} + \hat{k}L) = \Lambda(\mathbf{x}) \end{aligned} \quad (2.3)$$

is only preserved if periodic gauge functions $\Lambda(\mathbf{x}) \in SU(N)$ are admitted. It can be regarded as a continuous mapping from a three-dimensional torus to $SU(N)$, and it is characterised by an integer – the winding number n .

In the Schrödinger representation, quantum mechanical states of the theory are wave functionals $\psi[A]$, where A runs over all gauge fields. A scalar product is given by

$$\langle \psi | \chi \rangle = \int D[A] \psi[A]^* \chi[A], \quad D[A] = \prod_{\mathbf{x}, k, a} dA_k^a(\mathbf{x}). \quad (2.4)$$

Physical states are gauge invariant. So

$$\psi[A^\Lambda] = \psi[A] \quad (2.5)$$

has to apply for all gauge transformations Λ . Any wave functional state can be projected on the physical subspace,

$$\psi[A] \rightarrow \mathbb{P}\psi[A] = \int D[\Lambda] \psi[A^\Lambda], \quad D[\Lambda] = \prod_{\mathbf{x}} d\Lambda(\mathbf{x}). \quad (2.6)$$

Here $d\Lambda(\mathbf{x})$ denotes the Haar measure of $SU(N)$. The gauge field $A_k^a(\mathbf{x})$ can be interpreted as an operator field that acts on wave functionals $\psi[A]$. The canonically conjugate field,

$$F_{0k}^a(\mathbf{x}) = -i \frac{\delta}{\delta A_k^a(\mathbf{x})}, \quad (2.7)$$

is the colour-electric part of the colour field strength tensor. The magnetic components are

$$F_{kl}^a(\mathbf{x}) = \partial_k A_l^a(\mathbf{x}) - \partial_l A_k^a(\mathbf{x}) + f^{abc} A_k^b(\mathbf{x}) A_l^c(\mathbf{x}). \quad (2.8)$$

²Anti-hermitean vector potentials are used. With respect to a basis of group generators T^a in the adjoint representation, $a = 1 \dots N^2 - 1$, one obtains $A_k(\mathbf{x}) = A_k^a(\mathbf{x})T^a$ with real gauge fields $A_k^a(\mathbf{x})$.

The Hamiltonian of the theory, \mathbb{H} , is given by

$$\mathbb{H} = \int_0^L d^3x \left(\frac{g_0^2}{2} F_{0k}^a(\mathbf{x}) F_{0k}^a(\mathbf{x}) + \frac{1}{4g_0^2} F_{kl}^a(\mathbf{x}) F_{kl}^a(\mathbf{x}) \right), \quad (2.9)$$

whereas g_0 denotes the bare gauge coupling.

Each classical gauge field $C_k(\mathbf{x})$ defines a state $|C\rangle$ through

$$\langle C|\psi\rangle = \psi[C]. \quad (2.10)$$

Generally, such a state $|C\rangle$ is not gauge-invariant, but may be made so by applying the projector \mathbb{P} . The Euclidean Schrödinger functional $\mathcal{Z}[C', C]$ is now defined by

$$\mathcal{Z}[C', C] = \langle C'|e^{-\mathbb{H}T}\mathbb{P}|C\rangle. \quad (2.11)$$

The spectral representation may be written down by inserting an orthonormal basis $|\psi_n\rangle$, $n = 0, 1, 2, \dots$, of gauge-invariant and discrete energy eigenstates,

$$\mathcal{Z}[C', C] = \sum_{n=0}^{\infty} e^{-E_n T} \psi_n[C'] \psi_n[C]^*, \quad (2.12)$$

with real energy eigenvalues E_n .³ $\mathcal{Z}[C', C]$ is invariant under arbitrary gauge transformations since only physical intermediate states contribute.

Alternatively to the Hamiltonian approach, one may express the matrix elements of the Euclidean time evolution operator $e^{-\mathbb{H}T}$ between gauge-invariant states through a functional integral over all gauge field configurations A_μ in four dimensions, in a $L^3 \times T$ box, with $0 \leq x_0 \leq T$ and periodic boundary conditions in the spatial directions and Dirichlet boundary conditions at the $x_0 = 0, T$ hyperplanes,

$$A_k(x) = \begin{cases} C_k^\Lambda(\mathbf{x}) & \text{at } x_0 = 0, \\ C_k'(\mathbf{x}) & \text{at } x_0 = T. \end{cases} \quad (2.13)$$

In this formulation, the Euclidean gauge action is

$$S_G[A] = -\frac{1}{2g_0^2} \int d^4x \operatorname{tr} (F_{\mu\nu} F_{\mu\nu}), \quad (2.14)$$

³Lüscher has shown that this holds even on the lattice, chapter 2.4.1.

where the trace is taken over colour indices $a = 1 \dots N^2 - 1$ of the gauge fields in the adjoint representation. The field strength tensor has the well-known form

$$F_{\mu\nu} = \partial_\mu A_\nu - \partial_\nu A_\mu + [A_\mu, A_\nu]. \quad (2.15)$$

Finally, the definition of the Schrödinger functional in terms of the functional integral is

$$\mathcal{Z}[C', C] = \int D[A] \int D[\Lambda] e^{-S_G[A]}. \quad (2.16)$$

The integration over all gauge transformations Λ is required to account for the projector \mathbb{P} , eq. (2.6). The functional integral representation will be chosen for the definition on the lattice.

The issue of renormalisation of the Schrödinger functional is discussed (and numerically checked to a certain extent) in a wide range of literature, for instance [27, 28, 29, 32, 33, 34, 35]. It was shown up to 2-loop order in perturbation theory that, apart from the standard renormalisation of the bare coupling constant, no additional counterterms occur in the Yang-Mills theory.

2.1.3 Formulation with Fermions

The Schrödinger functional, as defined for the pure gauge, may be extended to QCD by including fermions [29]. It is useful to write the fermionic part of the action in the functional integral representation,

$$\begin{aligned} S_F[A, \bar{\psi}, \psi] = & \int_0^T dx_0 \int_0^L d^3\mathbf{x} \bar{\psi}(x) [\gamma_\mu D_\mu + m_0] \psi(x) \\ & - \int_0^L d^3\mathbf{x} [\bar{\psi}(x) P_- \psi(x)]_{x_0=0} - \int_0^L d^3\mathbf{x} [\bar{\psi}(x) P_+ \psi(x)]_{x_0=T}. \end{aligned} \quad (2.17)$$

This is the usual fermion action for manifolds without boundaries plus two extra surface terms at the $x_0 = 0, T$ boundaries. D_μ denotes the covariant derivative, $D_\mu = \partial_\mu + A_\mu$, and $P_\pm = \frac{1}{2}(1 \pm \gamma_0)$ the projector where standard Euclidean γ -matrices have been used.⁴ The quark fields are taken to be

⁴Their explicit form is given in appendix A.

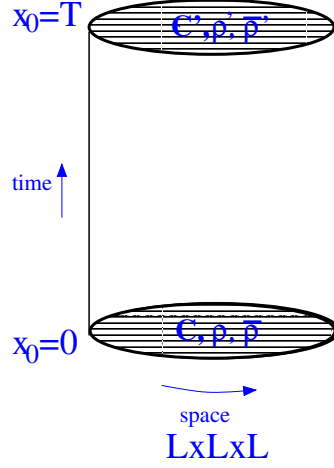


Figure 2.1: Visualisation of the Schrödinger functional as a four-dimensional cylinder.

periodic up to a phase in the spatial directions,

$$\psi(x + \hat{k}L) = e^{i\theta_k} \psi(x), \quad \bar{\psi}(x + \hat{k}L) = \bar{\psi}(x)e^{-i\theta_k}, \quad k = 1, 2, 3, \quad (2.18)$$

and have to obey on the $x_0 = 0, T$ boundaries,

$$P_+ \psi(x)|_{x_0=0} = \rho(\mathbf{x}), \quad P_- \psi(x)|_{x_0=T} = \rho'(\mathbf{x}), \quad (2.19)$$

$$\bar{\psi}(x)P_-|_{x_0=0} = \bar{\rho}(\mathbf{x}), \quad \bar{\psi}(x)P_+|_{x_0=T} = \bar{\rho}'(\mathbf{x}). \quad (2.20)$$

Since the Dirac operator is a first order differential operator, only half of the spinor components have to be specified at the boundaries.

The total action is the sum of the gauge and the fermion part,

$$S[A, \bar{\psi}, \psi] = S_G[A] + S_F[A, \bar{\psi}, \psi]. \quad (2.21)$$

It appears in the Boltzmannian of the QCD Schrödinger functional,

$$\mathcal{Z}[C', \bar{\rho}', \rho', C, \bar{\rho}, \rho] = \int D[A]D[\psi]D[\bar{\psi}] e^{-S[A, \bar{\psi}, \psi]}, \quad (2.22)$$

and an integration over all fields with specified boundary values is involved.

To write down correlation functions

$$\langle \mathcal{O} \rangle = \left(\frac{1}{\mathcal{Z}} \int \mathcal{D}[A] \mathcal{D}[\psi] \mathcal{D}[\bar{\psi}] \mathcal{O} e^{-S[A, \bar{\psi}, \psi]} \right) \Big|_{\bar{\rho}' = \rho' = \bar{\rho} = \rho = 0} \quad (2.23)$$

as expectation values of an operator \mathcal{O} , one may define 'boundary fields' that create quarks and antiquarks at $x_0 = 0, T$,

$$\zeta(\mathbf{x}) = \frac{\delta}{\delta \bar{\rho}(\mathbf{x})}, \quad \bar{\zeta}(\mathbf{x}) = -\frac{\delta}{\delta \rho(\mathbf{x})}, \quad (2.24)$$

$$\zeta'(\mathbf{x}) = \frac{\delta}{\delta \bar{\rho}'(\mathbf{x})}, \quad \bar{\zeta}'(\mathbf{x}) = -\frac{\delta}{\delta \rho'(\mathbf{x})}. \quad (2.25)$$

\mathcal{O} may contain gauge fields and matter fields ψ, ζ etc.⁵ As an application, the definition of the renormalised quark mass in the Schrödinger functional is discussed in chapter 2.6.

Some comments to the renormalisation of the Schrödinger functional with quarks are in order:

The existence of gauge-invariant composite fields of dimension three enforce counterterms. Sint [29, 32] showed in 1-loop order of perturbation theory that two counterterms at the $x_0 = 0, T$ boundaries have to be added to obtain a finite renormalised theory. This turned out to be equivalent to a wave function renormalisation of the boundary values,

$$\rho_R = Z_b^{-1/2} \rho, \quad \text{etc.} \quad (2.26)$$

For vanishing boundary values, no additional renormalisation is necessary.

2.1.4 Lattice Formulation

Starting from the formulation of the Schrödinger functional in continuum space-time, section 2.1.2 and 2.1.3, one discretises a physical volume $L^3 \times T$ by a finite lattice spacing a . As introduced in chapter 1, one defines gauge fields $U(x, \mu) \in \text{SU}(N)$ with direction $\mu = 0, 1, 2, 3$, as well as quark and antiquark fields, $\psi(x)$ and $\bar{\psi}(x)$, that carry Dirac, flavour and colour indices on each point x on the lattice. Fermion fields are assumed to be periodic in

⁵These derivatives, eqs. (2.24), (2.25), act on the Boltzmannian with the effect of inserting certain combinations of $\psi(x)$ and $\bar{\psi}(x)$ close to the lattice boundaries.

space up to the phase, $-\pi < \theta_k < \pi$, eq. (2.18). A compact notation for the phase in four dimensions is θ_μ with the time component θ_0 set to zero.

The Euclidean gauge field is subjected to the following boundary conditions,

$$U(x, k)|_{x_0=0} = W(\mathbf{x}, k), \quad \text{and} \quad U(x, k)|_{x_0=T} = W'(\mathbf{x}, k), \quad (2.27)$$

with lattice boundary fields W, W' . For example, W may be written as

$$W(\mathbf{x}, k) = P \exp \left(a \int_0^1 dt C_k(\mathbf{x} + a\hat{k} - ta\hat{k}) \right) \quad (2.28)$$

with continuum gauge potentials C_k , eq. (2.13). The expression for W' is analogous. The symbol P denotes the path-order operator.

A convenient choice for the matrices C_k and C'_k are constant Abelian fields. They are smooth, introduce only small lattice artefacts and are discussed in ref. [28]. The gauge field action is the Wilson plaquette action [36],

$$S_G[U] = \frac{1}{g_0^2} \sum_p w(p) \operatorname{tr} (1 - U(p)), \quad (2.29)$$

with the sum over all oriented plaquettes p , weights $w(p)$ and parallel transporters $U(p)$ around p .

In the interior, the weight is always set to 1, whereas

$$w(p) = \begin{cases} \frac{1}{2}c_s & \text{if } p \text{ is a spatial plaquette at } x_0 = 0 \text{ or } x_0 = T, \\ c_t & \text{if } p \text{ is time-like and attached to a boundary plane.} \end{cases} \quad (2.30)$$

The case $c_s = 1 = c_t$ corresponds to the standard Wilson action. For an $O(a)$ improved action, however, these coefficients depend on the bare coupling g_0 . This will be described in more detail in section 2.2.

Because the Schrödinger functional has Dirichlet boundary conditions imposed at $x_0 = 0, T$, it is suitable to use a 'padding with zeros',

$$\psi(x) = 0 \quad \text{if } x_0 < 0 \text{ or } x_0 > T, \quad (2.31)$$

and

$$P_- \psi(x)|_{x_0=0} = 0 = P_+ \psi(x)|_{x_0=T}, \quad (2.32)$$

similarly for the antiquark fields, to write down the fermion action more elegantly. Gauge fields that reside outside the manifold are set to 1. One may then write the fermion action as a sum over all space-time points without restrictions for the time coordinate,

$$S_F[U, \bar{\psi}, \psi] = a^4 \sum_x \bar{\psi}(x) (D + m_0) \psi(x), \quad (2.33)$$

with the standard Wilson-Dirac operator,

$$D = \frac{1}{2} \sum_{\mu=0}^3 \left(\gamma_\mu (\nabla_\mu^* + \nabla_\mu) - a \nabla_\mu^* \nabla_\mu \right). \quad (2.34)$$

The symbol m_0 denotes the diagonalised mass matrix in flavour space, and ∇_μ, ∇_μ^* are the covariant lattice forward/backward derivatives⁶

$$\begin{aligned} \nabla_\mu \psi(x) &= \frac{1}{a} [e^{i\theta_\mu/L} U(x, \mu) \psi(x + a\hat{\mu}) - \psi(x)], \\ \nabla_\mu^* \psi(x) &= \frac{1}{a} [\psi(x) - e^{-i\theta_\mu/L} U(x - a\hat{\mu}, \mu)^{-1} \psi(x - a\hat{\mu})]. \end{aligned} \quad (2.35)$$

The Schrödinger functional may then be written as [29, 32],

$$\mathcal{Z} = e^{-\Gamma} = \int D[\psi] D[\bar{\psi}] D[U] e^{-(S_G[U] + S_F[U, \bar{\psi}, \psi])}, \quad D[U] = \prod_{x, \mu} dU(x, \mu), \quad (2.36)$$

with the Haar measure dU . The symbol Γ denotes the effective action. One usually integrates $\psi, \bar{\psi}$ out by hand, as explained in appendix B. This gives rise to quark propagators and the fermion determinant.

2.1.5 The Renormalised Coupling $\bar{g}(L)$

The Schrödinger functional allows one to define a renormalisable coupling \bar{g} in finite volume that depends only on one scale $1/L$. It is chosen such that

$$\alpha_S(q) = \frac{\bar{g}^2(L)}{4\pi}, \quad q = 1/L \quad (2.37)$$

applies. Starting from the Schrödinger functional, there are many ways to define such a coupling non-perturbatively. One may choose a background

⁶The periodicity of fermion fields in space, eq. (2.18), may be rewritten such that the phase θ_μ is uniformly distributed over the lattice with a phase θ_μ/L between two neighbouring sites. This allows a more convenient numerical treatment.

field⁷ B that is a smooth function of some dimensionless parameter η , and differentiates the effective action $\Gamma = -\ln \mathcal{Z}[C', C]$, eq. (2.16),

$$\Gamma'[B] = \frac{\partial}{\partial \eta} \Gamma[B]. \quad (2.38)$$

That is defined to be \bar{g}^{-2} up to a normalisation factor,

$$\bar{g}^2 = (\Gamma'_0[B]/\Gamma'[B])|_{\eta=0, T=L}, \quad (2.39)$$

where $\Gamma'_0[B] = g_0^2 \partial_\eta S[B]$ ensures that \bar{g}^2 coincides with the bare coupling g_0^2 to leading order of perturbation theory. Non-perturbative determinations of the running coupling may be found in [34] for the quenched approximation, for a toy model with $N_f = -2$ sea quark flavours in [37] and for full QCD with $N_f = 2$ in [38]. Perturbative results up to two-loop order in g_0 are known [33].

2.2 $O(a)$ Improvement Programme

In this section, the $O(a)$ improved action S_{impr} is introduced. It may be obtained by adding suitable counterterms to the Wilson action S such that $O(a)$ contributions are cancelled out,

$$S_{\text{impr}}[U, \bar{\psi}, \psi] = S[U, \bar{\psi}, \psi] + \delta S[U, \bar{\psi}, \psi]. \quad (2.40)$$

This is done in the framework of Symanzik's improvement programme as introduced in section 1.3. Schrödinger functional boundaries have to be taken into account since they may enforce the presence of additional counterterms. Improvement of operators is not discussed here but is usually necessary.

2.2.1 Gauge Action

Because of boundaries, the gauge action in eq. (2.29) is not fully $O(a)$ improved. But it can be made so by adding a counterterm at the boundaries. This amounts to a redefinition of the weight in eq. (2.30),

$$w(p) = c_t(g_0), \quad (2.41)$$

⁷ Certain fields B are referred to as background fields. Such a field is induced by the boundary conditions, and $S[A] > S[B]$ holds for all A that are not equivalent to a gauge transform of B . Furthermore, B has to be a solution of the equation of motion satisfying the boundary conditions, eq. (2.13).

for time-like plaquettes attached to the boundary planes. For the other case, $w = 1$ remains. The improvement coefficient c_t is known up to two-loop order in perturbation theory [35]. For constant Abelian fields, as used throughout this work, the improvement coefficient c_s is not needed.

2.2.2 Fermion Action

In [26] it is shown that there are two sorts of improvement terms for the fermionic part of the action – a volume term (v) and a boundary term (b),

$$\delta S_F[U, \bar{\psi}, \psi] = \delta S_{F,v}[U, \bar{\psi}, \psi] + \delta S_{F,b}[U, \bar{\psi}, \psi]. \quad (2.42)$$

The first contribution is the Sheikholeslami-Wohlert (clover) term [39],

$$\delta S_{F,v}[U, \bar{\psi}, \psi] = a^5 \sum_x c_{sw}(g_0) \bar{\psi}(x) \frac{1}{4} \sigma_{\mu\nu} \hat{F}_{\mu\nu}(x) \psi(x). \quad (2.43)$$

It is independent of imposed boundary conditions. The improvement coefficient c_{sw} must be tuned such that $O(a)$ cutoff effects cancel. This tuning is a non-trivial task. The tree level value is $c_{sw} = 1$. A non-perturbative determination is found in [40, 41]. The symbol $\sigma_{\mu\nu} = \frac{i}{2}[\gamma_\mu, \gamma_\nu]$ is the commutator of Dirac matrices, and $\hat{F}_{\mu\nu} = \frac{1}{8a^2}(Q_{\mu\nu} - Q_{\nu\mu})$ the gluon field strength tensor on the lattice. The symbol $Q_{\mu\nu}$ is defined as

$$\begin{aligned} Q_{\mu\nu}(x) = & U(x, \mu)U(x + a\hat{\mu}, \nu)U(x + a\hat{\nu}, \mu)^{-1}U(x, \nu)^{-1} \\ & + U(x, \nu)U(x - a\hat{\mu} + a\hat{\nu}, \mu)^{-1}U(x - a\hat{\mu}, \nu)^{-1}U(x - a\hat{\mu}, \mu) \\ & + U(x - a\hat{\mu}, \mu)^{-1}U(x - a\hat{\mu} - a\hat{\nu}, \nu)^{-1}U(x - a\hat{\mu} - a\hat{\nu}, \mu)U(x - a\hat{\nu}, \nu) \\ & + U(x - a\hat{\nu}, \nu)^{-1}U(x - a\hat{\nu}, \mu)U(x + a\hat{\mu} - a\hat{\nu}, \nu)U(x, \mu)^{-1} \end{aligned}$$

and looks like a clover leaf. This is depicted in figure 2.2. Eq. (2.42) involves one more counterterm that originates in the presence of fermion fields at the boundaries. In [26] one may find all operators of dimension four that may occur in counterterms. There it is also shown how the number of operators can be reduced to four,

$$\hat{O}_s(\mathbf{x}) = \frac{1}{2}\bar{\rho}(\mathbf{x})\gamma_k(\nabla_k^* + \nabla_k)\rho(\mathbf{x}), \quad (2.44)$$

$$\hat{O}'_s(\mathbf{x}) = \frac{1}{2}\bar{\rho}'(\mathbf{x})\gamma_k(\nabla_k^* + \nabla_k)\rho'(\mathbf{x}), \quad (2.45)$$

$$\hat{O}_t(\mathbf{x}) = (\bar{\psi}(y)P_+\nabla_0^*\psi(y) + \bar{\psi}(y)\overleftarrow{\nabla}_0^*P_-\psi(y))|_{y=(a,\mathbf{x})}, \quad (2.46)$$

$$\hat{O}'_t(\mathbf{x}) = (\bar{\psi}(y)P_-\nabla_0\psi(y) + \bar{\psi}(y)\overleftarrow{\nabla}_0P_+\psi(y))|_{y=(T-a,\mathbf{x})}, \quad (2.47)$$

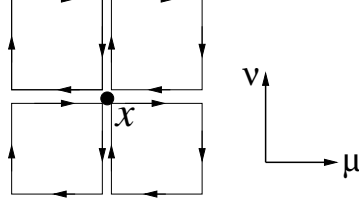


Figure 2.2: Visualisation of the contribution $Q_{\mu\nu}(x)$ in the SW clover term.

that are part of the counterterm,

$$\delta S_{F,b}[U, \bar{\psi}, \psi] = \quad (2.48)$$

$$a^4 \sum_{\mathbf{x}} \left((\tilde{c}_s - 1)[\hat{\mathcal{O}}_s(\mathbf{x}) + \hat{\mathcal{O}}'_s(\mathbf{x})] + (\tilde{c}_t - 1)[\hat{\mathcal{O}}_t(\mathbf{x}) - \hat{\mathcal{O}}'_t(\mathbf{x})] \right).$$

The result for \tilde{c}_t as a function of the bare coupling is given in [42] to one-loop order of perturbation theory.

Eq. (2.48) simplifies for vanishing fermionic boundary fields because in this case $\hat{\mathcal{O}}_s$ and $\hat{\mathcal{O}}'_s$ will drop out. So one is left with the tuning of $\tilde{c}_t(g_0)$.

2.3 The Correlation Functions f_A , f_P and f_1

In order to compute quantities of interest, for instance pseudoscalar masses and decay constants as well as current quark masses, one needs to choose operators \mathcal{O} and \mathcal{O}' , each of them creates a pair of a quark and an antiquark with flavours $i, j = 1 \dots N_f$ at the $x_0 = 0, T$ boundary,

$$\mathcal{O}^{ij}(\omega) = \frac{a^6}{L^3} \sum_{\mathbf{y}, \mathbf{z}} \bar{\zeta}_i(\mathbf{y}) \gamma_5 \omega(\mathbf{y} - \mathbf{z}) \zeta_j(\mathbf{z}), \quad (2.49)$$

$$(\mathcal{O}^{ij})'(\omega') = \frac{a^6}{L^3} \sum_{\mathbf{u}, \mathbf{v}} \bar{\zeta}'_j(\mathbf{u}) \gamma_5 \omega'(\mathbf{v} - \mathbf{u})^* \zeta'_i(\mathbf{v}). \quad (2.50)$$

The boundary fields are defined in eqs. (2.24), (2.25), and Euclidean γ -matrices are given in appendix A. The functions ω, ω' have to be smooth functions in space. Later in this work, they will be referred to as 'wave functions' and play a central role. The axial current and pseudoscalar density

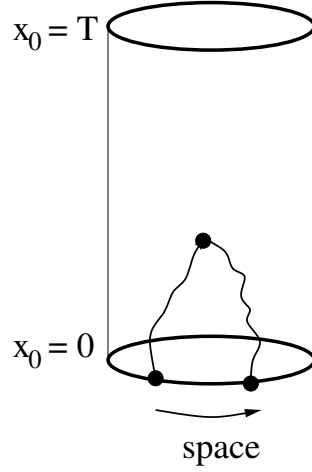


Figure 2.3: Visualisation of the correlators f_A and f_P , respectively. Currents A_0 or P are inserted in the interior.

are

$$A_\mu^{ij}(x) = \bar{\psi}_j(x) \gamma_\mu \gamma_5 \psi_i(x), \quad (2.51)$$

$$P^{ij}(x) = \bar{\psi}_j(x) \gamma_5 \psi_i(x). \quad (2.52)$$

Both are used to build up bare correlation functions. Then one has to renormalise both the currents and the operators.

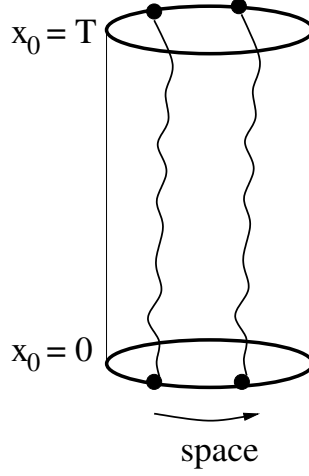
Bare correlation functions f_A, f_P and f_1 for finite quark masses can be defined as follows⁸,

$$f_A(x_0, \omega) = -\frac{a^3}{2} \sum_{\mathbf{x}} \langle A_0^{ij}(x) \mathcal{O}^{ij}(\omega) \rangle, \quad (2.53)$$

$$f_P(x_0, \omega) = -\frac{a^3}{2} \sum_{\mathbf{x}} \langle P^{ij}(x) \mathcal{O}^{ij}(\omega) \rangle. \quad (2.54)$$

Correlators f_A and f_P are depicted in figure 2.3. They are proportional to the transition probability amplitude that a quark-antiquark pair is created at the $x_0 = 0$ boundary, propagates to a point x in the interior of the box and is annihilated there.

⁸If expressions are explicitly written out, a trace over Dirac and SU(3) colour indices appears. But flavour indices are not summed over.

Figure 2.4: The boundary-boundary correlator f_1 .

In the context of $O(a)$ improvement [26], one needs to define an improved axial current $(A_I)_\mu$,

$$(A_I)_\mu^{ij}(x) = A_\mu^{ij}(x) + a c_A \cdot \frac{1}{2} (\partial_\mu^* + \partial_\mu) P^{ij}(x), \quad (2.55)$$

and correspondingly in the Schrödinger functional,

$$f_A^I(x_0, \omega) = f_A(x_0, \omega) + c_A \frac{1}{2} (f_P(x_0 + a, \omega) - f_P(x_0 - a, \omega)), \quad (2.56)$$

for $a < x_0 < T - a$. Values for c_A have been determined non-perturbatively in ref. [40]. The pseudoscalar density P does not need to be improved.

The boundary-boundary correlator f_1 for quark flavours i and j is shown in figure 2.4,

$$f_1(\omega, \omega') = -\frac{1}{2} \langle (\mathcal{O}^{ij})'(\omega') \mathcal{O}^{ij}(\omega) \rangle. \quad (2.57)$$

It is proportional to the transition amplitude that a pair consisting of a quark and an antiquark is created at the bottom $x_0 = 0$, propagates to the top $x_0 = T$ where it is annihilated. Since the propagation is between the two boundaries, f_1 may depend on two functions ω and ω' . An $O(a)$ improvement term is not necessary.

2.4 Spectral Representations of Correlation Functions

2.4.1 The QCD Transfer Matrix Formalism in the Schrödinger Functional

The transfer matrix is an important tool in solid state physics and field theory. Its knowledge for the studied model would allow to extract valuable information about the energy spectrum [36].

In this section, the Euclidean transfer matrix is introduced and related to correlation functions that can be computed non-perturbatively. They in turn allow to gain some knowledge about the spectrum of the transfer matrix.

The notation is taken from [43]. Lüscher showed in [44] how to construct a

- self-adjoint and bounded
- gauge-invariant
- strictly positive (i.e. all its eigenvalues are larger than zero)

transfer matrix \mathbb{T} for Wilson fermions.⁹ For the $O(a)$ clover improved case, however, one has to argue with universality in the continuum limit.

It is suitable to work in the Heisenberg picture¹⁰ of quantum mechanics,

$$\mathbb{T} = \exp(-a\mathbb{H}), \quad (2.58)$$

for the QCD Hamiltonian \mathbb{H} on the lattice with unknown energy spectrum $E_n^{(q)}$. Here $n \geq 0$ is the energy level of states with quantum numbers $(q) = (J, P, C, \dots)$. The action of the transfer matrix on a state $|E_n^{(q)}\rangle$ is

$$\mathbb{T}|E_n^{(q)}\rangle = \exp(-E_n^{(q)}a)|E_n^{(q)}\rangle. \quad (2.59)$$

States are normalised to one,

$$\langle E_n^{(q)} | E_{n'}^{(q')} \rangle = \delta_{n,n'} \delta_{q,q'}, \quad (2.60)$$

⁹One should not take these properties for granted. For example, RG improved actions do usually not fulfil positivity.

¹⁰As a short reminder: in the Heisenberg picture, operators are functions of time, and states are time-independent.

where $\delta_{,,}$ is the Kronecker symbol. Since only differences of energies are observable, one may define quantities with the vacuum energy subtracted,

$$\tilde{E}_n^{(q)} = E_n^{(q)} - E_0^{(0)}. \quad (2.61)$$

For convenience, the vacuum energy is from now on set to zero,

$$E_0^{(0)} = 0. \quad (2.62)$$

In the present case, homogeneous boundary conditions are imposed. The spatial components of the gauge potentials are set to zero

$$C_k = 0 = C'_k, \quad k = 1, 2, 3 \quad (2.63)$$

at the boundaries. That defines states $|i_0\rangle$ at $x_0 = 0$ and $\langle f_0|$ at the $x_0 = T$ hyperplane, and $|f_0\rangle = |i_0\rangle$ carries the quantum numbers of the vacuum.

Also the fermion fields are taken to vanish. The application of $\widehat{\mathcal{O}}^{ij}$, eq. (2.49), on $|i_0\rangle$ creates a pseudoscalar meson state,

$$|i_M(\omega)\rangle = \widehat{\mathcal{O}}^{ij}(\omega)|i_0\rangle, \quad (2.64)$$

at $x_0 = 0$. Correspondingly, $(\widehat{\mathcal{O}}^{ij})'$ creates a pseudoscalar meson at $x_0 = T$, and $|f_M(\omega)\rangle = |i_M(\omega)\rangle$ applies.

Schrödinger functional states are usually *no* eigenstates of \mathbb{T} . Rather, they are a mixture of all states that have the same set of quantum numbers q ,

$$\begin{aligned} |i_0\rangle &= c_0|E_0^{(0)}\rangle + c_1|E_1^{(0)}\rangle + \dots \\ |i_M(\omega)\rangle &= \widehat{\mathcal{O}}^{ij}(\omega)|i_0\rangle = d_0(\omega)|E_0^{(\text{PS})}\rangle + d_1(\omega)|E_1^{(\text{PS})}\rangle + \dots \end{aligned} \quad (2.65)$$

Analogous expressions hold for states at $x_0 = T$. Quantum numbers of the vacuum are labelled by '0', those for pseudoscalar mesons by 'PS'. The amplitudes $c_n, d_n(\omega)$ are overlap coefficients¹¹ of the n th energy eigenstate of \mathbb{T} with the SF boundary states at $x_0 = 0, T$, respectively,

$$c_n = \langle E_n^{(0)} | i_0 \rangle, \quad d_n(\omega) = \langle E_n^{(\text{PS})} | i_M(\omega) \rangle. \quad (2.66)$$

As discussed in the introduction of the Schrödinger functional, the partition function \mathcal{Z} can be written as a power of \mathbb{T} ,

$$\mathcal{Z} = \langle i_0 | \mathbb{T}^{T/a} | i_0 \rangle, \quad (2.67)$$

¹¹In this work, they are real and positive.

with \mathbb{P} projecting onto the gauge-invariant sector.

For correlation functions one obtains

$$f_X(x_0, \omega) = \frac{1}{\mathcal{Z}} \cdot \frac{L^3}{2} \langle i_0 | e^{-(T-x_0)\mathbb{H}} \mathbb{P} \mathbb{X} e^{-x_0\mathbb{H}} \mathbb{P} | i_M(\omega) \rangle, \quad (2.68)$$

$$a \leq x_0 \leq T - a,$$

$$f_1(\omega, \omega) = \frac{1}{\mathcal{Z}} \cdot \frac{1}{2} \langle i_M(\omega) | \mathbb{T}^{T/a} \mathbb{P} | i_M(\omega) \rangle, \quad (2.69)$$

with $f_X = f_A, f_P$ and the operator $\mathbb{X} = A_0, P$ in the Heisenberg picture. For simplicity, one has used translational invariance of the spatial sites, where $V_3 = (L/a)^3$ is the corresponding volume.

2.4.2 Spectral Decomposition of Correlators

The expansion of the partition function, eq. (2.67), is

$$\begin{aligned} \mathcal{Z}(T) &= \sum_q \sum_{m=0}^{\infty} \langle i_0 | E_m^{(q)} \rangle \langle E_m^{(q)} | \exp(-E_m^{(q)} T) | i_0 \rangle \\ &= \sum_q \sum_{m=0}^{\infty} \delta_{q,0} c_m^2 \exp(-E_m^{(0)} T), \quad c_m = \langle E_m^{(0)} | i_0 \rangle \\ &= c_0^2 \exp(-E_0^{(0)} T) \left(1 + \sum_{m=1}^{\infty} \frac{c_m^2}{c_0^2} \exp(-\tilde{E}_m^{(0)} T) \right) \\ &= c_0^2 \mathcal{Z}'(T). \end{aligned}$$

To get the result, a complete set of eigenstates

$$\mathbf{1} = \sum_q \sum_{m=0}^{\infty} |E_m^{(q)} \rangle \langle E_m^{(q)}| \quad (2.70)$$

has been inserted into eq. (2.67) and expanded in energy states, $|E_m^{(0)}\rangle$, with vacuum quantum numbers. The vacuum-to-SF boundary state overlap coefficients c_m are independent of the functions ω, ω' .¹² After factorising out the overlap with the vacuum, the remainder $\mathcal{Z}'(T)$ accounts for all contributions from vacuum excitations.

The behaviour of \mathcal{Z} for large time extents, such as $O(2 \text{ fm})$, is dominated by the vacuum ground state and its lowest excitation – the 0^{++} –glueball.¹³

¹²This is obvious, since the dependence on ω, ω' would be due to the application of meson operators $\widehat{\mathcal{O}^{ij}}$ and $(\widehat{\mathcal{O}^{ij}})'$.

¹³Glueballs have not been experimentally detected so far. Their nature originates in non-perturbative dynamics of gluons [45].

Since it is quite heavy, about 1.6 GeV in physical units [46], one expects negligible contributions for moderate time extents of the lattice.

With the notation taken from [43], the spectral representation of the correlator f_A is derived,

$$f_A(x_0, \omega) = \frac{L^3}{2} \cdot \frac{\sum_{n=0, g=0} \exp(-(T-x_0)E_n^{(0)}) \exp(-x_0 E_g^{(\text{PS})}) c_n d_g(\omega) \langle E_n^{(0)} | A_0 | E_g^{(\text{PS})} \rangle}{\sum_{m=0} c_m^2 \exp(-E_m^{(0)} T)}, \quad (2.71)$$

$$c_m = \langle E_m^{(0)} | i_0 \rangle, \quad d_g(\omega) = \langle E_g^{(\text{PS})} | i_M(\omega) \rangle.$$

Again, complete sets of eigenstates of the transfer matrix were inserted.

A qualitative discussion of the correlator follows for large time extents of order $O(2\text{ fm})$.

- Among the lowest state in the vacuum and the pseudoscalar channel, there are sizeable contributions from excited pseudoscalar meson states for small time separations $x_0 \ll T/2$. But because of their relatively large mass, they decay fast.
- In the limit $x_0 \gg T/2$ one expects contributions from vacuum excitations to be large because $T - x_0$ in the exponential gets small.
- For the intermediate region, $x_0 \approx T/2$, the leading behaviour is governed by the lightest pseudoscalar meson state, $n = 0$. Small contributions may come from the first excited meson state (its gap to the ground state is denoted by Δ) and from the glueball (with mass m_G),

$$f_A(x_0, \omega) = \frac{L^3}{2} \cdot \underbrace{\langle E_0^{(0)} | A_0 | E_0^{(\text{PS})} \rangle}_{\propto F_{\text{PS}}} \cdot \rho(\omega) \cdot \exp(-\tilde{E}_0^{(\text{PS})} x_0). \quad (2.72)$$

$$\left(1 - \frac{c_1^2}{c_0^2} \exp(-m_G T) + \eta_A^{\text{PS}}(\omega) \exp(-\Delta x_0) + \eta_A^0 \exp(-m_G(T - x_0)) + \dots \right).$$

The matrix element in front is proportional to the bare decay constant F_{PS} ,

$$\langle E_0^{(0)} | A_0 | E_0^{(\text{PS})} \rangle = F_{\text{PS}} m_{\text{PS}} \cdot \sqrt{\frac{1}{2m_{\text{PS}} L^3}}. \quad (2.73)$$

The last factor takes account of the conventional normalisation of one-particle states. In this convention, the experimental value of the pion

decay constant is 132 MeV. The overlaps of the boundary states with the corresponding ground states, here denoted by $\rho(\omega)$, appear in f_A . The amplitudes $\eta_A^{(\cdot)}$ are ratios of decay constants of different channels,

$$\rho(\omega) = \frac{c_0 d_0(\omega)}{c_0^2}, \quad (2.74)$$

$$\eta_A^{\text{PS}}(\omega) = \frac{d_1(\omega)}{d_0(\omega)} \frac{\langle E_0^{(0)} | A_0 | E_1^{(\text{PS})} \rangle}{\langle E_0^{(0)} | A_0 | E_0^{(\text{PS})} \rangle}, \quad \eta_A^0 = \frac{c_1}{c_0} \frac{\langle E_1^{(0)} | A_0 | E_0^{(\text{PS})} \rangle}{\langle E_0^{(0)} | A_0 | E_0^{(\text{PS})} \rangle}.$$

One should keep in mind that f_A has two contributions of vacuum excitations: both in the numerator and in the denominator. The spectral representation of $f_P(x_0, \omega)$ is not given here, but it may be derived analogously.

The boundary-boundary correlator, eq. (2.69), is

$$f_1(\omega, \omega') = \frac{1}{2} \frac{\sum_{g=0} d_g(\omega') d_g(\omega) \exp(-E_g^{(\text{PS})} T)}{\sum_{m=0} c_m^2 \exp(-E_m^{(0)} T)}, \quad (2.75)$$

and it becomes for large time extents,

$$f_1(\omega, \omega') = \frac{1}{2} \rho(\omega) \rho(\omega') \cdot \exp(-\tilde{E}_0^{(\text{PS})} T) \cdot \left(1 + \frac{d_1(\omega') d_1(\omega)}{d_0(\omega') d_0(\omega)} \exp(-\Delta T) - \frac{c_1^2}{c_0^2} \exp(-m_G T) + \dots \right). \quad (2.76)$$

This correlation function decays exponentially in T with the lowest pseudo-scalar mode. Corrections come from higher excitations, but are exponentially damped for large enough times. Again, one should keep in mind that there are glueball corrections from the denominator (partition function).

Because of universality in the continuum limit, one does not need to distinguish the spectral decomposition of correlators for Wilson fermions with or without $O(a)$ improvement. Though numbers may change, the formulae are the same.

2.5 Pseudoscalar Masses and Decay Constants

2.5.1 The Pseudoscalar Mass m_{PS} of the Ground State

The local (effective) mass from the axial current is usually taken to extract the meson ground state energy.¹⁴ Starting from the definition in the continuum,

$$m_{\text{eff}}(x_0) = -d \ln f_A(x_0, \omega) / dx_0, \quad (2.77)$$

one may discretise the derivative in x_0 up to $O(a^2)$ effects,

$$m_{\text{eff}}(x_0, \omega) a = \frac{1}{2} \ln \frac{f_A(x_0 - a, \omega)}{f_A(x_0 + a, \omega)}. \quad (2.78)$$

Obviously, partition functions and renormalisation factors of the boundary fields from individual correlators f_A drop out.

If one considers physical time extents of order $O(2 \text{ fm})$ and $x_0 \approx T/2$, one can assume to be in a region where the meson ground state dominates and excited state contributions are small. If so, eq. (2.72) may be applied. Then leading contributions are

$$m_{\text{eff}}(x_0, \omega) a = a \tilde{E}_0^{(\text{PS})} + \eta_A^{\text{PS}}(\omega) \sinh(a\Delta) \exp(-x_0\Delta) - \eta_A^0 \sinh(am_G) \exp(-m_G(T - x_0)) + \dots \quad (2.79)$$

Instead of using the axial current, the mass may also be defined by means of the pseudoscalar density f_P . Both versions of effective masses have to coincide within error bars in the plateau region.

Another way to extract the mass from correlators is

$$m_{\text{eff}}(T', T, \omega) a = \ln \left[\left(\frac{f_1(T', \omega, \omega)}{f_1(T, \omega, \omega)} \right)^{a/(T-T')} \right]. \quad (2.80)$$

For large time separations T, T' and $T - T'$ one expects a leading contribution from the meson ground state,

$$m_{\text{eff}}(T', T, \omega) a = a \tilde{E}_0^{(\text{PS})} + \frac{a}{T-T'} \left(\frac{d_1^2(\omega)}{d_0^2(\omega)} \exp(-\Delta T') \left(1 - e^{-\Delta(T-T')} \right) - \frac{c_1^2}{c_0^2} \exp(-m_G T') \left(1 - e^{-m_G(T-T')} \right) + \dots \right), \quad (2.81)$$

¹⁴In this work, all fermion fields have $\mathbf{p} = \mathbf{0}$. Then $m_{\text{PS}} \equiv \tilde{E}_0^{(\text{PS})}$ is the mass of the lowest pseudoscalar state, and similarly $m_{\text{PS}}^* \equiv \tilde{E}_1^{(\text{PS})}$ for its first excitation.

shown with its leading corrections in both the pseudoscalar and vacuum channel. But here, in contrast to the definition of $m_{\text{eff}}a$ involving f_A or f_P , glueball corrections from the partition functions are present.

If corrections from excited states are small, the latter definition gives a value for the pseudoscalar mass that is consistent with the two other versions.

2.5.2 The Pseudoscalar Decay Constant F_{PS} of the Ground State

Some ways to extract the pseudoscalar decay constant are described.

First, one defines the bare decay constant by means of lattice correlation functions, and then one renormalises the quantity. Given a bare pseudoscalar decay constant F_{PS} , eq. (2.73), one obtains the renormalised one, $(F_{\text{PS}})_{\text{R}}$, through

$$(F_{\text{PS}})_{\text{R}} = Z_A (1 + b_A a m_q) F_{\text{PS}}. \quad (2.82)$$

Because chiral symmetry is not preserved on the lattice, $Z_A \neq 1$ applies. It has been computed non-perturbatively in [47]. In contrast to the massless case, a fully $\mathcal{O}(a)$ improved axial current for massive quarks needs an additional improvement term with coefficient b_A . It is only known perturbatively to one-loop order so far [48]. The symbol m_q shall denote the subtracted quark mass which is further discussed in section 2.6.

The following dimensionless quantity is often used to extract the pseudoscalar decay constant,

$$X(x_0, T, \omega) = \frac{f_A(x_0, T, \omega)}{\sqrt{f_1(T, \omega, \omega)}}, \quad (2.83)$$

which decays exponentially with the mass of the meson ground state for large times. The factor $\sqrt{f_1}$ cancels the renormalisation factor of the boundary quark fields that also appears in f_A . Provided that the time extent is sufficiently large, the spectral representation of X around $x_0 \approx T/2$ is well described by

$$X(x_0, T, \omega) = \frac{1}{2} \sqrt{V_3} F_{\text{PS}} a \sqrt{\tilde{E}_0^{(\text{PS})}} a \exp(-(x_0 - T/2) \tilde{E}_0^{(\text{PS})}) (1 + R). \quad (2.84)$$

The factor appearing in front of the exponential term is proportional to the matrix element¹⁵ in eq. (2.73). The bare pseudoscalar decay constant $F_{\text{PS}}a$ may be determined through

$$F_{\text{eff}}a = \frac{2}{\sqrt{V_3} \tilde{E}_0^{(\text{PS})}a} X|_{x_0=T/2} \approx F_{\text{PS}}a, \quad (2.85)$$

provided that the pseudoscalar mass is known and contributions from excited states are small. Corrections, R , come from excitations in both the mesonic and the vacuum channel. The leading terms for large time extents and $x_0 \approx T/2$ are given here,

$$R = \eta_A^{\text{PS}}(\omega) \exp(-x_0\Delta) - \frac{d_1^2(\omega)}{2d_0^2(\omega)} \exp(-\Delta T) - \frac{c_1^2}{2c_0^2} \exp(-m_G T) + \eta_A^0 \exp(-m_G(T - x_0)) + \dots \quad (2.86)$$

Due to mesonic corrections in f_1 and contributions of vacuum excitations in the partition function, the curve of the effective decay constant is shifted independently of x_0 . The leading term of that shift is

$$\text{shift} = -\frac{d_1^2(\omega)}{2d_0^2(\omega)} \exp(-\Delta T) - \frac{c_1^2}{2c_0^2} \exp(-m_G T) + \dots \quad (2.87)$$

The other terms in eq. (2.87) depend on x_0 and may distort the curve but cannot shift it. A few comments are in order:

- As in the case of effective masses, excited mesons contribute for small times x_0 , vacuum excitations for $T - x_0$ small.
- Eq. (2.87) says that the leading contribution from excited mesons shifts $F_{\text{PS}}a$ downwards, that one from the glueball as well.

As an alternative definition, one could generalise eq. (2.83) using a distinct (usually smaller) time extent T' in f_1 ,¹⁶

$$\begin{aligned} X(x_0, T', T, \omega) &= \frac{f_A(x_0, T, \omega)}{\sqrt{f_1(T', \omega, \omega)}} \\ &= \frac{1}{2} \sqrt{V_3} \cdot F_{\text{PS}}a \sqrt{\tilde{E}_0^{(\text{PS})}a} \exp(-(x_0 - T'/2)\tilde{E}_0^{(\text{PS})}) \cdot (1 + R), \end{aligned} \quad (2.88)$$

¹⁵The definition in the static-light channel differs slightly. The chapter on B-physics will give more details.

¹⁶This case is considered because for large time extents, the signal-to-noise ratio decreases rapidly in the static approximation. So this formula gives an option to extract the decay constant there.

The leading corrections from excited states to the asymptotics, $T \rightarrow \infty$, are

$$R = \eta_A^{\text{PS}}(\omega) \exp(-x_0 \Delta) - \frac{d_1^2(\omega)}{2d_0^2(\omega)} \exp(-\Delta T') + \quad (2.89)$$

$$\frac{c_1^2}{c_0^2} \exp(-m_G T') \left(\frac{1}{2} - e^{-m_G(T-T')} \right) + \eta_A^0 \exp(-m_G(T-x_0)) + \dots$$

Contributions in the pseudoscalar sector decrease X . In the vacuum channel, however, this does not need to be the case. They could even cancel or change the sign depending on the size of the argument in the exponential.

Still another example, how to obtain the pseudoscalar decay constant is

$$aF_{\text{eff}}(x_0, T', T, \omega) = \frac{2}{\sqrt{V_3}} \frac{f_A(x_0, T, \omega)}{\sqrt{f_1(T', \omega, \omega)}} \exp(m_{\text{eff}} \cdot (x_0 - T'/2)) / \sqrt{m_{\text{eff}} a}, \quad (2.90)$$

with m_{eff} as defined in eq. (2.78). This is the version that is used in this work. For small corrections to the asymptotics one expects a plateau level at aF_{PS} . The expected approach to the plateau region is

$$aF_{\text{eff}} = aF_{\text{PS}} \cdot \left(1 - \frac{d_1^2(\omega)}{2d_0^2(\omega)} e^{-\Delta T'} + \frac{c_1^2}{c_0^2} e^{-m_G T'} \left(\frac{1}{2} - e^{-m_G(T-T')} \right) + \quad (2.91)$$

$$\left(\frac{x_0}{a} - \left[\frac{T'}{2a} + \frac{1}{2a\tilde{E}_0^{(\text{PS})}} - \frac{1}{\sinh(a\Delta)} \right] \right) \cdot \sinh(a\Delta) \eta_A^{\text{PS}}(\omega) e^{-x_0 \Delta} -$$

$$\left(\frac{x_0}{a} - \left[\frac{T'}{2a} + \frac{1}{2a\tilde{E}_0^{(\text{PS})}} + \frac{1}{\sinh(am_G)} \right] \right) \cdot \sinh(am_G) \eta_A^0 e^{-(T-x_0)m_G} + \dots \Bigg).$$

This version needs no prior knowledge of the pseudoscalar mass, and correlations between f_A 's for consecutive values of x_0 are fully taken into account. As in the previous definitions, there is a systematic shift, even of the plateau level, if contributions from excited states are not negligible.

2.6 The PCAC Relation on the Lattice

In the Schrödinger functional, it is suitable to define a renormalised quark mass by means of the PCAC relation. It says that the axial current, as defined in eq. (2.51), is partially conserved,

$$\partial_\mu A_\mu^{ij}(x) = (m_i + m_j) P^{ij}(x), \quad (2.92)$$

with the pseudoscalar density as defined in eq. (2.52) and bare quark masses $m_{i,j}$ for the flavour indices $i, j = 1 \dots N_f$. This equation is exact in the continuum. For finite lattice spacing a , however, it is valid up to corrections

with certain powers in the lattice spacing. This is because Wilson fermions explicitly break chiral symmetry. But chiral symmetry is restored when one approaches the continuum limit.

For the unimproved theory, the leading correction term is linear in a . The approach to the continuum can be accelerated by means of Symanzik's improvement programme. For the $O(a)$ improved theory [26], the leading lattice artefacts are quadratic¹⁷ in the lattice spacing a . The axial current needs an improvement term, eq. (2.55). The pseudoscalar density already converges with a rate proportional to a^2 . As a part of the research programme of the ALPHA collaboration, the improvement coefficient c_A has been determined non-perturbatively [40].

For Wilson fermions, masses are not protected through chiral symmetry. They are shifted because of an additive renormalisation. That means, even for massless quarks, there must be a bare mass. In other words, there is a critical line in the bare parameter space for which the renormalised quark mass vanishes,

$$m_0 = m_c(g_0) \quad \leftrightarrow \quad m_R = 0. \quad (2.93)$$

It is convenient to change to the subtracted quark mass $m_q = m_0 - m_c$. This quantity will be renormalised multiplicatively. Thus, the critical line is also described by the condition

$$m_q(g_0) = 0. \quad (2.94)$$

The renormalised versions of the axial current and pseudoscalar density

$$(A_R)_{\mu}^{ij} = Z_A \left(1 + \frac{1}{2} b_A a(m_q^i + m_q^j)\right) (A_I)_{\mu}^{ij}, \quad (2.95)$$

$$P_R^{ij} = Z_P \left(1 + \frac{1}{2} b_P a(m_q^i + m_q^j)\right) P^{ij} \quad (2.96)$$

define the renormalised quark mass through eq. (2.92).

For non-vanishing quark masses, one needs the coefficients b_A and b_P . Their difference has been computed non-perturbatively in [50], but they are only known to one-loop order of perturbation theory individually [48]. Because chiral Ward identities are only valid up to $O(a^2)$ lattice artefacts in the regularised theory, the factor Z_A gets a dependence on g_0 . But it does not depend on a renormalisation scale [47]. The renormalisation factor of the pseudoscalar density, Z_P , has not only a dependence on g_0 but also on the

¹⁷This is confirmed in scaling tests, for instance in [49].

scale. It can be used to compute running quark masses [51, 52]. The renormalised quark mass m_R may be defined by virtue of an operator identity,

$$\langle \frac{1}{2} (\partial_\mu + \partial_\mu^*) (A_R)_{\mu}^{ij}(x) \mathcal{O} \rangle = (m_R^i + m_R^j) \langle P_R^{ij}(x) \mathcal{O} \rangle + O(a^2), \quad (2.97)$$

for any operator \mathcal{O} apart from the location x .

Solved for the renormalised quark mass, eq. (2.97) reads¹⁸

$$m_R = \frac{Z_A}{Z_P} (1 + (b_A - b_P) am_q) m + O(a^2). \quad (2.98)$$

Translated in terms of correlation functions f_A and f_P , the bare PCAC mass m is given by

$$m(x_0, \omega) = \frac{\tilde{\partial}_0 f_A(x_0, \omega) + a c_A \partial_0^* \partial_0 f_P(x_0, \omega)}{2 f_P(x_0, \omega)} = r(x_0, \omega) + a c_A s(x_0, \omega) = \quad (2.99)$$

$$\frac{f_A(x_0+a, \omega) - f_A(x_0-a, \omega)}{4a f_P(x_0, \omega)} + c_A \frac{f_P(x_0+a, \omega) - 2f_P(x_0, \omega) + f_P(x_0-a, \omega)}{2a f_P(x_0, \omega)} + O(a^2).$$

There is more than one possibility to meet the condition of a vanishing quark mass, for instance one may choose $m|_{x_0=T/2} = 0$. Then one has to tune the bare parameters. such that eq. (2.93) holds there. On the lattice, this may be realised by

$$m = \begin{cases} m\left(\frac{T}{2a}, \omega\right) & \text{for } T/a \text{ even,} \\ \frac{1}{2} \left(m\left(\frac{T-a}{2a}, \omega\right) + m\left(\frac{T+a}{2a}, \omega\right) \right) & \text{for } T/a \text{ odd.} \end{cases} \quad (2.100)$$

In the general context one may introduce the hopping parameter κ as

$$\kappa = \frac{1}{2am_0 + 8r}, \quad 2am_q = \frac{1}{\kappa} - \frac{1}{\kappa_c}, \quad (2.101)$$

where κ_c describes the critical line, eq. (2.94). The hopping parameter κ usually serves as an input parameter for simulations.

¹⁸ Written down for two mass-degenerated quarks, as they are used in the light-light channel of this work.

Chapter 3

The b -quark on the Lattice

3.1 Introduction

The b -quark was the first discovered heavy quark of the predicted third family.¹ Heavy-light and heavy-heavy quarkonia may decay into many channels. Amongst purely hadronic channels, that are governed by QCD, there are also semi-leptonic decays, such as $B \rightarrow D^* l \bar{\nu}_l$, where quarks decay due to electroweak currents.²

The fact that there exist three families of fermions which are made up of fields with identical $SU(2)_L \otimes U(1)_Y$ transformation properties allows one to form invariant Yukawa couplings for arbitrary combinations of fields from the different families. This is flavour mixing in the charged current³ that is described by a unitary $SU(3)$ matrix, the Cabibbo-Kobayashi-Maskawa CKM matrix [54, 55],

$$d_{jL} \rightarrow \tilde{d}_{jL} = (U_{KM})_{jk} d_{kL}, \quad U_{KM} \in SU(3), \quad (3.1)$$

for the lower components of the left-handed doublets. One can show that the CKM matrix is determined by 4 (observable) parameters. Possible choices are 3 rotation angles and one phase or the approximate description by the Wolfenstein parametrisation [56]. Both versions contain a complex phase.

¹The existence of three quark families is due to lepton-quark duality in the electroweak sector. This cancels the chiral anomaly there, and this is essential for renormalisability of the Standard Model. A general introduction into the Standard Model is e. g. [53].

²This means, there is flavour number violation in charged weak interactions.

³The experimentally confirmed absence of flavour-changing neutral currents at tree-level is due to the GIM mechanism.

The latter may lead to complex effective couplings in the charge-changing currents and is therefore the cause of CP-violation. It is important to note that this may only occur for more than two families and non-degenerate quark masses. CP-violating effects have been observed in the kaon system [5, 6] and recently in the B-system [7, 8, 9].

To test if the Standard Model describes our world, a precise knowledge of independent CKM matrix elements and their ratios is, amongst other quantities, needed. Elements, such as $|V_{ud}|$ and $|V_{us}|$, are quite precisely known [57]. The Belle experiment at KEK [58] delivers still rough estimates for $|V_{ub}|$ and $|V_{cb}|$. The CP-violating phase depends very sensitively on a quantity $B_B f_B^2$ [59, 60, 61]. Therefore, the latter should be known precisely. Here, B_B is referred to as B -parameter and f_B is the decay constant of the B -meson. A good review for these issues is [62].

3.2 The Static Approximation

Heavy quark physics on the lattice is a great challenge for present computers, even quenched, because it requires a very fine discretisation of the lattice. This is because the masses of charm (c -), bottom (b -) and top (t -) quarks are above 1 GeV and therefore far heavier than the typical scale Λ_{QCD} of a few hundred MeV.⁴ Large masses $ma > 1$, as for heavy quarks for currently accessible lattice spacings $a \approx 0.05$ fm, result in large undesired discretisation errors. To treat the b -quark by means of relativistic lattice QCD reliably, one has to meet

$$m_b a \ll 1. \quad (3.2)$$

At the same time, to keep finite size effects due to pion propagation small,

$$m_\pi L \gg 1 \quad (3.3)$$

has to apply. Unfortunately, typical lattice sizes in nowadays quenched lattice QCD simulations are too small to meet both constraints.

But experimentally observable spectra of heavy-light and heavy-heavy bound states reveal that due to their large mass heavy quarks are non-relativistic

⁴The heaviest quark, the top, is not presently known to have bound states. It is too heavy to establish them and decays weakly. But those ones of the c - and b -quark may be investigated.

rather than relativistic particles. Therefore, using a non-relativistic treatment on the lattice should be a suitable choice from both the physical and numerical point of view.

In the Heavy Quark Effective Theory [63], one uses a Lagrangian that is expanded in inverse powers of the heavy quark mass,

$$\mathcal{L}^{\text{HQET}}(x) = \mathcal{L}_h^{\text{stat}}(x) + \frac{1}{m}\mathcal{L}_h^{(1)}(x) + \mathcal{O}(\frac{1}{m^2}), \quad (3.4)$$

where the Lagrangian $\mathcal{L}_h^{\text{stat}}$ of the static theory has mass dimension four and $\mathcal{L}_h^{(1)}$ is of mass dimension five etc. The Lagrangian of the static theory is

$$\mathcal{L}_h^{\text{stat}}(x) = \bar{\psi}_h(x)(D_0 + m + \delta m)\psi_h(x). \quad (3.5)$$

The mass term $m\bar{\psi}_h(x)\psi_h(x)$ is usually subtracted since it corresponds to a universal energy shift of all states that contain a heavy quark. Removing it makes explicit that the dynamics of heavy-light systems is independent of the scale m at lowest order of $1/m$. The symbol δm is a mass counter term. Composite fields of mass dimension higher than four are treated as perturbations to the static theory [64]. The perturbation in $\mathcal{O}(1/m)$ is

$$\mathcal{L}_h^{(1)}(x) = \bar{\psi}_h(x)(-\frac{1}{2}\vec{D}^2 - \vec{\sigma} \cdot \vec{B})\psi_h(x). \quad (3.6)$$

To compute expectation values, the fermionic action in the Boltzmannian is always the sum of the light and the static quark action. The remainder of the HQET action in the exponential, $S^{\text{stat}} - S^{\text{HQET}}$, has to be expanded to the given order $\mathcal{O}(1/m^n)$ of the action and appears as operator insertions into correlation functions. The reason to do so is that the static effective theory is renormalisable [65, 66, 67], as perturbative and non-perturbative tests support. And the continuum limit exists if the correlation function has been renormalised.

The natural starting point in this effective description of QCD is therefore the static case. It is a suitable tool to explore the heavy quark sector of QCD with a low numerical effort. It may serve as a guide for extrapolations of masses and decay constants from simulations with relativistic quarks, such as the charm [68], to the b .

In the limit $m \rightarrow \infty$, new symmetries appear [69, 70, 71]. Quarks become spatially static sources of colour charge with no spin and flavour.⁵

⁵On the lattice, the static propagator is just a product of links and therefore cheap to compute.

3.3 The Static b -quark in the Schrödinger Functional

This section complements chapter 2 in describing how the Eichten-Hill action for static quarks [63] is implemented in the Schrödinger functional. Correlation functions are defined from which physical observables, such as hadron masses and decay constants, may be extracted. The notation is taken from ref. [66].

3.3.1 The Action

As in the case of relativistic quarks, boundary fields ρ_h and $\bar{\rho}'_h$ are defined such that

$$\psi_h(x)|_{x_0=0} = \rho_h(\mathbf{x}), \quad \bar{\psi}_h(x)|_{x_0=T} = \bar{\rho}'_h(\mathbf{x}). \quad (3.7)$$

The projectors are not necessary because the theory is defined with two-component spinor fields only. The redundant two components are set to zero. For the same reason, $P_- \psi_h(x)$ will vanish. Since static quarks propagate only in time, spatial boundary conditions do not need to be discussed.

In the Schrödinger functional, the continuum static quark action is as for space-time without boundaries plus a boundary term [29],

$$S_h[A, \bar{\psi}_h, \psi_h] = \int dx_0 \int d^3\mathbf{x} \bar{\psi}_h(x) D_0 \psi_h(x) - \int d^3\mathbf{x} [\bar{\psi}_h(x) \psi_h(x)]_{x_0=T}. \quad (3.8)$$

Similarly to the relativistic case, the static quark field on the lattice is defined to be

$$\psi_h(x) = 0 \quad \text{if } x_0 < 0 \text{ or } x_0 \geq T, \quad (3.9)$$

such that the lattice counterpart of the continuum action, eq. (3.8), is

$$S_h[U, \bar{\psi}_h, \psi_h] = a^4 \sum_x \bar{\psi}_h(x) \nabla_0^* \psi_h(x). \quad (3.10)$$

The mass term in S_h , eq. (3.8), has been dropped in eq. (3.10) since it shifts all energies by a common value. The total action is

$$S[U, \bar{\psi}, \psi, \bar{\psi}_h, \psi_h] = S_G[U] + S_F[U, \bar{\psi}, \psi] + S_h[U, \bar{\psi}_h, \psi_h], \quad (3.11)$$

and the Schrödinger functional, eq. (2.36), now includes static quarks,

$$\mathcal{Z}[C', \bar{\rho}', \rho', \bar{\rho}_h, C, \bar{\rho}, \rho, \rho_h] = \int D[U] D[\psi] D[\bar{\psi}] D[\psi_h] D[\bar{\psi}_h] e^{-S[U, \bar{\psi}, \psi, \bar{\psi}_h, \psi_h]}. \quad (3.12)$$

The expectation value, eq. (2.23), of an operator \mathcal{O} is easily generalised. This operator may also contain static boundary fields,

$$\zeta'_h(\mathbf{x}) = \frac{\delta}{\delta \bar{\rho}'_h(\mathbf{x})}, \quad \bar{\zeta}_h(\mathbf{x}) = -\frac{\delta}{\delta \rho_h(\mathbf{x})}. \quad (3.13)$$

As for light quark boundary fields, static ones are explicitly set to zero after integration. The renormalisation of static quark boundary fields is multiplicative. This is analogous to the relativistic case.

The acceleration of the approach to the continuum limit by means of Symanzik's improvement programme to order a has been investigated in [66]. It turns out that the static quark action, eq. (3.10), is already $\mathcal{O}(a)$ improved. Operators, however, usually need improvement.

3.3.2 Correlation Functions

The static-light axial current is defined as

$$A_0^{j\text{stat}}(x) = \bar{\psi}_j(x) \gamma_0 \gamma_5 \psi_h(x), \quad j = 1 \dots N_f. \quad (3.14)$$

This quantity may be used to extract energies and decay constants. From now on, the flavour index j of the light quark will be considered irrelevant in the designation of A_0^{stat} and is therefore omitted.

The current needs $\mathcal{O}(a)$ improvement,

$$\delta A_0^{\text{stat}} = \bar{\psi}_j(x) \gamma_k \gamma_5 \frac{1}{2} (\bar{\nabla}_k + \bar{\nabla}_k^*) \psi_h(x), \quad j = 1 \dots N_f, \quad (3.15)$$

where the expression is summed over the spatial index $k = 1, 2, 3$. Thus, the $\mathcal{O}(a)$ improved static axial current is given by

$$(A_1^{\text{stat}})_0(x) = A_0^{\text{stat}}(x) + a c_A^{\text{stat}} \delta A_0^{\text{stat}}(x). \quad (3.16)$$

The improvement coefficient c_A^{stat} is only known in perturbation theory up to one-loop order [72, 66]. Unlike in the relativistic case, there is no symmetry that allows one to compute c_A^{stat} non-perturbatively.

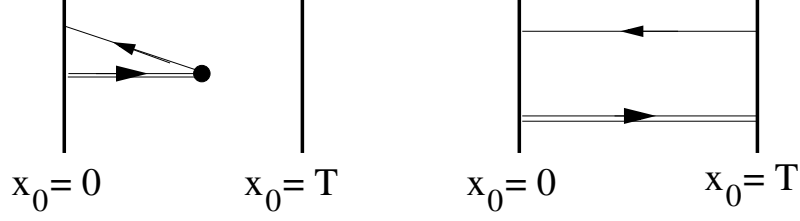


Figure 3.1: Visualisation of the correlators f_A^{stat} (left) and f_1^{stat} (right). The static quark is drawn with a double line. The current A_0^{stat} is inserted in the interior of the left figure.

Correlation functions, such as f_A^{stat} and f_1^{stat} , are built up with the boundary operators, eqs. (2.49) and (2.50), where the light flavour i is replaced by the static quark h ,

$$\mathcal{O}(\omega) = \frac{a^6}{L^3} \sum_{\mathbf{y}, \mathbf{z}} \bar{\zeta}_h(\mathbf{y}) \gamma_5 \omega(\mathbf{y} - \mathbf{z}) \zeta_j(\mathbf{z}), \quad (3.17)$$

$$\mathcal{O}'(\omega') = \frac{a^6}{L^3} \sum_{\mathbf{u}, \mathbf{v}} \bar{\zeta}'_j(\mathbf{u}) \gamma_5 \omega'(\mathbf{v} - \mathbf{u})^* \zeta'_h(\mathbf{v}), \quad (3.18)$$

$$f_A^{\text{stat}}(x_0, \omega) = -\frac{a^3}{2} \sum_{\mathbf{x}} \langle A_0^{\text{stat}}(x) \mathcal{O}(\omega) \rangle, \quad (3.19)$$

$$\delta f_A^{\text{stat}}(x_0, \omega) = -\frac{a^3}{2} \sum_{\mathbf{x}} \langle \delta A_0^{\text{stat}}(x) \mathcal{O}(\omega) \rangle. \quad (3.20)$$

The static quark can only propagate forward in time. The correlators are depicted in figure 3.1. The boundary-boundary correlator f_1^{stat} is given by

$$f_1^{\text{stat}}(\omega, \omega') = -\frac{1}{2} \langle \mathcal{O}'(\omega') \mathcal{O}(\omega) \rangle. \quad (3.21)$$

Their spectral representations, eqs. (2.71) and (2.75), are derived straightforwardly.

3.3.3 The Static Decay Constant

The renormalisation group invariant matrix element Φ_{RGI} of the axial current between the vacuum and the heavy-light pseudoscalar is defined by

$$\Phi_{\text{RGI}} = Z_{\text{RGI}} \langle E_0^{(0)} | A_0^{\text{stat}} | E_0^{(\text{PS})} \rangle, \quad (3.22)$$

with some renormalisation factor Z_{RGI} . The latter is proportional to the scale- and regularisation-dependent renormalisation factor $Z_{\text{A}}^{\text{stat}}(g_0, \mu = 1/L)$,

$$Z_{\text{RGI}}(g_0) = \frac{\Phi_{\text{RGI}}}{\Phi(\mu)} \Big|_{\mu=(1.436 r_0)^{-1}} \times Z_{\text{A}}^{\text{stat}}(g_0, L/a) \Big|_{L=1.436 r_0}. \quad (3.23)$$

For the Eichten-Hill action, it has been computed non-perturbatively [73, 67]. And the regularisation-independent part is

$$\Phi(\mu)/\Phi_{\text{RGI}} = 1.088(10) \quad \text{at} \quad \mu = (1.436 r_0)^{-1}, \quad (3.24)$$

with an error of 0.9% that has to be added in quadrature after the continuum extrapolation.

The RGI matrix element and the decay constant may be related through [67]

$$F_{\text{PS}} \sqrt{m_{\text{PS}}} = C_{\text{PS}}(M_{\text{b}}/\Lambda_{\overline{\text{MS}}}) \Phi_{\text{RGI}}, \quad (3.25)$$

up to leading corrections in $\mathcal{O}(1/m_{\text{PS}})$. The value of the mass-dependent function $C_{\text{PS}}(M_{\text{b}}/\Lambda_{\overline{\text{MS}}}) = 1.22(3)$ is known from perturbation theory. Its argument is the ratio of the RGI mass of the b -quark and the Lambda-parameter in the $\overline{\text{MS}}$ -scheme. If the experimental value for the spin-averaged B-meson mass, $m_B = m_{B_s} = 5.4 \text{ GeV}$, is used as input and Φ_{RGI} known from lattice calculations, eq. (3.25) may be solved for the decay constant F_{PS} . The matrix element Φ_{RGI} can be extracted from an x_0 -independent range, the plateau level, for a suitable combination of correlation functions,

$$\Phi_{\text{RGI}}(x_0) = -Z_{\text{RGI}} (1 + b_{\text{A}}^{\text{stat}} a m_{\text{q}}) \frac{2}{\sqrt{V_3}} \frac{f_{\text{A}}^{\text{stat}}(x_0, T, \omega)}{\sqrt{f_1^{\text{stat}}(T', \omega, \omega)}} e^{E_{\text{eff}}(x_0 - T'/2)}. \quad (3.26)$$

The effective energy is defined as in eq. (2.78), but with f_{A} replaced by $f_{\text{A}}^{\text{stat}}$. The coefficient $b_{\text{A}}^{\text{stat}}$ is required to improve the decay constant to order a for a massive light quark. Its tree-level value is $b_{\text{A}}^{\text{stat}} = 1/2$.

Some further comments are in order:

- correlation functions usually depend on the divergent mass counter term, but the dependence is known explicitly. For the decay constant, eq. (3.26), and energy differences (mass splittings) no knowledge of the counter term is needed.
- to extrapolate effective energies to the continuum, one needs to subtract the mass counter term. Unfortunately, there are only perturbative estimates [74], and there is no symmetry that allows a non-perturbative determination of the mass counter term. But there is a proposal to circumvent the problem [75, 76].
- following Eichten [77] it was noted in [74], that the signal in correlation functions decreases exponentially with Euclidean time separation x_0 . Using conventional methods, it is very difficult to obtain the decay constant with a satisfying statistical precision. Wave functions, also called 'smearing', may provide a way out [78, 79, 80, 81, 82].

Chapter 4

Wave Functions

4.1 Motivation

As eq. (2.65) indicates, Schrödinger functional boundary states are a superposition of eigenstates of the transfer matrix \mathbb{T} with the same set of quantum numbers q . They contribute to correlation functions, such as f_A , f_P and f_1 , eqs. (2.71) and (2.75), which are used to extract hadron masses and decay constants for a given state. Regarding the ground state, that is usually the state of interest, a safe extraction can only be obtained if contributions from excited states are negligible. To ensure that, one has several options:

- choose the time extent of the box sufficiently large, $T \gg 1$ fm,
- accelerate the approach to ground state dominance.

From the theoretical point of view, item number one is quite obvious but practically not always feasible. This is due to limited computational resources. In addition, especially in the static approximation, the signal-to-noise ratio is known to be rapidly decreasing with increasing Euclidean times x_0 [74]. Therefore, in this work, option two is investigated. In practice, one chooses an arbitrary operator $\widehat{\mathcal{O}}^{ij}(\omega)$ with the correct set of quantum numbers q . The overlap with the particular state of interest may be varied through the function ω . This 'wave function', that appears in eq. (2.49), depends on the relative displacement \mathbf{r} of the boundary quark fields.

A good meson interpolating operator $\widehat{\mathcal{O}}^{(n)}$ for the state n has a large overlap with the n th energy eigenstate of \mathbb{T} . Since it is not a priori known, one may choose a set of operators with different wave functions ω_i , $i = 1 \dots N_\omega$, and try

to approximate the improved interpolating field $\widehat{\mathcal{O}}^{(n)}$ by a linear combination of $\widehat{\mathcal{O}}(\omega_i)$ with unknown weight factors $\alpha_i^{(n)}$,

$$\widehat{\mathcal{O}}^{(n)} \approx \widehat{\mathcal{O}}(\omega_{\text{opt}}^{(n)}), \quad \omega_{\text{opt}}^{(n)}(\mathbf{r}) = \sum_{i=1}^g \alpha_i^{(n)} \omega_i(\mathbf{r}), \quad g \leq N_\omega. \quad (4.1)$$

Eq. (4.1) defines $\omega_{\text{opt}}^{(n)}$. A technique to find the coefficients $\alpha_i^{(n)}$ is based on the variational principle.

4.2 The Variational Principle

It is typically applied to the static potential [83], the extraction of glueball masses [84], the computation of phase shifts in elastic $\pi - \pi$ -scattering [85] or in heavy quark physics in the static approximation [78].

The variational principle will be introduced following [86, 87, 88] but with an emphasis on hadron physics. The notation of section 2.4.1 is used. Concerning the Schrödinger functional, some points need a separate discussion.

The General Case

It is a well-known fact from elementary quantum mechanics that the variational principle may serve as a suitable tool to estimate the ground state and its energy. It is based on an extremal principle. One chooses some set of meson operators $\widehat{\mathcal{O}}(\omega_i)$, that create 'trial states' with quantum numbers of pseudoscalar mesons from the vacuum state $|0\rangle$, and varies within them such that the energy expectation $\langle \mathbb{H} \rangle$ gets minimal,

$$\delta \left\{ \frac{\langle \text{i}_M(\omega) | \mathbb{H} | \text{i}_M(\omega) \rangle}{\langle \text{i}_M(\omega) | \text{i}_M(\omega) \rangle} \right\} = 0. \quad (4.2)$$

On the lattice, however, the transfer matrix $\mathbb{T} = \exp(-a\mathbb{H})$ is considered. Therefore, eq. (4.2) changes to

$$\delta \left\{ \frac{\langle \text{i}_M(\omega) | \mathbb{T} | \text{i}_M(\omega) \rangle}{\langle \text{i}_M(\omega) | \text{i}_M(\omega) \rangle} \right\} = 0, \quad (4.3)$$

and the expectation value of the transfer matrix needs to be maximised. For a positive and bounded operator \mathbb{T} , eq. (4.3) gives an upper bound on the true ground state value

$$\langle \mathbb{T} \rangle \leq \exp(-a\tilde{E}_0^{(\text{PS})}). \quad (4.4)$$

Equality holds if the state $|\mathbf{i}_M(\omega)\rangle$ is the true ground state $|E_0^{(\text{PS})}\rangle$. For any power $p \geq 0$ one obtains $\langle \mathbb{T}^{p/a} \rangle \leq \exp(-p\tilde{E}_0^{(\text{PS})})$. In particular, for $p = T - T'$ and a basis transformation $|\mathbf{i}_M(\omega)\rangle = \mathbb{T}^{T'/(2a)}|\psi\rangle$, eq. (4.3) changes to

$$\delta \langle \mathbb{T}^{p/a} \rangle = 0 = \delta \left\{ \frac{\langle \psi | \mathbb{T}^{T/a} | \psi \rangle}{\langle \psi | \mathbb{T}^{T'/a} | \psi \rangle} \right\}, \quad (4.5)$$

that has to be maximised. As introduced in section 2.4.1, correlation functions with time separation T may be expressed by means of the transfer matrix,

$$C_{ij}(T) = \langle 0 | \hat{\mathcal{O}}^\dagger(\omega_j) \mathbb{T}^{T/a} \hat{\mathcal{O}}(\omega_i) | 0 \rangle, \quad (4.6)$$

for $i, j = 1 \dots N_\omega$. Under the model assumption that the N_ω lowest eigenstates of \mathbb{T} with non-degenerate energies contribute for large time extents, the spectral representation of $C(T)$ is approximated by

$$C_{ij}(T) = \sum_{n=0}^{N_\omega-1} e^{-\tilde{E}_n^{(\text{PS})}T} \psi_i^{(n)} \psi_j^{*(n)}, \quad (4.7)$$

where the unknown overlap of the operator $\hat{\mathcal{O}}(\omega_i)$ with state n is denoted by

$$\psi_i^{(n)} = \langle 0 | \hat{\mathcal{O}}^\dagger(\omega_i) | E_n^{(\text{PS})} \rangle = d_n(\omega_i).$$

It is suitable to introduce a set of vectors $v^{(m)}$ dual to the $\psi^{(n)}$,

$$\langle v^{(m)}, \psi^{(n)} \rangle = \delta_{mn}.$$

Demonstrating for the ground state, the application of $v^{(0)}$ to $C(T)$ and $C(T')$ from the left and right yields the variational principle, eq. (4.5),

$$\frac{\langle v^{(0)}, C(T) v^{(0)} \rangle}{\langle v^{(0)}, C(T') v^{(0)} \rangle} = e^{-\tilde{E}_0^{(\text{PS})}(T-T')}, \quad (4.8)$$

if the model assumption is fulfilled. In general, state vectors and energies may be extracted by means of the *generalised eigenvalue problem* (GEVP),

$$\sum_j C_{ij}(T) v_j^{(n)}(T, T') = \lambda_n(T, T') \cdot \sum_j C_{ij}(T') v_j^{(n)}(T, T'), \quad T > T'. \quad (4.9)$$

Effective generalised eigenvalues are denoted by $\lambda_n(T, T')$, and corresponding generalised eigenvectors are the $v^{(n)}(T, T')$. They are the weight factors $v^{(n)} = (\alpha_1^{(n)}, \dots, \alpha_{N_\omega}^{(n)})$ to obtain an approximative interpolating operator for the n th energy state of the meson, eq. (4.1).

A few remarks are in order:

- The correlation matrices are symmetrised by hand in order to ensure that their eigenvalues are real. Negative eigenvalues or those close to zero with large statistical errors may be present due to limited statistical precision. They are the cause of numerical instabilities and should be discarded.
- A formulation of eq. (4.9) as an ordinary eigenvalue problem for a symmetric matrix $\hat{C}(T, T') = C^{-1/2}(T')C(T)C^{-1/2}(T')$ may be used to compute $\lambda_n(T, T')$ and orthonormal vectors $\hat{v}^{(n)}(T, T')$ that are related to the $v^{(n)}(T, T')$ through

$$\hat{v}_i^{(n)}(T, T') = \sum_j [C^{1/2}(T')]_{ij} v_j^{(n)}(T, T').$$

- Because the signal decreases exponentially with time separation, one usually inverts $C(T')$ for $T' < T$.
- Eq. (4.9) should be solved for several time extents. All other parameters have to be equal.
- Reference [85] proposes to extract the energy of state n by

$$m_{\text{eff}} a = \frac{a}{T-T'} \ln \left(\frac{\lambda_n(T, T'')}{\lambda_n(T', T'')} \right) = a \tilde{E}_n^{(\text{PS})} + \mathcal{O}(\exp(-T \Delta \tilde{E}_n^{(\text{PS})})), \quad (4.10)$$

for $T > T' > T''$ and T'' fixed such that $C(T'')$ has no noisy eigenvalues close to zero. The symbol

$$a \Delta \tilde{E}_n^{(\text{PS})} = \min_{n \neq m} |\tilde{E}_n^{(\text{PS})} a - \tilde{E}_m^{(\text{PS})} a|$$

is the distance of $a \tilde{E}_n^{(\text{PS})}$ to some other energy $a \tilde{E}_m^{(\text{PS})}$. The practicality in the Schrödinger functional is discussed in the chapter on data analysis.

The Variational Principle in the Schrödinger Functional

Some facts of the previous subsection need to be modified in the Schrödinger functional. For instance, the vacuum state $|0\rangle$ is replaced by the boundary state $|i_0\rangle$, eq. (2.65),

$$|0\rangle \rightarrow |i_0\rangle = c_0 |E_0^{(0)}\rangle + c_1 |E_1^{(0)}\rangle + \dots \quad (4.11)$$

In the Schrödinger functional, one simulates the correlation matrix

$$C_{ij}(T) = f_1(T, \omega_i, \omega_j) = \tilde{C}_{ij}(T) \mathcal{Z}^{-1}(T),$$

as given by eq. (2.75). Different time arguments refer to different statistically independent simulations of the correlation matrix. *All facts mentioned in the general case of the variational principle apply to $\tilde{C}(T)$ but not to the directly accessible quantity $C(T)$.* The latter involves an unknown scalar time-dependent function – the partition function $\mathcal{Z}(T)$. It modifies the generalised eigenvalues

$$\lambda(T, T') = \tilde{\lambda}(T, T') \cdot \frac{\mathcal{Z}(T')}{\mathcal{Z}(T)} > \tilde{\lambda}(T, T'), \quad (4.12)$$

with the consequence that the meson energies are *systematically shifted downwards* due to excited vacuum states. The eigenvectors, however, remain unchanged by this scalar factor.

4.3 The Variational Principle in Practice

A recipe to reliably solve the generalised eigenvalue problem, eq. (4.9), is proposed in [89] and well-described in [88]:

1. symmetrisation of the correlation matrices $C(T)$ and $C(T')$,
2. diagonalisation of $C(T')$,

$$C(T')b_i = \mu_i b_i, \quad \mu_0 \geq \dots \geq \mu_{N_\omega-1}, \quad (4.13)$$

and projection of the correlation matrices to the space of eigenvectors corresponding to the M highest eigenvalues¹,

$$C_{ij}^M(t) = \langle b_i, C(t)b_j \rangle, \quad i, j = 0 \dots M-1, \quad t = T', T. \quad (4.14)$$

Since correlators of the operator basis may not be statistically precise enough on the Monte-Carlo sample with finite statistics, small or even negative eigenvalues with large statistical errors may appear. They introduce undesired numerical instabilities. To avoid them, one has to choose the subspace of dimension $M \leq N_\omega$ appropriately.² The final

¹Eigenvalues that are close to zero, for instance within two standard deviations, as well as negative or complex ones have to be projected away.

²One should be aware that one therefore discards noisy linear combinations of operators rather than individual operators. That keeps physical information from all operators.

result should not depend on the choice of M . This has to be checked afterwards.

3. solving of the generalised eigenvalue problem, eq. (4.9), but with correlation matrices $C^M(T)$ and $C^M(T')$ in the truncated basis. This yields vectors $v^{(n)}(T, T')$ and eigenvalues $\lambda_n(T, T')$ for $n = 0 \dots M - 1$, $M \leq N_\omega$. For the extraction of glueball masses [88], the problem is reported to be still too sensitive to statistical fluctuations. There it is proposed to restrict the problem to a more stable subspace, $K \leq M$,

$$C_{ij}^K(t) = \langle v^{(i)}, C_{ij}^M(t) v^{(j)} \rangle, \quad i, j = 0 \dots K - 1, t = T', T. \quad (4.15)$$

4. fit of all correlation matrices $C_{ij}^K(t)$ according to the expected functional behaviour. This yields the energies $a\tilde{E}_m^{(\text{PS})}$ and the overlap amplitudes $\psi_i^{(m)}$ for the 'optimal operator' with eigenstate $|E_m^{(\text{PS})}\rangle$.

Apart from the last step, this proposal has been implemented in this work. A direct comparison of effective masses, eq. (4.10), is not reliable because the factor $\mathcal{Z}^{-1}(T)$ in eq. (2.75) changes the effective eigenvalues, eq. (4.12), from which the masses are extracted. So it is difficult to justify which pair of $(T'/a, T/a)$ values delivers weights $v^{(n)}$ to obtain a satisfying suppression of contributions from $m \neq n$ energy eigenstates.

One way to assess the quality of $v^{(n)} = (\alpha_1^{(n)}, \dots, \alpha_{N_\omega}^{(n)})$ consists in applying eq. (4.1) to build up $\omega_{\text{opt}}^{(n)}$ and the computation of the effective pseudoscalar mass $m_{\text{eff}}(x_0, \omega_{\text{opt}}^{(n)})a$ for correlators f_A, f_P and the effective pseudoscalar decay constant $aF_{\text{eff}}(x_0, \omega_{\text{opt}}^{(n)})$. An early and long plateau region in x_0 for all quantities is desirable.³

The variational principle should be applied for each β -value since the components of the solution vectors may have relevant intrinsic $O(a)$ -effects.

4.4 The Program Implementation

This chapter deals with technical details of the simulations. The implementation of correlation functions f_A, f_1 etc. in terms of quark two-point functions is described. Compared to the standard ALPHA case with no wave function,

³The check with several observables avoids the case that cancellations among excited state contributions show up.

the 'naive' implementation with smeared quark sources at the boundaries is shown to increase the numerical effort considerably. But there are possibilities to reduce the effort.

4.4.1 General Remarks

Numerical simulations in the quenched approximation have been carried out on the APEmille parallel computer; very early stages of this work on its predecessor APE-100. Random number generation is described in [90].

Hybrid Overrelaxation (HOR) is used for updating. It is a local algorithm and numerically inexpensive. It consists of some n_{OR} overrelaxation steps followed by heatbath updates. The overrelaxation update [91] is known to effectively decorrelate successive configurations but is not ergodic. For that reason, ergodic heatbath steps [92] are necessary. In practice, one heatbath step follows n_{OR} overrelaxation updates, where the number of the latter should be chosen such that autocorrelations will be small.

Fermionic correlators may be expressed by quark two-point functions as derived in section B.4. To obtain the propagator, the Dirac equation has to be solved, section B.1. This is done by the BiCGstab solver with SSOR preconditioning [93, 94].

The action is always $O(a)$ improved. Non-perturbatively obtained values for improvement coefficients are used where possible.

Existing code with a non-trivial hydrogen-like wave function in the static case was the basis. This version has first been extended to several wave functions and partially optimised for the APEmille.⁴ After that, smearing of light quark boundary fields has been implemented.

4.4.2 Propagators and Correlation Functions

This section will give explicit expressions for correlation functions in terms of quark propagators. To keep this section concise, the derivation of the quark propagator, its properties and the form of f_A as well as f_1 in terms of quark two-point functions may be found in appendix B. Important results of the latter are given here where appropriate.

⁴Apart from more memory and computational power, this machine provides far more registers and nice features such as complex conjugation during loading data.

Eqs. (2.53) and (2.57) for f_A and f_1 may be expressed in terms of quark propagators that are defined in eqs. (B.22) and (B.27),

$$f_A(x_0, \omega) = -\frac{a^9}{2L^3} \sum_{\mathbf{x}, \mathbf{y}, \mathbf{z}} \langle \text{Tr}' (S^j(x, \mathbf{z})^\dagger \gamma_0 S^i(x, \mathbf{y}) \omega(\mathbf{y} - \mathbf{z})) \rangle_G, \quad (4.16)$$

$$f_1(\omega, \omega') = \frac{a^{12}}{2L^6} \sum_{\mathbf{y}, \mathbf{z}, \mathbf{u}, \mathbf{v}} \langle \text{Tr}' (S_T^j(\mathbf{u}, \mathbf{z})^\dagger S_T^i(\mathbf{v}, \mathbf{y}) \omega(\mathbf{y} - \mathbf{z}) \omega'(\mathbf{v} - \mathbf{u})^*) \rangle_G. \quad (4.17)$$

The trace extends over Dirac and SU(3) colour but not over flavour indices i, j . The notation $\langle \dots \rangle_G$ means that only the gauge part of the action is used to compute the expectation value. One realises in the formulae above that quark propagators are needed from all points at the bottom to all points with $x_0 > 0$. In the case of a constant wave function, $\omega_{std} = 1$, one may significantly reduce the computational effort by a factor $V_3 = (L/a)^3$ because the summations over \mathbf{y} and \mathbf{z} may be performed independently,

$$f_A(x_0, \omega_{std}) \equiv f_A(x_0) = -\frac{1}{2V_3} \sum_{\mathbf{x}} \langle \text{Tr}' (\bar{S}^j(x)^\dagger \gamma_0 \bar{S}^i(x)) \rangle_G, \quad (4.18)$$

$$\bar{S}^i(x) = a^3 \sum_{\mathbf{y}} S^i(x, \mathbf{y}). \quad (4.19)$$

Thus, it remains to solve a single Dirac equation for each value of x , where the propagator $\bar{S}^i(x)$ is defined through

$$(D_I + m_0^i) \bar{S}^i(x) = a^{-1} \delta_{x_0, a} \tilde{c}_t U^\dagger(x - a\hat{0}, 0) P_+. \quad (4.20)$$

Thus, a constant wave function allows one to take advantage of translational invariance in the boundary quark fields.⁵ One expects a sizeable reduction of the statistical error of order $\sqrt{V_3}$ compared to an ordinary point-to-point quark propagator.

With similar arguments one may write f_1 as

$$f_1 = \frac{1}{2V_3^2} \langle \text{Tr}' ((\bar{S}_T^j)^\dagger \bar{S}_T^i) \rangle_G, \quad \bar{S}_T^i = a^3 \sum_{\mathbf{x}} \tilde{c}_t P_+ U^\dagger(x, 0) \bar{S}^i(x)|_{x_0=T-a}. \quad (4.21)$$

For a general wave function ω , however, eqs. (4.18) and (4.21) unfortunately do not apply. In order to avoid the computation of all point-to-point propagators, one may think of

⁵This is the usual program implementation in the ALPHA collaboration.

1. giving up one summation in eqs. (4.16) and (4.17),
2. introducing a stochastic estimator as demonstrated in [95].

Both proposals are briefly discussed here. Since point one may be regarded as a special case of the stochastic estimator, the latter is discussed first. The basic idea to sum independently in eqs. (4.16) and (4.17) is to introduce a stochastic estimator for the delta function,

$$a^{-3}\delta_{\mathbf{z},\mathbf{z}'} = \langle \sigma(\mathbf{z})\sigma(\mathbf{z}') \rangle_\sigma, \quad \sum_{\mathbf{z}'} \delta_{\mathbf{z},\mathbf{z}'} = 1, \quad (4.22)$$

with a scalar field σ . It may be taken as a random Ising field at inverse temperature $\hat{\beta} = 0$. As the Ising field and the gauge field are completely decoupled the averages may be performed trivially, for instance by picking one random Ising field per gauge field considered in the gauge field average. One obtains for the correlators,

$$\begin{aligned} f_A(x_0, \omega) &= -\frac{a^9}{2L^3} \sum_{\mathbf{x}, \mathbf{y}, \mathbf{z}, \mathbf{z}'} \langle \text{Tr}' (S^j(x, \mathbf{z}')^\dagger \delta_{\mathbf{z}, \mathbf{z}'} \gamma_0 S^i(x, \mathbf{y}) \omega(\mathbf{y} - \mathbf{z})) \rangle_G \\ &= -\frac{1}{2V_3} \sum_{\mathbf{x}} \langle \text{Tr}' \left(\left[a^3 \sum_{\mathbf{z}'} S^j(x, \mathbf{z}')^\dagger \sigma(\mathbf{z}') \right] \gamma_0 \left[a^6 \sum_{\mathbf{y}, \mathbf{z}} S^i(x, \mathbf{y}) \omega(\mathbf{y} - \mathbf{z}) \sigma(\mathbf{z}) \right] \right) \rangle_{G\sigma}. \end{aligned}$$

The sums over \mathbf{z}' and \mathbf{y} may be done independently. To keep notation short, it is suitable to introduce new symbols that are defined through

$$(D_I + m_0^i) S_\sigma^i(x) = a^{-1} \delta_{x_0, a} \tilde{c}_t U^\dagger(x - a\hat{0}, 0) P_+ \sigma(\mathbf{x}), \quad (4.23)$$

$$\begin{aligned} (D_I + m_0^i) S_{\omega, \sigma}^i(x) &= a^6 \sum_{\mathbf{y}, \mathbf{z}} (D_I + m_0^i) S^i(x, \mathbf{y}) \omega(\mathbf{y} - \mathbf{z}) \sigma(\mathbf{z}) \\ &= a^{-1} \delta_{x_0, a} \tilde{c}_t U^\dagger(x - a\hat{0}, 0) P_+ \cdot a^3 \sum_{\mathbf{z}} \omega(\mathbf{x} - \mathbf{z}) \sigma(\mathbf{z}). \end{aligned} \quad (4.24)$$

The final result for f_A is

$$f_A(x_0, \omega) = -\frac{1}{2V_3} \sum_{\mathbf{x}} \langle \text{Tr}' (S_\sigma^j(x)^\dagger \gamma_0 S_{\omega, \sigma}^i(x)) \rangle_{G\sigma}. \quad (4.25)$$

Thus, one needs to compute $N_\omega + 1$ propagators for a set of N_ω non-trivial wave functions. The term

$$a^3 \sum_{\mathbf{z}} \omega(\mathbf{x} - \mathbf{z}) \sigma(\mathbf{z}) \quad (4.26)$$

has a numerical effort proportional to $V_3^2 = (L/a)^6$ and needs to be determined after each update of the Ising field.

The summations for f_1 , eq. (4.17), may be separated similarly. A compact notation is obtained by the introduction of

$$S_{T,\sigma}^i(\mathbf{u}) = a^3 \sum_{\mathbf{z}'} S_T^i(\mathbf{u}, \mathbf{z}') \sigma(\mathbf{z}') = \tilde{c}_t P_+ U^\dagger(u, 0) S_\sigma^i(u)|_{u_0=T-a}, \quad (4.27)$$

$$S_{T,\omega,\sigma}^i(\mathbf{v}) = a^6 \sum_{\mathbf{y}, \mathbf{z}} S_T^i(\mathbf{v}, \mathbf{y}) \omega(\mathbf{y} - \mathbf{z}) \sigma(\mathbf{z}) = \tilde{c}_t P_+ U^\dagger(v, 0) S_{\omega,\sigma}^i(v)|_{v_0=T-a}. \quad (4.28)$$

Then f_1 may be written as

$$f_1(\omega, \omega') = \frac{1}{2V_3^2} \sum_{\mathbf{u}, \mathbf{v}} \langle \text{Tr}' (S_{T,\sigma}^j(\mathbf{u})^\dagger S_{T,\omega,\sigma}^i(\mathbf{v}) \omega'(\mathbf{v} - \mathbf{u})^*) \rangle_{G\sigma}. \quad (4.29)$$

The computation of f_1 amounts to $\propto V_3^2$ operations and is therefore numerically expensive.

Another way to reduce the computational effort of eqs. (4.16) and (4.17) is to give up one summation. This corresponds to the case $\sigma(\mathbf{x}) = \delta_{\mathbf{x}, \mathbf{0}}$ in the stochastic estimator. Here, the unsmeared propagator is always taken at the origin $\mathbf{z} = \mathbf{0}$ of the bottom of the Schrödinger functional. In this special case, the numerically expensive term in eq. (4.26) needs to be computed only once rather than after each update of the Ising spin field. This special case is therefore numerically less expensive than the general case. Some more comments are in order:

- the default implementation of many programs of the ALPHA collaboration uses an independent summation over boundary quark fields. This actually corresponds to using a constant wave function. Since other, rather non-trivial, wave functions are not implemented there, the case will be labelled by 'noWF'.
- in the static case one smears the static quark fields. This amounts to computing N_ω static quark propagators. For static-light correlation functions, it is necessary to solve the Dirac equation for a point source. The label is 'statWF'.
- In the relativistic case one needs to solve the Dirac equation N_ω times for the different wave functions and additionally for the point source, therefore $N_\omega + 1$ times in total. This case is labelled by 'relWF'.

Thus: the reduction of the number of propagators that are required to compute the correlators, eqs. (4.16) and (4.17), is expected to be at the cost of the statistical precision. Because of translational invariance, expectation values have to be the same. The issue of statistical precision will be discussed later in this chapter.

4.4.3 Details of used Wave Functions

So far, the wave functions have not been specified. Three types of them have been used in this work: a localised, a constant and exponential ones⁶,

$$\omega_\delta(\mathbf{r}) = \delta_{\mathbf{r},\mathbf{0}}, \quad (4.30)$$

$$\omega_{std}(\mathbf{r}) = 1, \quad (4.31)$$

$$\omega(\mathbf{r}) = \omega(r) = N^{-1} \cdot r^n \exp(-r/r_H), \quad (4.32)$$

given here for the infinite volume. The second one, eq. (4.31), is the 'standard' wave function. In the third case, there is a radial dependence, $r = |\mathbf{x} - \mathbf{y}|$, upon the boundary quark fields. Eq. (4.32) is motivated from the non-relativistic picture of heavy-light mesons that is similar to the hydrogen atom. Wave functions of that kind were studied in the static approximation very early, for instance in [78]. There, they had quite effective projection properties.

In the present work, they have been used in the static approximation and later also for light quarks. The parameter n is a non-negative integer value. The case $n = 0$ corresponds to purely exponential functions. The parameter r_H is the Bohr radius. As an example, the values $r_H/r_0 = \text{const}$, where $r_H/r_0 = 0.1863, 0.3726, 0.7457$, have been used in this work.

Hydrogen-like wave functions $\omega(r)$ are radially symmetric around $\mathbf{0}$. On a finite lattice, eq. (4.32) is modified to

$$\omega(\mathbf{x}) = N^{-1} \cdot \sum_{m \in \mathbb{Z}^3} e^{-|\mathbf{x} - m\mathbf{L}|/r_H} \cdot \left(\frac{|\mathbf{x} - m\mathbf{L}|}{r_0} \right)^n, \quad (4.33)$$

where \mathbf{x} runs over all lattice sites. The wave function gets L -periodic through the sum. The prefactor N ensures $\sum_{\mathbf{x}} \omega^2(\mathbf{x}) = 1$. The summation will be stopped in the program if the relative change in N is below a certain value, say 10^{-3} , between the current step and the previous one.

⁶The latter class will be referred to as hydrogen-like wave functions throughout this work.

4.4.4 Program Tests

The following numerical tests have been successfully done:

- for any wave function used, the stochastic estimator is expected to give the same averages within statistical errors as the case where one summation in the correlators is given up...✓
- for a constant wave function ω_{std} one expects 'noWF' and the stochastic estimator to give statistically compatible results...✓
- correlators for the point-like source ω_δ are to be obtained from a hydrogen-like wave function in the limit $r_H \rightarrow 0$ for each fixed lattice spacing...✓
- for large time extents, extracted masses and decay constants from a plateau in x_0 should be compatible for any used wave function...✓

4.4.5 Performance and Scaling

The implementation of several wave functions implies the computation of several quark propagators. Light quark propagators are numerically expensive. So the static case has first been studied because static propagators are just products of gauge fields and therefore numerically inexpensive. But regardless of the relativistic or static case, the computation of the correlation matrix will turn out to have a large numerical effort.

In this section, statistical precision and computational costs are compared to the standard case $\omega_{std} = 1$. Issues such as the quality of plateaux in the effective pseudoscalar mass and decay constant are discussed in the chapter on data analysis.

Comparison of Estimators

Both estimators of chapter 4.4.2 are now compared with respect to their statistical errors for the same number of measurements. Table 4.1 shows data of

$$f_A^{\text{stat}}(T/4), \quad f_A^{\text{stat}}(T/2), \quad f_1^{\text{stat}} \quad \text{and} \quad X^{\text{stat}}(T/2) = \frac{f_A^{\text{stat}}(T/2)}{\sqrt{f_1^{\text{stat}}}} \quad (4.34)$$

for some $(L/a)^3 \times T/a$ lattices at $\beta = 6.0$, $\kappa = 0.132$, $\theta = 0$, $\omega \propto \exp(-r/a)$ and $N_{\text{meas}} = 800$ measurements. $O(a)$ improvement has been employed.

lattice	estimator	$f_A^{\text{stat}}(T/4)$	$f_A^{\text{stat}}(T/2)$	f_1^{stat}	$X^{\text{stat}}(T/2)$
$6^3 \times 6$	stochastic	-0.980(9)	-0.1580(36)	0.285(12)	-0.2958(19)
	$\sigma(\mathbf{x}) = \delta_{\mathbf{x},\mathbf{0}}$	-0.986(1)	-0.1611(6)	0.297(3)	-0.2952(12)
$6^3 \times 12$	stochastic	-0.1553(9)	-0.0177(7)	0.0079(6)	-0.200(7)
	$\sigma(\mathbf{x}) = \delta_{\mathbf{x},\mathbf{0}}$	-0.1560(3)	-0.0184(3)	0.0089(4)	-0.195(4)
$12^3 \times 12$	stochastic	-0.1247(9)	-0.00942(17)	0.00254(15)	-0.187(4)
	$\sigma(\mathbf{x}) = \delta_{\mathbf{x},\mathbf{0}}$	-0.1245(3)	-0.00923(6)	0.00258(11)	-0.182(4)
$16^3 \times 16$	stochastic	-3.772(20)E-4	-1.345(15)E-5	4.6(7)E-9	-0.198(15)
	$\sigma(\mathbf{x}) = \delta_{\mathbf{x},\mathbf{0}}$	-3.769(14)E-4	-1.355(14)E-5	5.5(9)E-9	-0.182(15)
$16^3 \times 32$	stochastic	-1.352(19)E-5	-3.96(39)E-8	-3(6)E-12	?
	$\sigma(\mathbf{x}) = \delta_{\mathbf{x},\mathbf{0}}$	-1.325(13)E-5	-3.77(50)E-8	2.0(7)E-11	-8(2)E-3

Table 4.1: Comparison of the statistical errors for different estimators.

Obviously, data are statistically compatible. The estimator with one summation given up, $\sigma(\mathbf{x}) = \delta_{\mathbf{x},\mathbf{0}}$, shows smaller statistical errors in the correlators than the stochastic estimator, $\sigma(\mathbf{x}) = \text{random}$. This especially applies for small lattices, whereas statistical errors are about the same for large L/a , except for f_1^{stat} on the largest lattice. As already pointed out, the first mentioned case, $\sigma(\mathbf{x}) = \delta_{\mathbf{x},\mathbf{0}}$, is even numerically cheaper. For that reason, all following simulations in this work have used it.

An application of the stochastic estimator to light quarks has been investigated in [95]. It turns out, however, that the method is not as competitive as conventional techniques there. This is another argument to disregard the 'noisy' estimator, $\sigma(\mathbf{x}) = \text{random}$, in the present work.

Compared to the standard case $\omega_{\text{std}} = 1$, it still remains to investigate how large the increase in variance for $\sigma(\mathbf{x}) = \delta_{\mathbf{x},\mathbf{0}}$ is. Naively, one expects that the standard case has a smaller error of order $\sqrt{V_3}$. This could for instance be investigated by setting the wave function explicitly to one everywhere and using either translation invariance, case 'noWF', or not, case $\sigma(\mathbf{x}) = \delta_{\mathbf{x},\mathbf{0}}$. The central values are expected to be the same within statistical errors due to translational invariance. Table 4.2 shows results.

Thus, giving up translational invariance leads to an increase of the statistical error of usually less than a factor two. This is exciting. The same observation has been made in the relativistic case.

lattice	estimator	$f_A^{\text{stat}}(T/4)$	$f_A^{\text{stat}}(T/2)$	f_1^{stat}	$X^{\text{stat}}(T/2)$
$6^3 \times 6$	noWF	-2.201(3)	-0.932(4)	34.48(39)	-0.15876(55)
	$\sigma(\mathbf{x}) = \delta_{\mathbf{x},\mathbf{0}}$	-2.198(7)	-0.933(6)	34.59(43)	-0.15865(66)
$6^3 \times 12$	noWF	-0.887(4)	-0.1766(25)	1.130(46)	-0.1661(23)
	$\sigma(\mathbf{x}) = \delta_{\mathbf{x},\mathbf{0}}$	-0.887(6)	-0.1767(28)	1.113(53)	-0.1674(29)
$12^3 \times 12$	noWF	-0.939(2)	-0.1963(14)	5.88(17)	-0.0809(8)
	$\sigma(\mathbf{x}) = \delta_{\mathbf{x},\mathbf{0}}$	-0.943(5)	-0.1968(16)	6.10(20)	-0.0797(12)

Table 4.2: Comparison of the statistical error with/out translational invariance. The same set of parameters is used.

Scaling with L/a

The dependence of the numerical effort for the Dirac inversion and the correlation matrix on the number of lattice points is considered. In all cases, $(L/a)^4$ lattices are used at $\beta = 6.2$, $\theta = 0$ and $\kappa = 0.13490$. The latter is approximately the hopping parameter of the strange quark. All simulations have been carried out on an APEmille board.⁷ The labels 'relWF', 'statWF' and 'noWF' refer to different program versions and were introduced at the end of chapter 4.4.2.

Dirac Inversion:

Table 4.3 shows how much time is taken to build up a complete quark propagator for the specified geometry. The given times include the computation of the Sheikholeslami-Wohlert term, eq. (2.43). The total effort for the inversion scales with $(L/a)^n$, $4 < n < 5$.

⁷It has a topology of $2 \times 2 \times 2$ CPU nodes.

L/a	time [secs]
6	6
8	6
10	16
12	32
14	63
16	115

Table 4.3: Scaling of the time [secs] to solve the Dirac equation on a $(L/a)^4$ lattice on a board, quenched case.

L/a	relWF	statWF	noWF
6	2	1	1
8	4	2	1
10	11	3	1
12	27	7	1
14	63	15	1
16	135	32	1

Table 4.4: Total time in seconds to build up a 2×2 correlation matrix (as given in column 2 & 3) as a function of L/a on a board, quenched case.

The Correlation Matrix:

A large amount of execution time is taken for the computation of the correlation matrix $C(T)$. For $N_\omega = 2$, times are listed in column 2 and 3 of table 4.4. As expected the standard case, which is labelled by 'noWF', is the cheapest one. There, f_1 does not need to be convoluted with non-trivial wave functions and may be computed as a volume-independent product of two boundary-boundary propagators, eq. (4.21). In all other cases, a scaling with $A \cdot (L/a)^6$ is expected, eq. (4.29).⁸ From the numerical point of view, the coefficient A depends on the size of the structures that are convoluted. For static quarks, the propagator is an SU(3) matrix. For light quarks, however, it is a 4-spinor with an SU(3) matrix in each component. Therefore, the times should differ by a factor 4, at least for large values of L/a where terms in $O((L/a)^3)$ may be neglected. This scaling behaviour is confirmed.

Scaling with the Number of Wave Functions

is investigated on a 12^4 lattice for $\kappa = 0.13490$, $\theta = 0$ at $\beta = 6.2$ and a variable number of wave functions. The static case is listed twice. This is because in the optimised case, new features of the APEmille have been used. But the extensive usage of register variables limits to simulate 4 wave functions simultaneously. However, this is sufficient in most cases.

⁸This is because the boundary-to-boundary propagator depends on a spatial variable and has to be multiplied with a spatially dependent wave function.

Dirac Inversion:

In the static case, only one light quark propagator is needed. Thus only the relativistic case needs to be discussed here. To build up correlation functions, one has to compute $N_\omega + 1$ light quark propagators. Therefore, compared to the standard ALPHA case, smearing of light quarks will increase the numerical effort by a factor $N_\omega + 1$.

Computation of the Correlation Matrix:

Since f_1 is an $N_\omega \times N_\omega$ -matrix, one expects a scaling of the effort proportional to N_ω^2 . But the prefactor may differ in the cases considered. This can be seen in table 4.5. The additional optimisation in the static case amounts to about 15% gain in performance. Since the size of the propagator for light quarks is four times larger than the static one, execution times for the former are expected to be four times larger. This is indeed the case for $N_\omega > 1$, where N_ω -independent operations are almost negligible in expense.

N_ω	relWF	statWFopt	statWF
1	13	5	5
2	27	7	8
3	46	11	13
4	74	18	20
5	106	not avail.	29
6	147	not avail.	39

Table 4.5: Total time in seconds to build up the correlation matrix as a function of N_ω for $L/a = 12$ on a board.

4.4.6 A brief Remark on the Static Approximation

The choice whether the static propagator or the one of the light quark is smeared has a crucial influence on the statistical precision of correlators. This is illustrated here on a particular example. Figure 4.1 shows an effective energy plot for $f_A^{\text{stat}}(x_0, \omega)$ on a $24^3 \times 36$ lattice at $\beta = 6.2$, $\theta = 0$ and $\kappa = 0.13485$ for the estimator with $\sigma(\mathbf{x}) = \delta_{\mathbf{x}, \mathbf{0}}$. About 300 measurements have been taken. In both cases, the same hydrogen-like wave function $\omega(r) \propto r e^{-r/r_H}$, $r_H/a \approx 2.75$ has been used. The case where the light quark

is smeared and not the static one is the blue curve. Statistical errors are very large, even for small Euclidean times x_0 . This curve is expected to have the same average as the red one which uses a smeared static propagator and a local one for the light quark. This follows from translational invariance. Starting from eqs. (B.23) and (B.25) for the definitions of light quark and static quark propagators, one obtains for f_A^{stat} , eq. (4.25),

$$\begin{aligned}
f_A^{\text{stat}}(x_0, \omega) &= -\frac{1}{2V_3} \sum_{\mathbf{x}} \langle \text{Tr}' (S_\sigma^h(x)^\dagger \gamma_0 S_{\omega, \sigma}^i(x)) \rangle_{G\sigma} \\
&= -\frac{a^{12}}{2L^3} \sum_{\mathbf{x}} \langle \text{Tr}' \left(\left(\sum_{\mathbf{z}'} S^h(x, \mathbf{z}')^\dagger \sigma(\mathbf{z}') \right) \gamma_0 \sum_{\mathbf{y}, \mathbf{z}} S^i(x, \mathbf{y}) \omega(\mathbf{y} - \mathbf{z}) \sigma(\mathbf{z}) \right) \rangle_{G\sigma} \\
&= -\frac{a^9}{2L^3} \sum_{\mathbf{x}} \langle \text{Tr}' \left((W(x) P_+)^\dagger \sigma(\mathbf{x}) \gamma_0 \sum_{\mathbf{y}, \mathbf{z}} S^i(x, \mathbf{y}) \omega(\mathbf{y} - \mathbf{z}) \sigma(\mathbf{z}) \right) \rangle_{G\sigma} \\
&= -\frac{a^6}{2L^3} \sum_{\mathbf{x}} \langle \text{Tr}' \left((W(x) P_+)^\dagger \gamma_0 \sum_{\mathbf{y}} S^i(x, \mathbf{y}) \omega(\mathbf{y} - \mathbf{x}) \right) \rangle_G \\
&= -\frac{a^9}{2L^3} \sum_{\mathbf{x}, \mathbf{z}} \langle \text{Tr}' \left((W(x) P_+ \sum_{\mathbf{y}, \mathbf{z}'} \delta_{\mathbf{x}, \mathbf{z}'} \omega(\mathbf{y} - \mathbf{z}') \sigma(\mathbf{z}'))^\dagger \gamma_0 S^i(x, \mathbf{z}) \sigma(\mathbf{z}) \right) \rangle_{G\sigma} \\
&= -\frac{a^{12}}{2L^3} \sum_{\mathbf{x}} \langle \text{Tr}' \left(\left(\sum_{\mathbf{y}, \mathbf{z}'} S^h(x, \mathbf{z}') \omega(\mathbf{y} - \mathbf{z}') \sigma(\mathbf{z}') \right)^\dagger \gamma_0 \sum_{\mathbf{z}} S^i(x, \mathbf{z}) \sigma(\mathbf{z}) \right) \rangle_{G\sigma} \\
&= -\frac{1}{2V_3} \sum_{\mathbf{x}} \langle \text{Tr}' (S_{\omega, \sigma}^h(x)^\dagger \gamma_0 S_\sigma^i(x)) \rangle_{G\sigma}.
\end{aligned}$$

Therefore, both expectation values are the same. In contrast to the blue curve, the red one has much smaller statistical errors. For that reason, static-light correlators are from now on meant to consist of a smeared static quark propagator and a local propagator for the light quark.

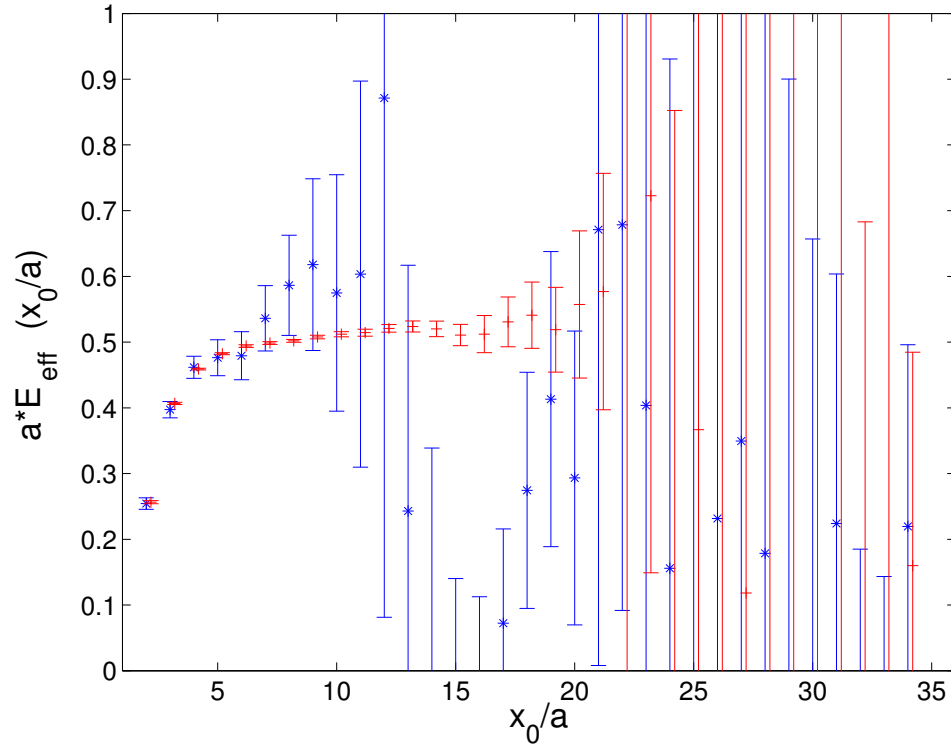


Figure 4.1: An effective energy plot from the static axial current on a $24^3 \times 36$ lattice at $\beta = 6.2$, $\theta = 0$ and $\kappa \approx \kappa_s$. Symbols are displaced horizontally for clarity. The static quark is either smeared (red plusses) or not (blue stars). Due to symmetry relations, the same average is expected. Obviously, this fact does not need to hold for statistical errors.

Chapter 5

Alternative Extraction Techniques

The variational principle, as introduced in the previous chapter, allows one to extract information about the ground state and low-lying excitations. But to obtain reliable information, it is essential to apply it to *several* pairs of time extents (T, T') , (T, T'') , (T', T'') etc., where all other parameters are kept fixed. It would be desirable to reduce the numerical effort. The alternative methods introduced here only need one lattice.¹ They allow to gain knowledge about the ground state and the lowest excitation in the pseudoscalar as well as vacuum channel.

5.1 Ground State Masses and Decay Constants

Effective masses or decay constants themselves may be used to obtain an early ground state dominance. For simplicity, the case with a pair of wave functions is considered. Generalisations using a larger operator basis may be done easily.

The spectral representation of correlators, as given in chapter 2.4.2, should be kept in mind. Masses and decay constants are defined through eqs. (2.78) and (2.90) with their spectral representations, eqs. (2.79) and (2.91), for

¹With a usually large time extent T of a few fermi.

large time extents. If one knew a ratio

$$R_{ij} = \frac{d_1(\omega_i)}{d_1(\omega_j)}, \quad i, j = \text{fix}, \quad (5.1)$$

for any two trial wave functions, one may find an optimal one for which the contribution from the first excited meson state vanishes,

$$\omega_{\text{opt}} = \omega_i - R_{ij}\omega_j. \quad (5.2)$$

The symbol R_{ij} is the weight factor between both trial wave functions ω_i and ω_j , eq. (4.1). Its determination is described here.

For two Euclidean times $x_0 = T_1$, $y_0 = T_2$, $x_0 \neq y_0$ in the range of $[T/4, T/2]$ and fixed wave function ω_i , the expression

$$\begin{aligned} \frac{m_{\text{eff}}(T_1, \omega_i)a}{m_{\text{eff}}(T_2, \omega_i)a} - 1 &= \frac{a\tilde{E}_0^{(\text{PS})} + \eta_A^{\text{PS}}(\omega_i) \sinh(a\Delta)e^{-T_1\Delta} + \dots}{a\tilde{E}_0^{(\text{PS})} + \eta_A^{\text{PS}}(\omega_i) \sinh(a\Delta)e^{-T_2\Delta} + \dots} - 1 \\ &= \eta_A^{\text{PS}}(\omega_i) \frac{\sinh(a\Delta)}{a\tilde{E}_0^{(\text{PS})}} (e^{-T_1\Delta} - e^{-T_2\Delta}) + \dots \end{aligned} \quad (5.3)$$

is computed.² Divided by the same expression but ω_i replaced by another wave function ω_j one obtains $k_{ij} = k(T_1, T_2, \omega_i, \omega_j)$,

$$k_{ij} = \frac{\frac{m_{\text{eff}}(T_1, \omega_i)a}{m_{\text{eff}}(T_2, \omega_i)a} - 1}{\frac{m_{\text{eff}}(T_1, \omega_j)a}{m_{\text{eff}}(T_2, \omega_j)a} - 1} = \frac{\eta_A^{\text{PS}}(\omega_i)}{\eta_A^{\text{PS}}(\omega_j)} + \dots = \frac{d_1(\omega_i)/d_0(\omega_i)}{d_1(\omega_j)/d_0(\omega_j)} + \dots, \quad (5.4)$$

where eq. (2.74) has been used. The quantity k_{ij} is a ratio of overlap coefficients. An estimate for k_{ij} may also be obtained by a combination of effective decay constants,

$$k_{ij} = \frac{\frac{F_{\text{eff}}(T_1, \omega_i)a}{F_{\text{eff}}(T_2, \omega_i)a} - 1}{\frac{F_{\text{eff}}(T_1, \omega_j)a}{F_{\text{eff}}(T_2, \omega_j)a} - 1} = \frac{\eta_A^{\text{PS}}(\omega_i)}{\eta_A^{\text{PS}}(\omega_j)} + \dots = \frac{d_1(\omega_i)/d_0(\omega_i)}{d_1(\omega_j)/d_0(\omega_j)} + \dots, \quad (5.5)$$

which is completely analogous to eq. (5.4). Provided that there is ground state dominance, one may extract

$$\frac{d_0(\omega_i)}{d_0(\omega_j)} \approx \frac{\sqrt{f_1(T, \omega_i, \omega_i)}}{\sqrt{f_1(T, \omega_j, \omega_j)}} \quad (5.6)$$

²One may also take the effective mass from f_P , and coefficients η_A change to η_P .

from f_1 , or alternatively from $f_X \in \{f_A^I, f_P\}$ correlation functions,

$$\frac{d_0(\omega_i)}{d_0(\omega_j)} \approx \frac{f_X(x_0^*, \omega_i)}{f_X(x_0^*, \omega_j)}, \quad x_0^* \approx T/2 \text{ and fixed.} \quad (5.7)$$

The weight factor R_{ij} is obtained by multiplying both expressions,

$$R_{ij} = k_{ij} \frac{d_0(\omega_i)}{d_0(\omega_j)} \approx \frac{d_1(\omega_i)}{d_1(\omega_j)}. \quad (5.8)$$

A few comments are in order:

- Even in the case of only one wave function, eq. (5.4) may be applied. A modified correlator $(f_A^I)'$ may be found such that no contributions from the first excited meson state appear. For that, one has to use two distinct definitions of the effective mass *instead* of two distinct wave functions. So m_{eff} defined through f_A^I and f_P could be used instead of $m_{\text{eff}}(\omega_i)$ and $m_{\text{eff}}(\omega_j)$ for the *same fixed* correlator. In this case, eq. (5.4) has to be changed as follows,

$$\begin{aligned} k_{ij} \rightarrow k_{f_A^I f_P} &= \left(\frac{m_{\text{eff}}(f_A^I, T_1)a}{m_{\text{eff}}(f_A^I, T_2)a} - 1 \right) / \left(\frac{m_{\text{eff}}(f_P, T_1)a}{m_{\text{eff}}(f_P, T_2)a} - 1 \right) \\ &= \eta_A^{\text{PS}} / \eta_P^{\text{PS}} + \dots \\ &= \frac{\langle E_0^{(0)} | A_0 | E_1^{(\text{PS})} \rangle}{\langle E_0^{(0)} | A_0 | E_0^{(\text{PS})} \rangle} / \frac{\langle E_0^{(0)} | P | E_1^{(\text{PS})} \rangle}{\langle E_0^{(0)} | P | E_0^{(\text{PS})} \rangle} + \dots \end{aligned} \quad (5.9)$$

To compensate the undesired factor $\langle E_0^{(0)} | P | E_0^{(\text{PS})} \rangle / \langle E_0^{(0)} | A_0 | E_0^{(\text{PS})} \rangle$, one has to replace eq. (5.6) by f_A^I / f_P in the region $x_0^* \approx T/2$. Then, the axial current correlator with an absent first excited meson contribution is

$$(f_A^I)'(x_0) = f_A^I(x_0) - R_{f_A^I f_P} f_P(x_0), \quad R_{f_A^I f_P} = \frac{\langle E_0^{(0)} | A_0 | E_1^{(\text{PS})} \rangle}{\langle E_0^{(0)} | P | E_1^{(\text{PS})} \rangle}. \quad (5.10)$$

Unlike in the case of different wave functions, the correlator f_1 cannot be improved in this sense. Therefore, only observables *without* f_1 may approach the ground state faster.

- The considerations of the previous point may be extended. The knowledge of matrix elements between the vacuum and the first excited pseudoscalar meson state is necessary. As an operator identity, the PCAC relation holds up to $O(a^2)$ lattice artefacts in the clover improved theory and gives for any wave function ω ,

$$\frac{\eta_A^{\text{PS}}(\omega)}{\eta_P^{\text{PS}}(\omega)} \approx \frac{m_{\text{PS}}}{m_{\text{PS}} + \Delta} \rightarrow R_{f_A^I f_P} = \frac{\langle E_0^{(\text{PS})} | A_0 | E_1^{(\text{PS})} \rangle}{\langle E_0^{(\text{PS})} | P | E_1^{(\text{PS})} \rangle} \approx \frac{m_{\text{PS}}}{m_{\text{PS}} + \Delta} \frac{\langle E_0^{(\text{PS})} | A_0 | E_0^{(\text{PS})} \rangle}{\langle E_0^{(\text{PS})} | P | E_0^{(\text{PS})} \rangle}. \quad (5.11)$$

- The numerical behaviour of the different formulations for R_{ij} requires investigation. Some of these aspects are considered in the chapter on data analysis.

5.2 The First Excited State

It is suitable to extend the notation for the effective mass,

$$am_{\text{eff}}(x_0, \omega_i, X) = \frac{1}{2} \ln \left(\frac{f_X(x_0 - a, \omega_i)}{f_X(x_0 + a, \omega_i)} \right), \quad (5.12)$$

with an explicit reference to correlators $f_X \in \{f_A^I, f_P\}$ and wave functions. The pseudoscalar gap may be extracted from a plateau of a local mass in x_0 , where the latter is defined similarly to eq. (2.78),

$$a\Delta_{\text{eff}} = \frac{1}{2} \ln \left[\frac{m_{\text{eff}}(x_0 - a, \omega_i, X)a - m_{\text{eff}}(x_0 - a, \omega_j, Y)a}{m_{\text{eff}}(x_0 + a, \omega_i, X)a - m_{\text{eff}}(x_0 + a, \omega_j, Y)a} \right]. \quad (5.13)$$

Written in terms of correlators one obtains

$$a\Delta_{\text{eff}} = \frac{1}{2} \ln \left[\frac{\ln \left(\frac{f_X(x_0 - 2a, \omega_i)}{f_Y(x_0 - 2a, \omega_j)} \right) - \ln \left(\frac{f_X(x_0, \omega_i)}{f_Y(x_0, \omega_j)} \right)}{\ln \left(\frac{f_X(x_0, \omega_i)}{f_Y(x_0, \omega_j)} \right) - \ln \left(\frac{f_X(x_0 + 2a, \omega_i)}{f_Y(x_0 + 2a, \omega_j)} \right)} \right]. \quad (5.14)$$

Leading corrections to ground state dominance are expected from the glueball with mass m_G and from the two lowest meson excitations above the ground state with gaps $\Delta < \Delta^*$ relative to m_{PS} . The expression

$$\begin{aligned} \ln \left(\frac{f_X(x_0, \omega_i)}{f_Y(x_0, \omega_j)} \right) &= \ln \left(\frac{d_0(\omega_i) \langle E_0^{(0)} | X | E_0^{(\text{PS})} \rangle}{d_0(\omega_j) \langle E_0^{(0)} | Y | E_0^{(\text{PS})} \rangle} \right) + \\ &\quad \ln \left(\frac{1 + \eta_X^{\text{PS}}(\omega_i) e^{-x_0 \Delta} + \eta_X^{*\text{PS}}(\omega_i) e^{-x_0 \Delta^*} + \eta_X^0 e^{-(T-x_0)m_G} + \dots}{1 + \eta_Y^{\text{PS}}(\omega_j) e^{-x_0 \Delta} + \eta_Y^{*\text{PS}}(\omega_j) e^{-x_0 \Delta^*} + \eta_Y^0 e^{-(T-x_0)m_G} + \dots} \right) \\ &= \ln \left(\frac{d_0(\omega_i) \langle E_0^{(0)} | X | E_0^{(\text{PS})} \rangle}{d_0(\omega_j) \langle E_0^{(0)} | Y | E_0^{(\text{PS})} \rangle} \right) + \\ &\quad \left(1 + \hat{\eta}^* e^{-x_0(\Delta^* - \Delta)} + \hat{\eta}^0 e^{-Tm_G} e^{x_0(m_G + \Delta)} + \dots \right) \hat{\eta} e^{-x_0 \Delta}, \\ \hat{\eta} &= [\eta_X^{\text{PS}}(\omega_i) - \eta_Y^{\text{PS}}(\omega_j)], \quad \hat{\eta}^* = \frac{[\eta_X^{*\text{PS}}(\omega_i) - \eta_Y^{*\text{PS}}(\omega_j)]}{[\eta_X^{\text{PS}}(\omega_i) - \eta_Y^{\text{PS}}(\omega_j)]}, \quad \hat{\eta}^0 = \frac{[\eta_X^0 - \eta_Y^0]}{[\eta_X^{\text{PS}}(\omega_i) - \eta_Y^{\text{PS}}(\omega_j)]} \end{aligned}$$

is likewise computed for the other time separations and inserted in eq. (5.14),

$$a\Delta_{\text{eff}} = a\Delta + A_{\Delta^*} \hat{\eta}^* e^{-x_0(\Delta^* - \Delta)} + A_0 \hat{\eta}^0 e^{-Tm_G} e^{x_0(m_G + \Delta)} + \dots, \quad (5.15)$$

with amplitudes

$$A_{\Delta^*} = \frac{\sinh(a\Delta^*)}{\sinh(a\Delta)} \sinh(a(\Delta^* - \Delta)),$$

$$A_0 = \frac{\sinh(am_G)}{\sinh(a\Delta)} \sinh(a(m_G + \Delta)).$$

The contribution of the meson ground state drops out. For $f_X = f_Y$, vacuum excitations are cancelled because $\eta_X^0 = \eta_Y^0$ implies $\hat{\eta}^0 = 0$ in eq. (5.15).

5.3 The Mass of the 0^{++} -Glueball

The method to determine the mass gap between the meson ground state and the first excited one for $x_0 < T/2$ may be applied in the region $x_0 > T/2$ to extract the lowest-lying glueball with mass m_G ,

$$am_{G,\text{eff}} = -\frac{1}{2} \ln \left[\frac{\left(\frac{f_X(x_0-2a, \omega_i)}{f_Y(x_0-2a, \omega_j)} \right) - \left(\frac{f_X(x_0, \omega_i)}{f_Y(x_0, \omega_j)} \right)}{\left(\frac{f_X(x_0, \omega_i)}{f_Y(x_0, \omega_j)} \right) - \left(\frac{f_X(x_0+2a, \omega_i)}{f_Y(x_0+2a, \omega_j)} \right)} \right], \quad (5.16)$$

where $X \neq Y$ is required since otherwise vacuum corrections will cancel each other out. The term f_X/f_Y may also be replaced by its logarithm. Contributions from excited mesons are expected to be negligible for $x_0 \geq T/2$ if T has been chosen sufficiently large. Furthermore, those from the 0^{++} -glueball and the state above (labelled by a star) have to be taken into account,

$$\frac{f_X(x_0, \omega_i)}{f_Y(x_0, \omega_j)} = \frac{d_0(\omega_i) \langle E_0^{(0)} | X | E_0^{(\text{PS})} \rangle}{d_0(\omega_j) \langle E_0^{(0)} | Y | E_0^{(\text{PS})} \rangle} \times \frac{1 + \eta_X^{\text{PS}}(\omega_i) e^{-x_0 \Delta} + \eta_X^0 e^{-(T-x_0)m_G} + \eta_X^{0*} e^{-(T-x_0)m_G^*} + \dots}{1 + \eta_Y^{\text{PS}}(\omega_j) e^{-x_0 \Delta} + \eta_Y^0 e^{-(T-x_0)m_G} + \eta_Y^{0*} e^{-(T-x_0)m_G^*} + \dots}.$$

The spectral representation of $m_{G,\text{eff}}$ for $a \ll T - x_0 \leq T/2$ is

$$am_{G,\text{eff}} = am_G + A_{\Delta} (\hat{\eta}^0)^{-1} e^{Tm_G} e^{-x_0(\Delta+m_G)} + A_{0^*} \hat{\eta}^{0*} e^{-(T-x_0)(m_G^*-m_G)} + \dots,$$

$$\hat{\eta}^0 = \frac{[\eta_X^0 - \eta_Y^0]}{[\eta_X^{\text{PS}}(\omega_i) - \eta_Y^{\text{PS}}(\omega_j)]}, \quad \hat{\eta}^{0*} = \frac{[\eta_X^{0*} - \eta_Y^{0*}]}{[\eta_X^0 - \eta_Y^0]},$$

with amplitudes

$$A_{\Delta} = \frac{\sinh(a\Delta)}{\sinh(am_G)} \sinh(a(\Delta + m_G)),$$

$$A_{0^*} = \frac{\sinh(am_G^*)}{\sinh(am_G)} \sinh(a(m_G^* - m_G)).$$

Chapter 6

Numerical Results

The techniques which were described in the preceding chapters are applied to the data and discussed with respect to their practicality. They are tools to extract the decay constant of the B_s meson in the static approximation. A continuum estimate for $r_0(E - \Gamma^{\text{stat}})$ is also provided. This quantity is used in the computation of the RGI-quark mass M_b , as proposed in refs. [75, 76]. Also the mass gap to the lowest radial excitation above the ground state is investigated.

For the light quarkonium system, the mass and decay constant of the ground state as well as the mass of the first excited state are discussed.

In section 6.7, the results are summarised and compared with those from other references.

All simulations have been carried out in the quenched approximation. Correlators have been $O(a)$ -improved where necessary. The spatial extent of the boxes is approximately $L = 1.5 \text{ fm}$, the time extent T ranges up to $3L/2$, as summarised in tables C.2 and C.3 in the appendix. Results are obtained with a basis of $N_\omega = 4$ hydrogen-like wave functions, table C.1. The dimensionless ratio r_H/r_0 is kept constant.

The mass of the light quark has usually been set the one of the strange quark. The way how to obtain corresponding hopping parameters κ is described in the next section.

6.1 The Choice of the light Quark Mass

The determination of the subtracted quark mass (or hopping parameter) for the strange quark can be done following refs. [51, 96]. The running of the quark mass is computed non-perturbatively in the first reference. In the $O(a)$ improved lattice theory, the relation between the renormalisation group invariant (RGI-) quark mass M and the bare current quark mass m , eq. (2.99), is

$$M = Z_M(g_0) m(g_0) + O(a^2). \quad (6.1)$$

The symbol Z_M relates both types of masses to each other. One may find Z_M in ref. [51], table 2, for the relevant range of β -values. An interpolation formula for the range $6.0 \leq \beta \leq 6.5$ is also provided,

$$Z_M(\beta = 6/g_0^2) = 1.752 + 0.321 (\beta - 6) - 0.220 (\beta - 6)^2. \quad (6.2)$$

This parametrisation yields Z_M with an accuracy of about 1.1%. However, this determination neglects an $O(a)$ contribution $\propto (b_A - b_P) am_q$ to Z_M . Since $b_A - b_P$ is small in the relevant range of β [50], one may neglect the term $(b_A - b_P) am_q$ for small quark masses. The next step is to use the result

$$r_0(M_s + \hat{M}) = 0.362(12), \quad M_s/\hat{M} = 24.4 \pm 1.5, \quad (6.3)$$

from ref. [96] and r_0/a from ref. [83] to solve for $m_s a$ in the range of β -values one is interested in. Here, M_s shall denote the RGI strange quark mass and \hat{M} is the averaged RGI mass of the u - and d -quark. The given ratio relies on chiral perturbation theory [97].

Finally, the desired hopping parameter κ_s may be obtained through a linear interpolation of bare current quark masses m in κ . For this work, those in table 1 of ref. [96] have been used.

6.2 The Variational Principle

This section discusses eigenvalues (masses) and -vectors (weights) that are obtained in realising the variational principle, eq. (4.3), by the generalised eigenvalue problem. For that, eq. (4.9) is solved for several time extents (T', T) while keeping the other parameters fixed.

6.2.1 The Relativistic Case

Effective Masses

Effective masses of the ground and first excited state are listed in tables C.4–C.6 for $\beta = 6.0$ and in C.10 for $\beta = 6.2$. They have been extracted in two different ways: (1) directly from the generalised eigenvalue problem, eq. (4.9), and (2) using the Lüscher-Wolff proposal as given by eq. (4.10). Formally, option (1) may be obtained from (2) by setting $T'' = \infty$. Results of the gap in the pseudoscalar channel may be found in the tables as well. For option (1) it may be defined through

$$a\Delta_{\text{eff}} = -\frac{a}{T-T'} \ln(\lambda_1(T, T')/\lambda_0(T, T')), \quad (6.4)$$

for option (2) as the difference of extracted LW-masses between the first excited and the ground state.

The Ground State Mass, $\beta = 6.0$

From the tables C.4–C.6 and figure 6.1 one can read off a complicated non-monotonic behaviour of the effective mass from f_1 in the Euclidean time extents of the Schrödinger functional. This is due to contributions of excited states in the meson *as well as* vacuum channel.

In figure 6.1, the effective mass is shown as a function of T . The separations $T - T' = 2a, 4a, 6a, 8a$ and $T'' = 3a, 6a, 8a, 10a$ are kept fixed. First, the case $T - T' = 2a$ is discussed. The typical situation is: (1) for small time extents, $T/a \sim 10$, the effective mass comes from below, increases, and (2) forms a more or less pronounced peak around $T/a = 15$, and (3) the approach to the asymptotic value $m_{\text{PS}}a \approx 0.340$ from above for large times T/a . (4) These effects are particularly pronounced for very small values of T''/a .

Point (1) can be understood by means of eqs. (2.75) and (2.82). Contributions from excited mesons in the numerator of f_1 and those with vacuum quantum numbers in f_1 's denominator have opposite sign to leading order in T' . For small Euclidean times, vacuum excitations push the effective ground state mass down. And because of their large mass they are strongly suppressed as T' increases. Points (2) and (4) indicate that at $T \approx 1.5 \text{ fm}$ excited mesons still give sizeable corrections to the asymptotics. The height of the peak decreases for increasing values of T'' . Statement (3) reflects what one naively expects from the variational principle: approaching of the true ground state mass from above. Qualitatively, the statements (1) to (4) also

hold for $T - T' = 4a$, etc. But even for small values of T'' , the peaks get less pronounced. The reason is that the factor $1/(T - T')$ in eq. (2.82) also suppresses excited state contributions.

Summary:

The extraction of the pseudoscalar ground state mass by means of the variational principle with f_1 -correlation matrices is possible. A safe extraction requires $T' \geq 18a$, $T - T' \gg a$ (in practice $4a$ or more). The subspace dimension M , eq. (4.14), is two for $T/a \leq 20$, and one otherwise. Extracted masses are stable under changing $M = 2 \dots 4$ for $T/a \leq 20$ and for all M otherwise.

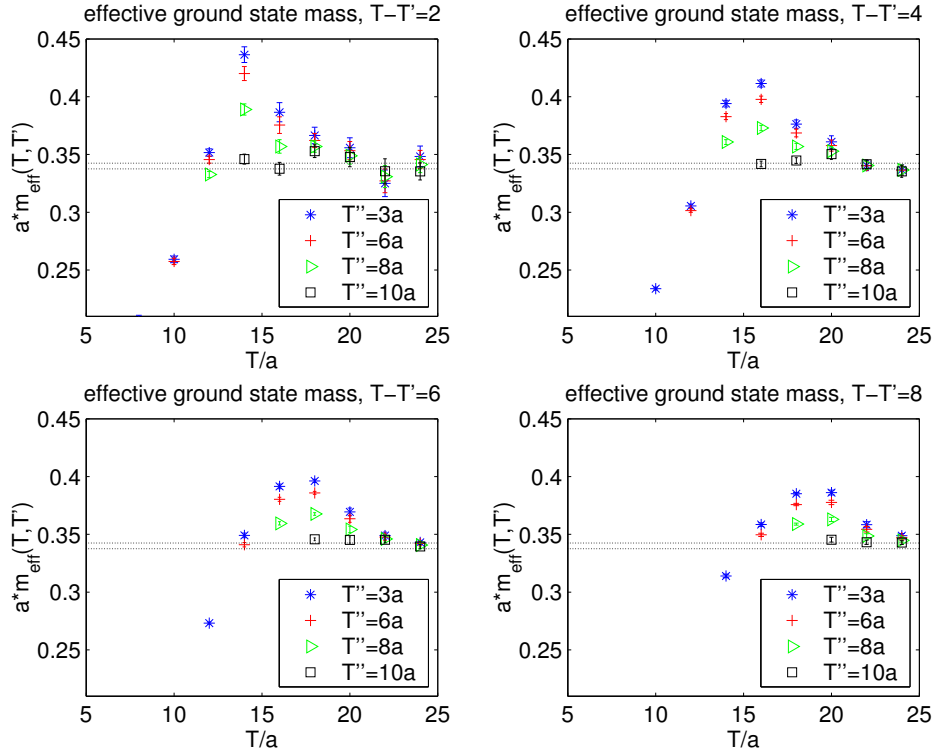


Figure 6.1: Effective pseudoscalar ground state mass from the variational principle, relativistic case, $\beta = 6.0$, $\kappa = \kappa_s$, in comparison to the extracted mass $m_{\text{PS}}(f_A^1)a = 0.340(3)$ (dotted lines).

The Ground State Mass, $\beta = 6.2$

This case is depicted in figure 6.2. Because there are runs for only four different time extents, determinations of m_{eff} directly from the GEVP have been included. The situation looks different from the one in figure 6.1. Since all points at $\beta = 6.2$ yield compatible results one may conclude that the asymptotic value $m_{\text{PS}}a = 0.250(5)$ is already reached at $T'/a = 15$. The complicated non-monotonic behaviour of effective masses for time extents ~ 1 fm at $\beta = 6.0$ could be due to large discretisation effects of excitations close to the cutoff scale.

To extract the masses, one has used subspace dimension $M = 2$, eq. (4.14), except for the case (no T'' , $T' = 24a$, $T = 36a$). Again, ground state masses are stable under changes of M .

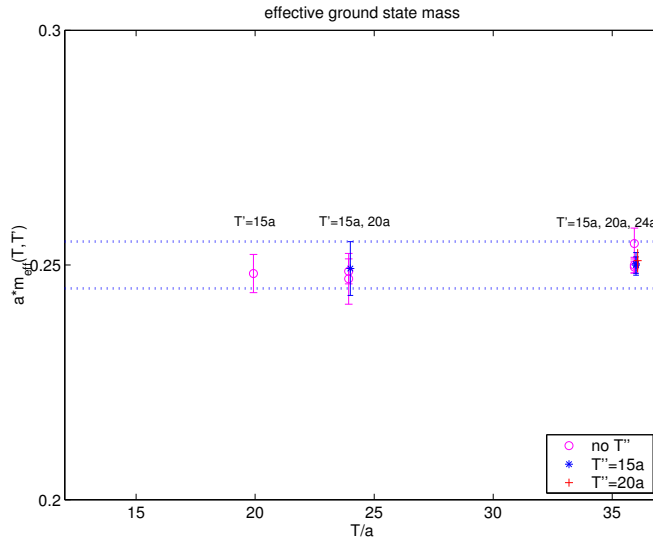


Figure 6.2: Effective mass of the pseudoscalar ground state from the variational principle, relativistic case, $\beta = 6.2$, $\kappa \approx \kappa_s$, in comparison to the extracted mass $m_{\text{PS}}(f_A^I)a = 0.250(5)$ (dotted lines).

The First excited State Mass, $\beta = 6.0$

The case for the first excited meson mass, figure 6.3, also shows a non-monotonic approach to the asymptotics from below. Data are collected in tables C.4–C.6 and may be compared with the extracted value $m_{\text{PS}}^*a = 0.83(5)$ from a plateau in the effective mass of the axial current (or pseudoscalar

density) for a suitable choice of $\omega_{\text{opt}}^{(1)}$. They agree well within their statistical errors. But for statistical reasons one is limited to use small time extents in the GEVP. Since excited meson contributions in eq. (2.82) are always positive, one may conclude that contributions of vacuum excitations are sizeable at $T'/a \sim 10$. One has used subspace dimension $M = 2$. A weak variation of masses with M has been observed.

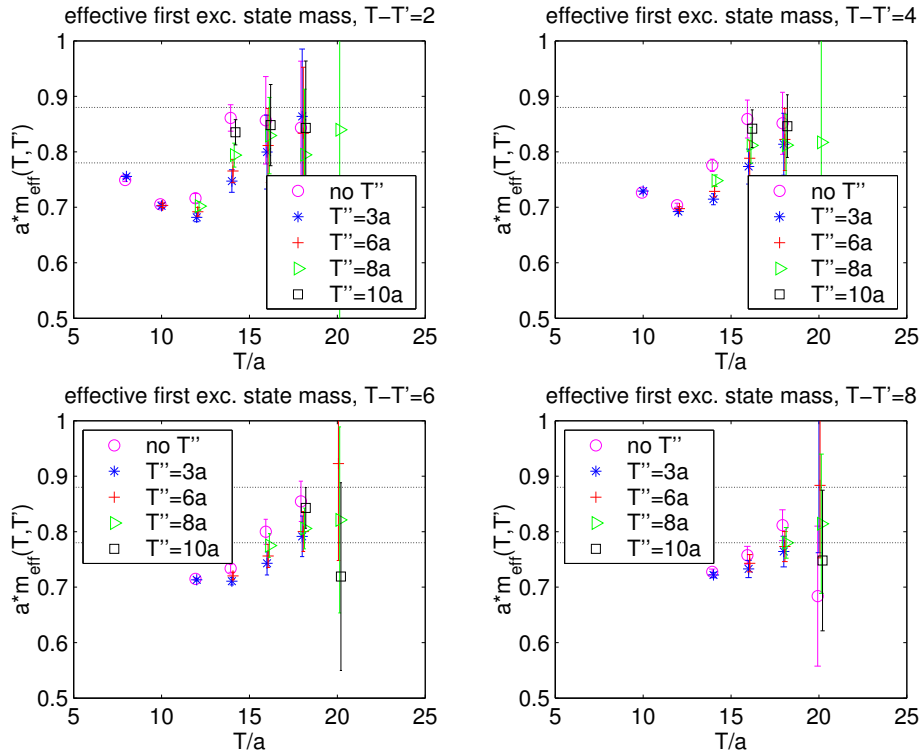


Figure 6.3: Effective mass of the first excited pseudoscalar state from the variational principle, relativistic case, $\beta = 6.0$, $\kappa = \kappa_s$, in comparison to the result $m_{\text{PS}}^*a = 0.83(5)$ from f_A^I or f_P (dotted lines).

The First excited State Mass, $\beta = 6.2$

A reliable extraction of m_{PS}^*a for these few (and large) time extents is not possible. On the smallest lattices (with $M = 2$), one may extract $m_{\text{PS}}^*a = 0.63(3)$ which fits to the determination via f_A^I or f_P . For the other combinations, the central value decreases while statistical errors grow. There are strong variations in M .

The First pseudoscalar Mass Gap, $\beta = 6.0$

In contrast to pseudoscalar masses from the variational principle, the mass gap Δ , eq. (6.4), has no contaminations from vacuum excitations. Contributions at time extents (T', T) are

$$a\Delta_{\text{eff}} = a\Delta + \frac{a}{T-T'} \left[\frac{d_1^2(\omega)}{d_0^2(\omega)} (\exp(-\Delta T') - \exp(-\Delta T)) - \frac{d_2^2(\hat{\omega})}{d_1^2(\hat{\omega})} (\exp(-\Delta^* T') - \exp(-\Delta^* T)) \right] + \dots \quad (6.5)$$

This follows from eq. (2.82) and the corresponding one for the first excited state mass. Additional leading corrections appear when using the LW-proposal, eq. (4.10). The case for $\beta = 6.0$ is shown in figure 6.4. At small time extents T' , excited states with masses larger than m_{PS}^* give sizeable contributions and push the gap downwards. The positive contribution proportional to the gap itself decays most slowly, eq. (6.5), and the asymptotic value $a\Delta = 0.50(10)$ is approached at $T/a = 18$. The dotted lines are error bands for $a\Delta = 0.55(5)$ which stem from an alternative extraction of the gap in section 6.4.

The First pseudoscalar Mass Gap, $\beta = 6.2$

With present data, one obtains a plot as in figure 6.5. Horizontal lines give $a\Delta = 0.41(5)$ which is obtained in section 6.4.

Eigenvectors

have been computed following the recipe given in section 4.3. They are listed in tables C.7–C.11 in the appendix. The set of eigenvectors of the lowest states of $C(T')$ are denoted by B . Projecting out negative eigenvalues or those compatible with zero determines the subspace dimension M . The generalised eigenvectors in the subspace of dimension M will be given in terms of the basis B . One usually works with $M = 2$.

The components of the eigenvectors are relatively stable for intermediate to large (T', T) . But it is not at all understood why the M th component gets pronounced. Also, eigenvectors of the lowest states form a cone that gets very narrow for large time arguments (T', T) . And statistical errors may not always allow to safely determine the vectors $v^{(0)}$ and $v^{(1)}$. This behaviour may indicate that the chosen basis of trial wave functions is not a very good one to describe the light-light system. This may not be very surprising since

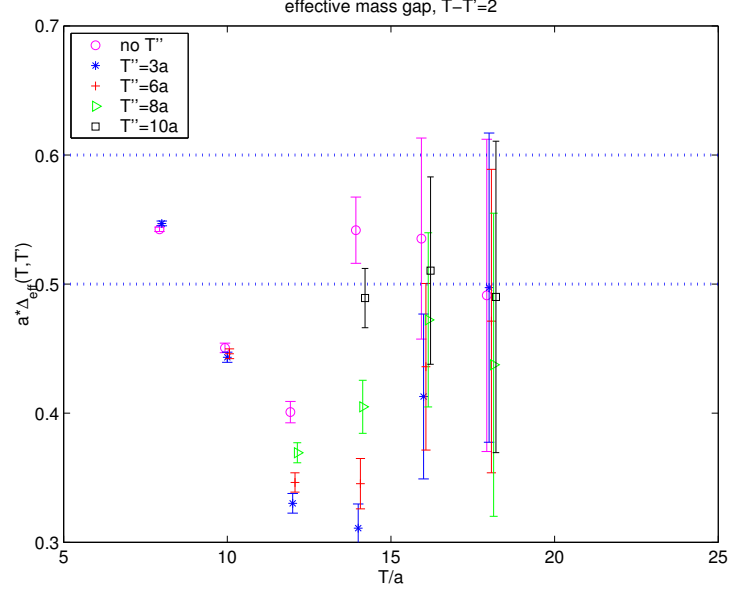


Figure 6.4: Effective pseudoscalar mass gap from the variational principle, relativistic case, $\beta = 6.0$, $\kappa = \kappa_s$. Error bands: $a\Delta = 0.55(5)$ (text).

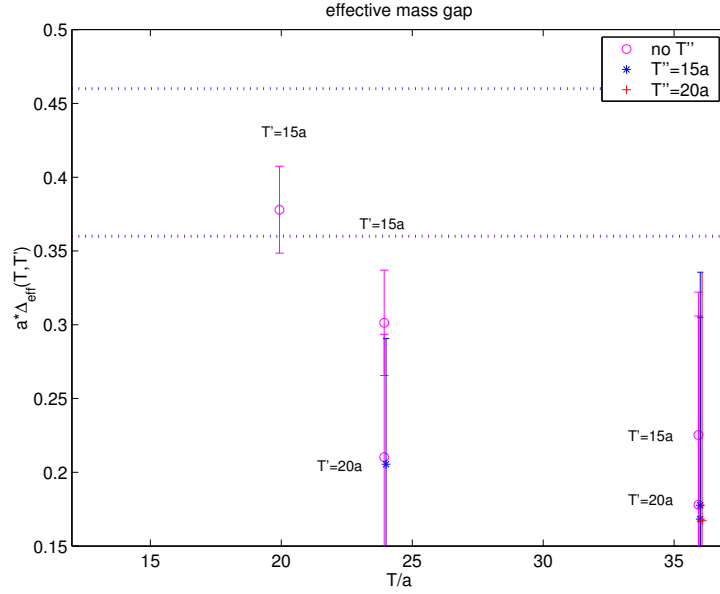


Figure 6.5: Effective pseudoscalar mass gap from the variational principle, relativistic case, $\beta = 6.2$, $\kappa \approx \kappa_s$. Error bands: $a\Delta = 0.41(5)$ (text).

the non-relativistic picture of an hydrogen atom does not apply to light-light pseudoscalars. Best results are obtained for $T \geq T' = 10a$ at $\beta = 6.0$ and $T \geq T' = 15a$ at $\beta = 6.2$. One may understand that by means of an effective mass plot, such as figure 6.1. The second and any higher excited state has practically died out at these Euclidean time extents of roughly 1 fm, and one may get v for the lowest two states well. Increasing T' will exponentially suppress the signal of the first excited state relative to the ground state. Therefore, the extraction of $v^{(1)}$ gets more and more unreliable for large T' .

6.2.2 The Static Case

Effective Energies

A severe problem in the static approximation (with Eichten-Hill action for the static quark) is the exponentially deteriorating quality of the signal in correlation functions. With the current data sets and statistical precision, one can only discuss the results of the variational principle at $\beta = 6.0$.

The Ground State Energy, $\beta = 6.0$

Data from table C.12 (for $M = 2$; stable under changes of M) is discussed here and plotted in figure 6.6. The dotted horizontal lines estimate the corridor of the ground state energy as obtained from $E_{\text{eff}}(f_{\text{A}}^{\text{stat}})$ with an $\mathcal{O}(a)$ -improved static axial current. Effective energies in figure 6.6 increase monotonically, and the asymptotic value $E_{\text{eff}}(f_{\text{A}}^{\text{stat}})$ is overshoot. This somehow reminds one of observation (1) in the relativistic case. This could be an indication that vacuum corrections are still present at $T'/a = 14$ (considering the case $T - T' = 2a$). Increasing the difference between T and T' decreases the overshoot but cannot eliminate it. Therefore, one is not able to safely extract the ground state binding energy from the GEVP alone.

The First excited State Energy, $\beta = 6.0$

The binding energy of the first excited state ($M = 2$) also shows large corrections to the asymptotics. From the effective energy plot of the static axial current one obtains $aE^* = 0.88(3)$, as drawn in with dotted lines in figure 6.7. This estimate is indeed reached at $T/a \sim 15$. So it seems to be easier to obtain an estimate for the first excited state energy out of the variational principle than for the ground state. Extracted energies vary weakly in M .

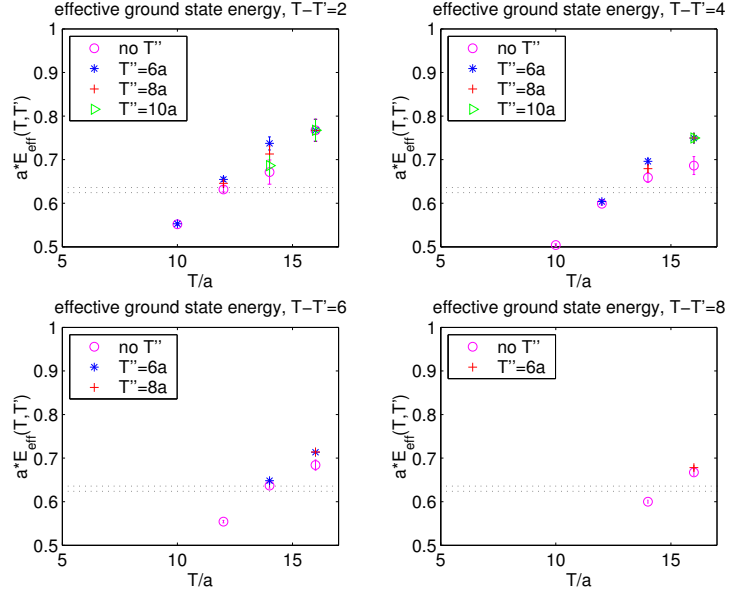


Figure 6.6: Effective ground state binding energy from the variational principle, static case, $\beta = 6.0$, $\kappa = \kappa_s$.

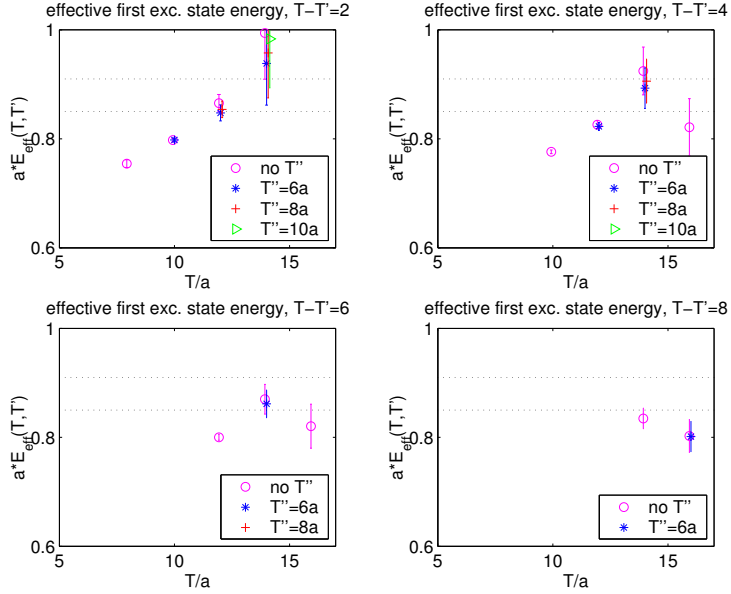


Figure 6.7: Effective binding energy of the first excited state, obtained from the variational principle, static case, $\beta = 6.0$, $\kappa = \kappa_s$.

The Energy Gap, $\beta = 6.0$

Figure 6.8 shows the gap as a function of T . The gap decreases monotonically to an estimated value as small as 0.2 or 0.3 (given in lattice units). No plateau in T can be seen. But the smallness of the gap may explain the late on-set of ground state dominance.

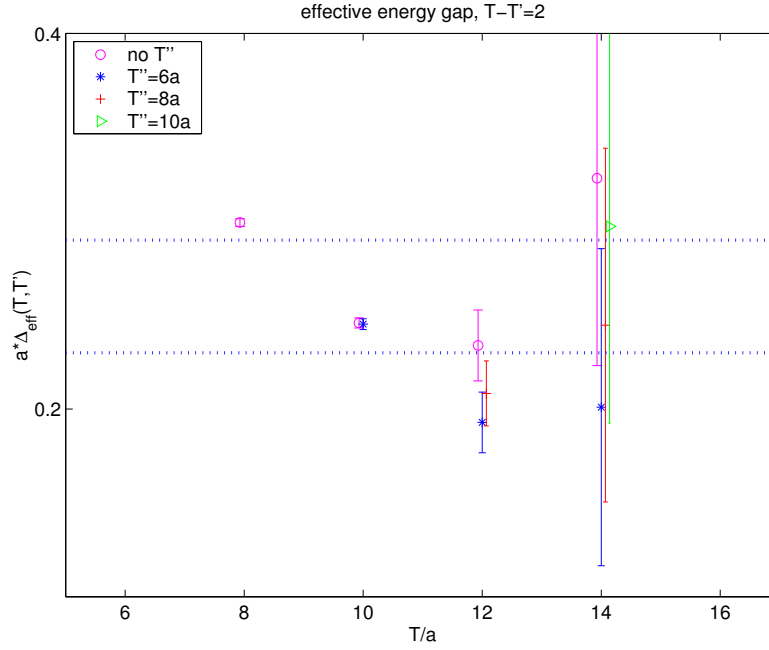


Figure 6.8: Effective energy gap from the variational principle, static case, $\beta = 6.0$, $\kappa = \kappa_s$.

Eigenvectors

In the static-light case, one expects a physical picture that is similar to the hydrogen atom. Therefore, wave functions of that kind should be a suitable choice. The generalised eigenvalue problem has been applied and the vectors are collected in table C.13. Good vectors can be obtained at $T' = 10a$ and $T = 12a, 14a$.

6.3 Extraction of Masses with optimal Wave Functions

Assuming that the generalised eigenvalue problem provides ground and first excited state vectors $v^{(0)}$ and $v^{(1)}$, one may use them to build up 'optimal' correlators, eq. (4.1), that have a large overlap with the ground and first excited state, respectively. This section considers the quality of extracted $v^{(n)}$ in the sense how well the mass of the n th energy eigenstate appears as a constant in the effective mass plot of the (static) axial current correlator.

6.3.1 The Relativistic Case

Figure 6.9 shows effective masses from f_A^I for $n = 0, 1$ at $\beta = 6.0$ and two sets of optimal wave functions from the variational principle with $T' = 10a$ and some $T > T'$. For the ground state, they are given by

$$\begin{aligned} v^{(0)} &= (-0.7694, -0.5161, 0.1651, 0.3383), \\ v^{(0)'} &= (-0.7894, -0.4933, 0.1909, 0.3113), \end{aligned} \quad (6.6)$$

and for the first excited state by

$$\begin{aligned} v^{(1)} &= (0.5688, -0.3523, -0.5142, 0.5366), \\ v^{(1)'} &= (0.7624, -0.0387, -0.5709, 0.3024). \end{aligned} \quad (6.7)$$

The $v^{(0)}$'s give a long plateau of the effective mass in x_0 . Different vectors will have different excited state contributions, but plateau values are expected to be independent of the wave functions. This can be confirmed. The plateau region of the ground state mass, which yields $m_{\text{PS}}a = 0.340(3)$, ranges between $[6a, 13a]$ *with smearing*. Compared to the standard case ω_{std} , the gain is about four lattice spacings. Excited mesons give sizeable contributions for smaller Euclidean times, and vacuum excitations for larger ones.¹ In contrast to the first kind of contributions, the latter cannot be minimised through hadron wave functions.

The plateau region of the first excited state is stable but very short. It gives $m_{\text{PS}}^*a = 0.83(5)$, and therefore a large gap $a\Delta = 0.49(5)$ between the first excited and the ground state. One may similarly proceed with data for $\beta = 6.2$.

¹As a rule of thumb, the influence of excited mesons is negligible after 1 fm (without smearing) from the bottom of the box and vacuum excitations about 1 fm from the top.

The following vectors, for which the GEVP has been solved at $T' = 15a$ and some $T > T'$, give flat effective mass plots,

$$\begin{aligned} v^{(0)} &= (0.7407, 0.5831, -0.0082, -0.3336), \\ v^{(1)} &= (0.6209, -0.1631, -0.6060, 0.4698). \end{aligned} \quad (6.8)$$

Finally, one may plot $r_0 m_{\text{eff}}$ versus x_0/r_0 (or $(T - x_0)/r_0$), as done in figure 6.10. The Sommer scale r_0 is computed in [83] and makes the quantities of interest dimensionless. The physical value of r_0 is approximately 0.5 fm. Scaling can be observed if the mass of the light quark was chosen correctly. Concerning the effective mass of the ground state, one observes scaling violations for Euclidean time separations $x_0 < r_0$ and much stronger ones for $x_0 \geq 3r_0$. To large extent, these violations at given times come from not exactly scaled box extents, as this can be seen by changing x_0/r_0 to $(T - x_0)/r_0$. Data from figure 6.10 are summarised in table 6.1. The pseudoscalar gap between both states is estimated by the mass difference.

β	$r_0 m_{\text{PS}}$	$r_0 m_{\text{PS}}^*$	$r_0 \Delta$
6.0	1.823(8)	4.40(15)	2.58(15)
6.2	1.834(13)	4.98(13)	3.15(13)

Table 6.1: Pseudoscalar masses for the light-light case taken at $x_0 \approx 2r_0$ (ground state) and at $x_0 \approx r_0$ for the first excited one.

6.3.2 The Static Case

As mentioned in the introduction of chapter 4, it is very difficult to extract the ground state energy in the static approximation and smearing techniques must therefore be applied. The signal decreases exponentially and is typically very noisy at $x_0 \geq 1.5 \text{ fm}$. Without smearing, the on-set of ground state dominance is in the same range of x_0 . This is shown in figure 6.11.

Taking two different vectors for the ground and first excited state, $n = 0, 1$, $v^{(n)} = (\alpha_1^{(n)}, \dots, \alpha_g^{(n)})$, and building up 'optimal' correlators, eq. (4.1), one obtains estimates for the effective energy, as shown in figure 6.12. Two choices of optimal wave functions for the ground state are

$$\begin{aligned} v^{(0)} &= (0.2103, 0.4400, 0.5969, 0.6371), \\ v^{(0)'} &= (0.3927, 0.5301, 0.5222, 0.5404), \end{aligned} \quad (6.9)$$

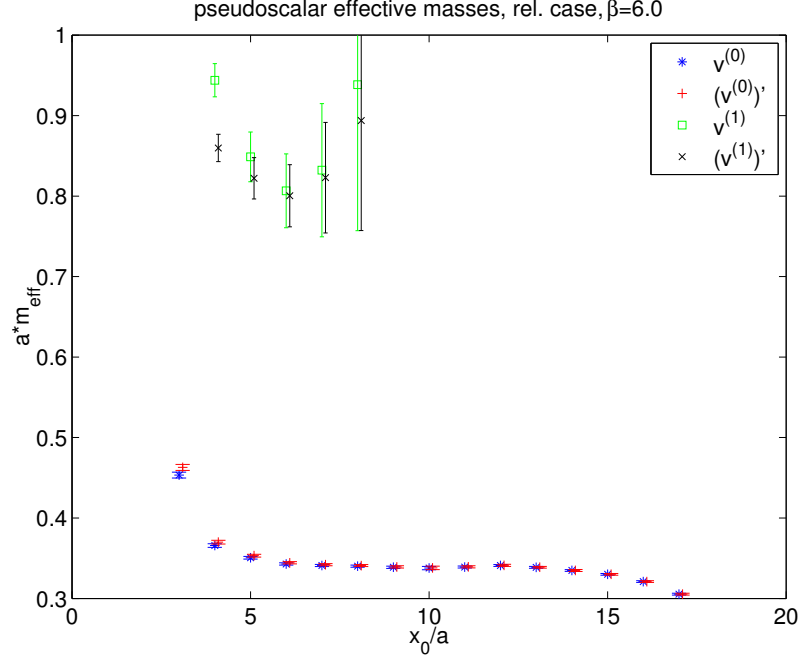


Figure 6.9: Effective ground and first excited state mass, $\beta = 6.0$, $\kappa = \kappa_s$, relativistic case.

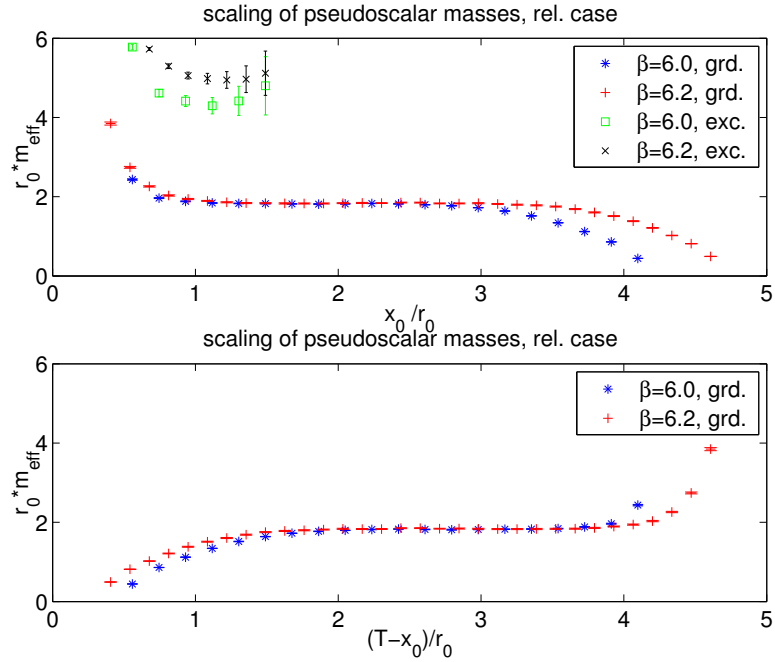


Figure 6.10: Scaling of effective ground and first excited state masses, $\beta = 6.0$ and 6.2 for the relativistic case. Symbols are as in figure 6.9.

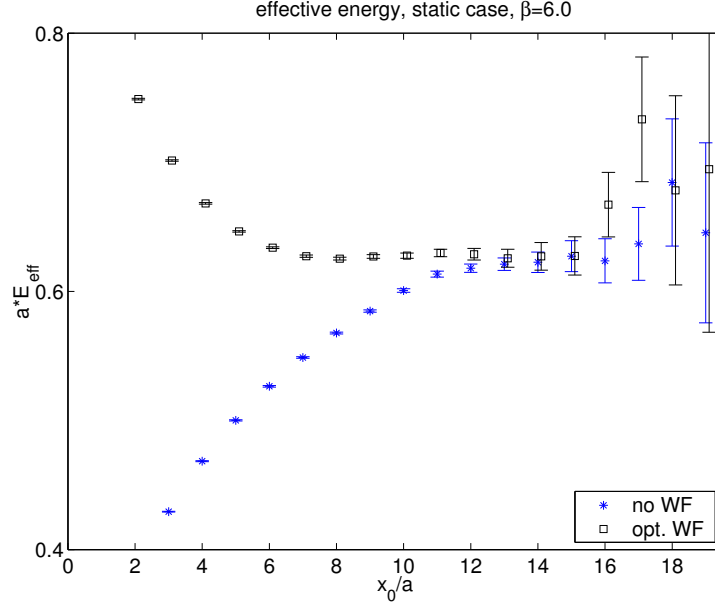


Figure 6.11: Smearing is essential in the static case: Effective energy plot of the static axial current correlator with(out) smearing, $\beta = 6.0$, $\kappa = \kappa_s$.

and for the first excited state,

$$\begin{aligned} v^{(1)} &= (-0.2342, -0.6905, -0.0417, 0.6831), \\ v^{(1)'} &= (0.0137, -0.6909, -0.1721, 0.7020). \end{aligned} \quad (6.10)$$

For the best choice of the ground state vector, the effective energy has a plateau in $x_0 = 7a \dots 13a$. And for the first excited state there is one for $x_0 = 8a \dots 11a$. This allows to extract binding energies $aE = 0.630(6)$ and $aE^* = 0.88(3)$ at $\beta = 6.0$. Obviously, the influence of the second excited meson state is sizeable up to $x_0 \approx 8a$. This is an indication for a rather small mass gap between the first and the second excited state.

Scaling is considered and shown in figure 6.13. For static data, there is a run with a third value, $\beta = 6.45$, available. Because of the flatness of effective binding energies in x_0 for $v^{(0)}$ (ground state) and $v^{(1)'}$ (the first excited state), they have been taken at all β -values.

In order to take the continuum limit of the binding energies, one has to subtract the divergent self-energy of the static quark. This is done following

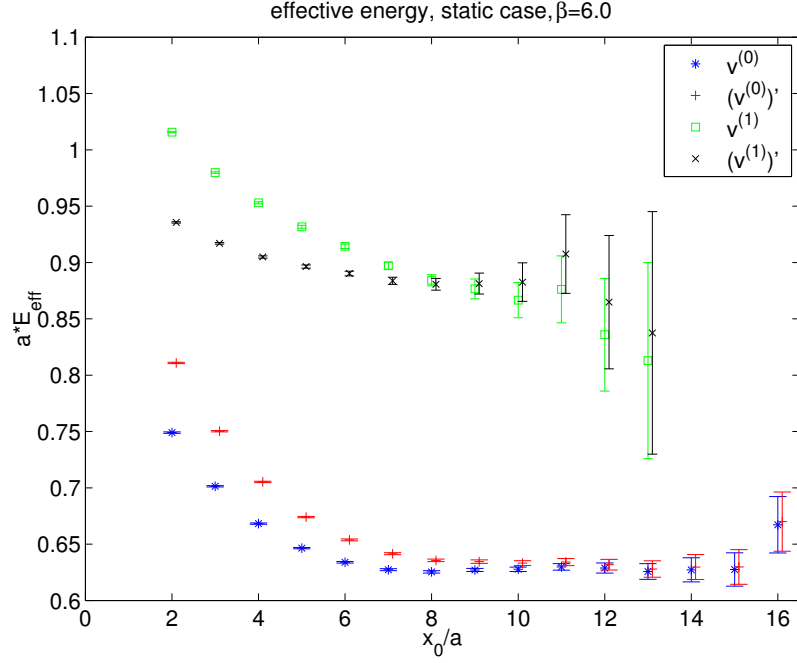


Figure 6.12: Effective energy plot of the static axial current corr., $\beta = 6.0$.

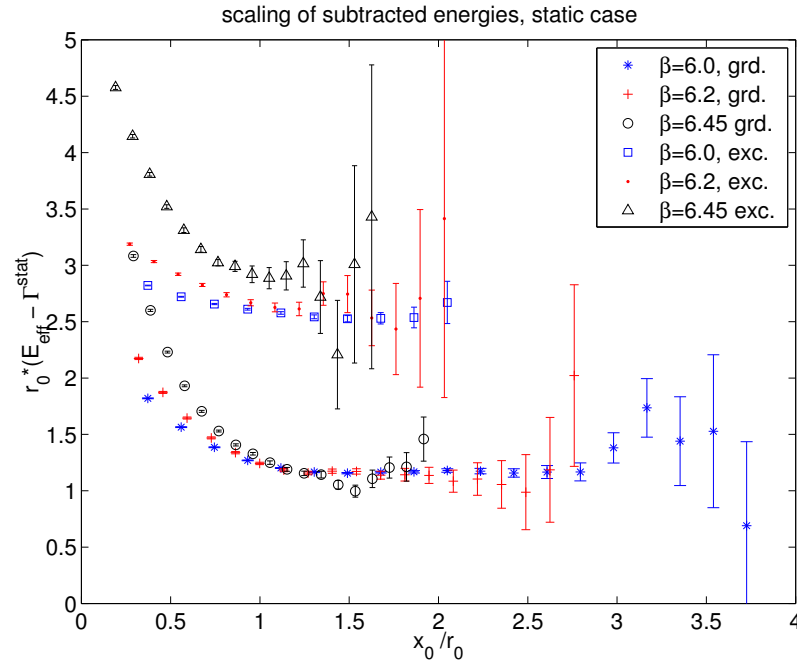


Figure 6.13: Scaling of $r_0(E - \Gamma^{\text{stat}})$ using vectors $v^{(0)}$, $v^{(1)'} at all β 's.$

the strategy in refs. [75, 76]. One computes

$$r_0 \Delta E_a = r_0(E - \Gamma^{\text{stat}}(L_2)), \quad \Gamma^{\text{stat}}(L) = -\frac{\partial_0 + \partial_0^*}{2} \ln f_A^{\text{stat}}(x_0)|_{x_0=L/2} \quad (6.11)$$

at $L_2 \approx 0.8 \text{ fm}$. The value for Γ^{stat} has been taken from ref. [64]. Results are summarised in table 6.2 and plotted in figure 6.13. It shows a rough scaling of the plateau for the ground state that starts at $x_0 \approx 1.2r_0$. For $\beta = 6.45$, small deviations of data at $x_0 \approx 1.5r_0$ are attributed to poor statistical precision. This situation should be improved in future studies. Also, a faster approach to the plateau region at $\beta > 6.0$ may be achieved through solving the variational principle at these particular β 's. The scaling of the first excited state shows sizeable violations between $\beta = 6.45$ and the other β -values.

To obtain the continuum limit, figure 6.13, one could make fit ansätze of the following form: fit to a constant (fit A) or one to a constant plus a term quadratic in a/r_0 (fit B). This has been done at $x_0 \approx 1.3r_0$ (columns 2 and 3) and $x_0 \approx 1.8r_0$ (columns 4 and 5). Both ansätze agree within errors for the ground state energy. To get a reasonable result for the first excitation, one has to use fit A or B for the smaller time extent, where one has to exclude the point at $\beta = 6.0$ for fit A. Data are very noisy at $x_0 \approx 1.8r_0$.

β	$r_0 \Delta E_a$	$r_0 \Delta E_a^*$	$r_0 \Delta E_a$	$r_0 \Delta E_a^*$
6.0	1.16(1)	2.54(2)	1.17(2)	2.5(1)
6.2	1.18(2)	2.75(11)	1.15(7)	2.4(4)
6.45	1.14(4)	2.77(21)	1.43(19)	4(3)
CL, fit A	1.17(1)	2.75(11)	1.17(2)	2.54(9)
CL, fit B	1.17(4)	2.93(18)	1.22(13)	2.4(9)

Table 6.2: Results for the static-light case, eq. (6.11), taken at $x_0 \approx 1.3r_0$ (resp. $x_0 \approx 1.8r_0$), $\Gamma^{\text{stat}}(L_2) = 0.410024 - 0.131595(\beta - 6)$ for $6.0 \leq \beta \leq 6.45$.

With $L_0/r_0 = 1.436/4$ from ref. [51] multiplied by the continuum result $r_0 \Delta E_a = 1.17(4)$ from table 6.2, one yields a more precise result than given in ref. [76],

$$L_0 \Delta E_a = 0.420(14).$$

One obtains an estimate for the energy gap from table 6.2,

$$r_0 \Delta = r_0 \Delta E_a^* - r_0 \Delta E_a = 2.75(11) - 1.17(4) = 1.58(12).$$

6.3.3 An Alternative Way without applying the Variational Principle

The numerical treatment of the proposal in section 5.1 is considered here. It allows to improve the correlators in the sense that a faster approach to ground state dominance is obtained on a single lattice *without* solving the variational principle for several lattice sizes. This is illustrated in the relativistic case at $\beta = 6.2$ and in the static approximation at $\beta = 6.45$.²

The quantity R_{ij} is computed at $x_0^* = T/2 + a = \text{fix}$ (relativistic case only), $T_2 = T/2 - a$ as the reference point and several times T_1 ranging from r_0 to $T_2 - 3a$. All pairs of trial wave functions are taken into account.

The Relativistic Case

The computation of R_{ij} may be done through the decay constant as well as the effective mass. Table C.14 lists the results for R_{ij} in dependence of the pair (i, j) of trial wave functions, several correlators and $x_0 = T_1$.

All versions give similar results. Error bars are in the same order, but they are somewhat larger for the implementation using the decay constant.

Disregarding the case (3, 4) for a while, one notices: For time separations $x_0/a < 10$, $R_{ij}(x_0)$ grows fast. This is followed by a narrow 'plateau region' of $3a$ length. At $x_0/a \approx 14$, coefficients may fluctuate and errors start to grow quickly. This behaviour is expected since effective masses (or decay constants) approach the region of ground state dominance for each trial wave function individually at these Euclidean times, hence their ratio is close to one. Meaningful information with small errors can only be extracted if effective masses (decay constants) are significantly spread. The case (3, 4) differs because it still has not entered the region of ground state dominance.

Since $R_{ij} \approx d_1(\omega_i)/d_1(\omega_j)$, one may read off from the table that the trial basis $\omega_1, \dots, \omega_4$ has increasing absolute overlaps with the first excited state, as indicated by R_{ij} getting smaller for $i < j$ at fixed x_0 and i .³

The optimal wave function is given by eq. (5.2). This translates into a difference of correlation functions, for instance

$$f_A^I(x_0, \omega_{\text{opt}}) = f_A^I(x_0, \omega_i) - R_{ij} f_A^I(x_0, \omega_j). \quad (6.12)$$

²With the intention to obtain a better plateau in the effective energy, figure 6.13.

³One may also get this impression in plotting the effective mass for the individual correlators $f_A^I(x_0, \omega_i)$ versus x_0/a . Then $m_{\text{eff}}(x_0, \omega_1)a$ turns out to be the flattest.

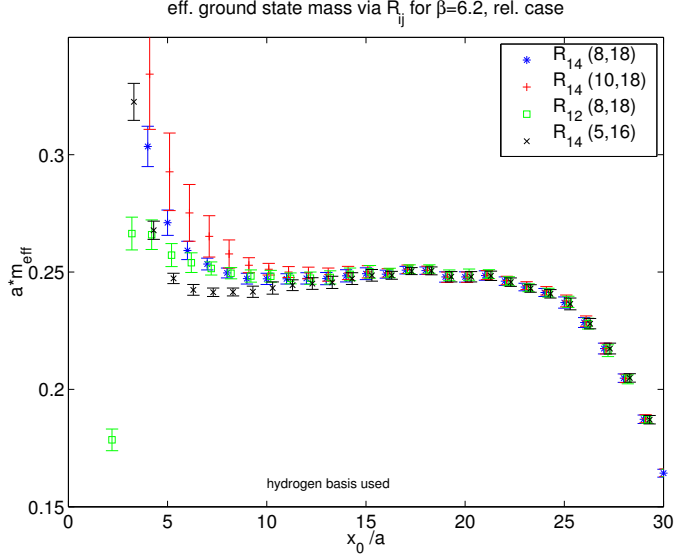


Figure 6.14: Effective mass plot using f_A^I and various values of R_{ij} , $\beta = 6.2$, $\kappa \approx \kappa_s$, relativistic case. Values for R_{ij} are taken from table C.14.

For numerical reasons, it is desirable to work with wave functions that approach the plateau region for effective masses (decay constants) from different directions, such that R_{ij} is negative.⁴ Otherwise, extra statistical noise will be introduced. Figure 6.14 shows some effective masses and summarises given facts. The statistical errors of the coefficients R_{ij} have been propagated. If T_1 is too small, such as $5a$, R_{ij} will not be well approximated due to the influence of highly excited meson states, and the plateau region of $m_{\text{eff}}a$ in x_0/a starts late. Taking R_{ij} for larger values of T_1 provides better results, even independent of the pair (i, j) . These effective mass plateaux are equally good with those where the ground state vector $v^{(0)}$ has been computed by means of the variational principle. At $T_1 \approx 14a$ (and above), the coefficients R_{ij} cannot be reliably computed anymore and the effective mass gets noisy. One may also consider eq. (5.10) which provides an interesting option to accelerate ground state dominance for effective masses (only!) even if there is only one wave function at hand. The quantity $R_{f_A^I f_P}$ is related to the PCAC-relation and is expected to be independent of ω . Results for $R_{f_A^I f_P}$ are given

⁴such as the basis $(\omega_{std}, \omega_\delta)$

in table C.15 for $\beta = 6.2$ and in table C.16 for some more β -values. Table C.15 confirms ω -independence within statistical errors for ω_i , $i = 2, 3, 4$ and $x_0 \approx 7a \dots 10a$ (or $r_0 \dots 1.5r_0$). Obviously, ω_1 is not suitable for the computation of $R_{f_A^I f_P}$. Within the trial basis, this wave function has the smallest absolute overlap with the first excited meson state and a reliable extraction of $R_{f_A^I f_P}$ at present statistical precision was not possible.

One can read off from table C.16 that $R_{f_A^I f_P}$ changes only weakly as the quark mass is increased from the strange to twice the strange. But a further increase to roughly four times the strange quark mass doubles $R_{f_A^I f_P}$.

A direct comparison of effective mass plots with the original correlators $f_A^I(x_0, \omega_i)$ and 'improved' ones $(f_A^I)'(x_0, \omega_j)$ is shown in figure 6.15, where $R_{f_A^I f_P} = 0.12(2)$ at $\beta = 6.2$ and $\kappa = 0.13485$ has been determined from ω_4 .⁵ For all 'improved' axial current correlators, effective masses include error propagation of the R -coefficient. They approach the plateau region around $x_0 = 8a$ and are therefore as good as those from previously described techniques. However, the price to pay for this earlier on-set is an increased statistical error.

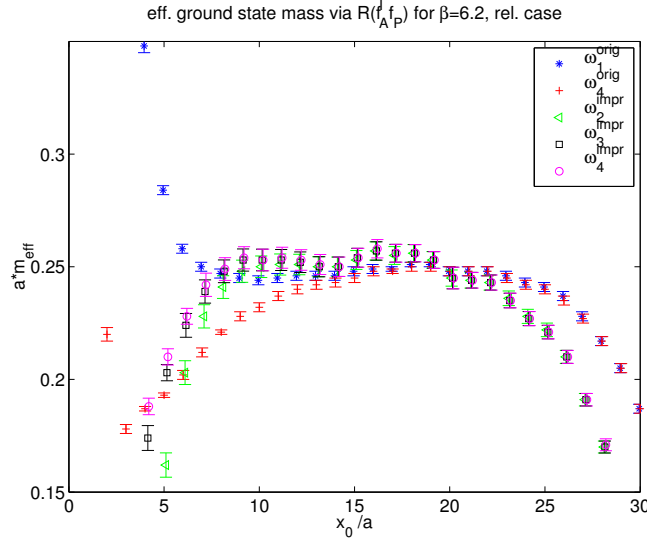


Figure 6.15: Effective mass plot using f_A^I for the original basis and an improved case with R from eq. (5.10), at $\beta = 6.2$, $\kappa \approx \kappa_s$, relativistic case.

⁵Since ω_4 has the largest overlap with the first excited pseudoscalar state.

The Static Case

A safe extraction of the ground state energy would be of particular interest. Because f_1 gets noisy for large time extents, a computation of R_{ij} will be only possible if the effective energy version is used. For the same reason, the factor $d_0(\omega_i)/d_0(\omega_j)$ has to be extracted from $O(a)$ –improved f_A^{stat} correlators.

Table C.17 shows the time dependence of corresponding weights R_{ij} for all pairs of wave functions. Since ω_3 and ω_4 show a much flatter behaviour in the effective energy plot than ω_1, ω_2 , they are now written in the first place. Central values for R_{ij} vary only weakly in x_0 . However, combinations involving ω_1 have errors of the same size as the central value. R_{43} , the best case, has only 20% statistical uncertainty.

Applying some R_{ij} –values to the data and taking error propagation from the R_{ij} into account, one obtains effective energy plots as shown in figure 6.16. Unfortunately, plateaux in the effective energy have large statistical errors.

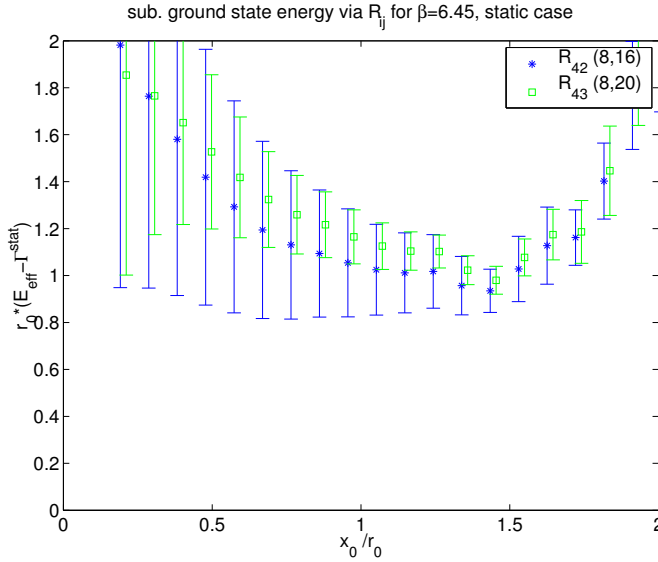


Figure 6.16: Effective energy plot from the static axial correlator, for two R_{ij} –values, $\beta = 6.45$, $\kappa = \kappa_s$.

6.4 Alternative Extraction of the Pseudoscalar Mass Gap

A method to obtain estimates of the pseudoscalar mass gap *on a single lattice* through effective masses themselves was described in section 5.2. It will now be applied to available data in the relativistic and static case.

6.4.1 The Relativistic Case

The estimate for the gap has been done via eq. (5.14) and several combinations of correlators f_A^I and f_P . It turned out that, for the presently available statistical precision, the version with f_P gives the most precise results. The version containing f_A^I alone gives consistent values to the f_P case but is too noisy. This behaviour is not surprising: For the same set of parameters, f_P is known to have larger contributions of excited meson states and the approach to ground state dominance is at larger Euclidean time separations than for the improved axial current correlator f_A^I .

The mixed form, that is f_A^I in one and f_P in the other definition of the effective mass, is disfavoured. Though this is a theoretically allowed combination, it suffers from corrections of excited meson states and those with vacuum quantum numbers, eq. (5.15). A plateau of the gap in x_0 could not be seen.

Therefore, effective masses constructed from the pseudoscalar density are used to determine the gap. One furthermore could vary the time extent of the box since glueball corrections will cancel each other exactly. Consistent results are confirmed at $\beta = 6.0$ and $T/a = 18, 20, 22, 24$ as well as $\beta = 6.2$ and $T/a = 24, 36$. Such a plot is figure 6.17. At $\beta = 6.0$, the effective pseudoscalar gaps for the six possible twin combinations of wave functions are shown. The combination (3,4) approaches the plateau region around 0.55 (in lattice units) only for large Euclidean times. This is due to large contributions from higher meson states. The other twin combinations give indistinguishable results around $x_0 = 8a$ ($x_0/r_0 \approx 1.5$). The case at $\beta = 6.2$ gives worse estimates for the gap. This could be improved by increasing the statistical precision. Figure 6.18 shows the scaling plot of the gap.⁶

⁶If the quark mass is close to the strange one, one obtains $r_0\Delta|_{x_0=r_0} \approx 3.0(3)$ (no continuum limit taken). At $\beta = 6.2$ and twice the strange quark mass one gets $r_0\Delta|_{x_0=r_0} \approx 2.5(2)$ and at roughly four times the strange quark mass it yields $r_0\Delta|_{x_0=r_0} \approx 2.0(1)$.

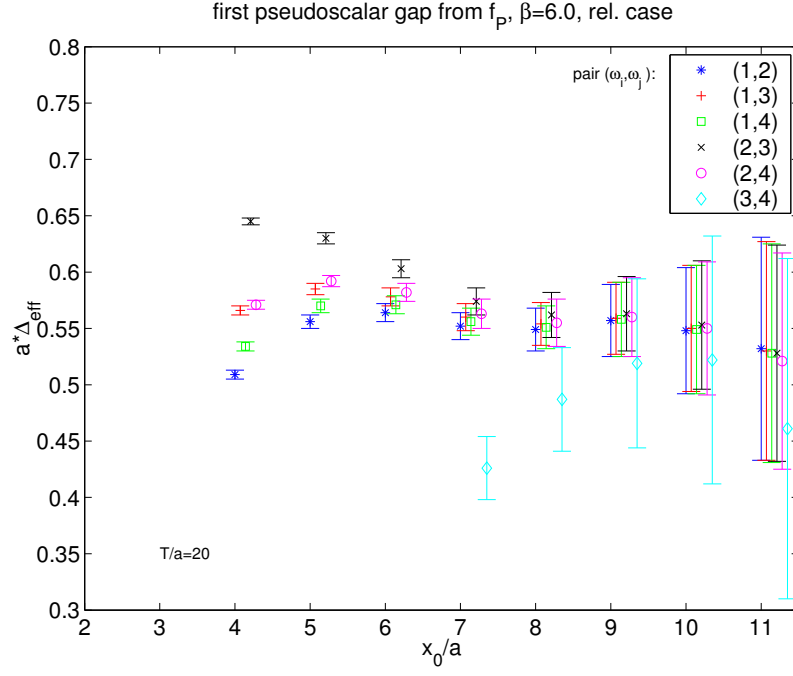


Figure 6.17: Effective pseudoscalar mass gap, $\beta = 6.0$, $\kappa = \kappa_s$, relativistic case. Effective masses from f_P and several pairs of wave functions are used.

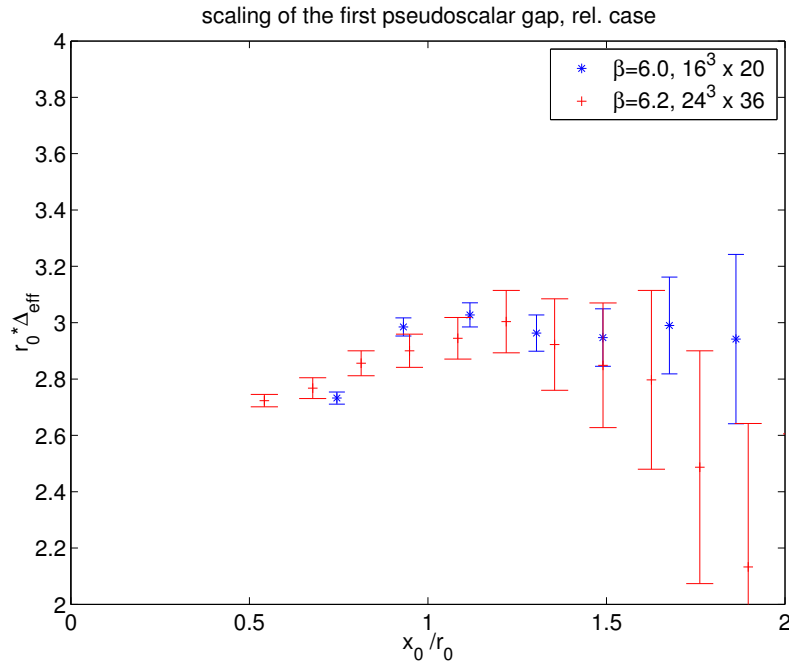


Figure 6.18: Scaling of the eff. pseudoscalar gap, relativistic case, $\kappa \approx \kappa_s$.

6.4.2 The Static Case

Similarly to the relativistic case, one may apply the procedure to static-light correlators. The choice f_A^{stat} ($O(a)$ –improved) and several combinations of wave functions allow for a safe extraction of the gap. This is done at three different β –values, as shown in figure 6.19 and summarised in table 6.3. The

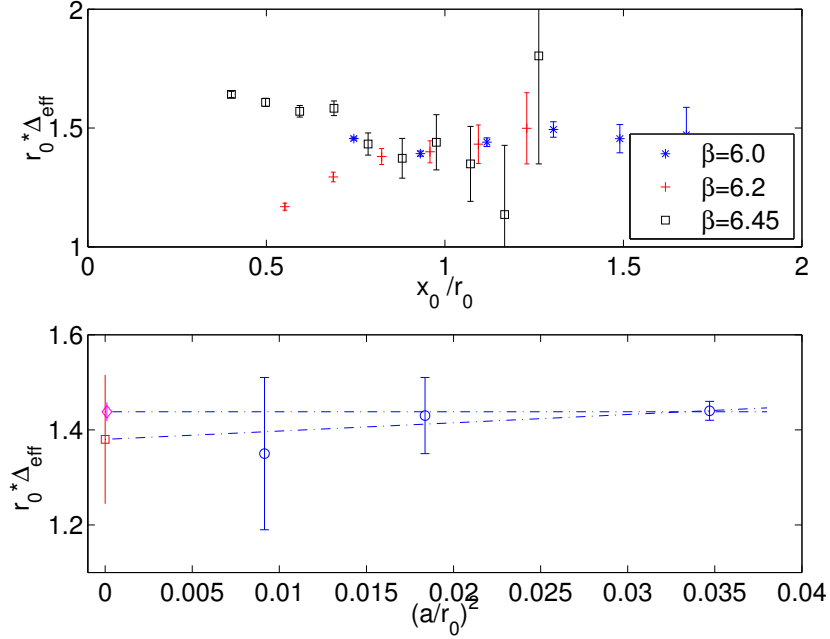


Figure 6.19: Scaling of the effective energy gap (upper plot) and the continuum extrapolation for $x_0 \approx r_0$ (lower plot), static case, $\kappa = \kappa_s$.

plateau region of $r_0 \Delta_{\text{eff}}$ in x_0 starts around r_0 . To obtain the continuum limit, figure 6.19, one may think of a polynomial fit to a constant (fit A) or one to a constant plus a term quadratic in a/r_0 (fit B). This has been done at $x_0 \approx r_0$, as listed in table 6.3.

β	6.0	6.2	6.45	CL:	fit A	fit B
$r_0 \Delta$	1.44(2)	1.43(8)	1.35(16)		1.44(2)	1.38(13)

Table 6.3: Energy gap for the static-light case taken at $x_0 \approx r_0$.

6.5 Decay Constants

Eq. (2.90) and the corresponding version in the static approximation, eq. (3.26), have been used to compute decay constants.

The relativistic case is considered first since the signal is clear there, and one may study the theory at large time separations. This is essential to understand the qualitative behaviour of corrections in the vacuum and meson channel. The static case is investigated afterwards.

6.5.1 The Relativistic Case

The dependence of the bare decay constant upon the time extent T of the Schrödinger functional box is investigated and plotted in figure 6.20. Corrections from excited states are described by eq. (2.91). The boxes at $\beta = 6.2$ roughly correspond to scaled ones at $\beta = 6.0$. One uses

$$\begin{aligned} v^{(0)} &= (-0.7894, -0.4933, 0.1909, 0.3113) & \text{at } \beta = 6.0, \\ v^{(0)'} &= (0.7407, 0.5831, -0.0082, -0.3336) & \text{at } \beta = 6.2 \end{aligned}$$

to define ω_{opt} and ω'_{opt} . There are long plateau regions for the largest values $T/a = 24, 36$ at $\beta = 6.0$ and 6.2 , respectively, and the decay constant may be safely extracted there.⁷ Thus, wave functions allow a reduction of the time extent from $T = 2L$ to $T = 3L/2$ without changing results. At $\beta = 6.2$, even $T = L$ seems to be safe.

Contributions from vacuum excitations get sizeable for $T - x_0 \leq 1$ fm. The plateau region is shortened for smaller T and disappears if T is too small. This is because vacuum contributions cannot be affected by meson wave functions, and contributions in the pseudoscalar channel can only be minimised to a certain extent. Additionally, eq. (2.90) is very sensitive to both types of corrections because the factor $\exp(+ (x_0 - T/2) \tilde{E}_0^{(\text{PS})})$ contains the effective mass in the exponential.

The analysis of figure 6.20 with ω_1 had yielded the same results for $x_0 \geq 9a$ ($\beta = 6.0$) and $x_0 \geq 11a$ ($\beta = 6.2$). Therefore, the 'bump' is caused by x_0 -dependent vacuum contributions.

Another way to study the influence of excited states on the decay constant is

⁷Their values are checked through interpolation of data from [96] linearly in κ . There one has used the standard wave function and $T = 2L$.

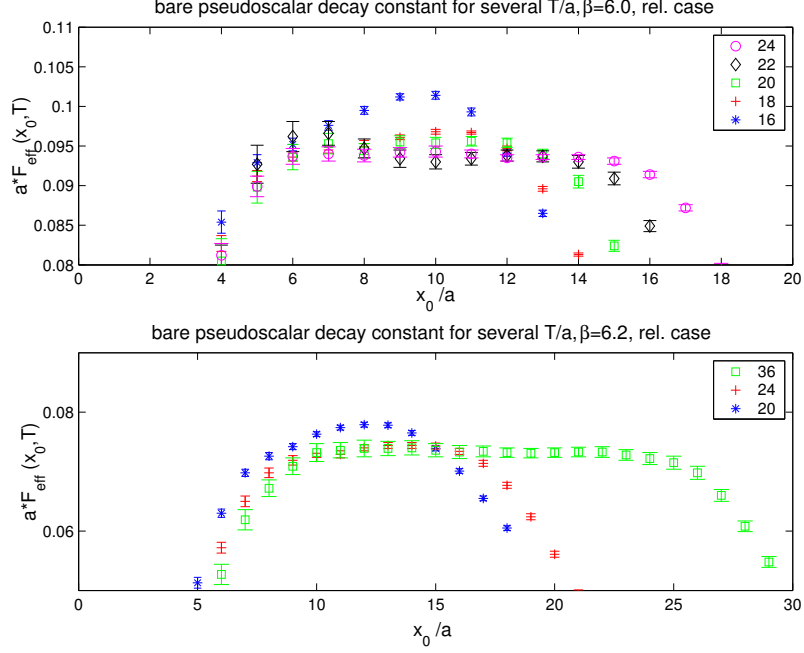


Figure 6.20: Change of the effective bare pseudoscalar decay constant (ground state) for several time extents T , a suitable ω_{opt} (given in the text), $\beta = 6.0$ and 6.2 , $\kappa \approx \kappa_s$, relativistic case.

to insert $f_1(T')$ for $T' \leq T$. The exponential factor has to be modified appropriately. The potential advantage of this method is that the plateau region should be almost unchanged. However, the *plateau level* may significantly change since $f_1(T')$ has more contaminations by excited states.⁸ Table 6.4 summarises the dependence of the plateau value $aF_{\text{PS}}(T, T')$ as a function of T' for two wave functions.

As expected, the result of aF_{PS} becomes independent of the wave function if $T = T'$ is large enough to neglect excited state contributions. Meson contributions always decrease the plateau level, whereas those from vacuum excitations always increase it.⁹ By means of eq. (2.91) one concludes for given T' that excited mesons have stronger contributions than vacuum cor-

⁸And the asymptotic value, $T \geq T' \rightarrow \infty$, for F_{PS} is independent of the wave function.

⁹One should keep in mind that shifts in the plateau level only indicate the *difference* of excited state contributions in both channels.

β	T/a	T'/a	$aF_{\text{PS}}(\omega_{\text{opt}})$	$aF_{\text{PS}}(\omega_1)$
6.0	24	10	0.0926(6)	0.0832(4)
		12	0.0909(5)	0.0824(4)
		14	0.0916(5)	0.0881(6)
		16	0.0919(6)	0.0904(6)
		18	0.0935(6)	0.0928(5)
		20	0.0946(11)	0.0939(10)
		22	0.0938(10)	0.0932(10)
		24	0.0938(7)	0.0938(4)
6.2	36	15	0.0692(9)	0.0656(9)
		20	0.0726(10)	0.0718(11)
		24	0.0726(13)	0.0721(13)
		36	0.0734(9)	0.0733(8)

Table 6.4: Systematic shift of the plateau level for aF_{PS} (bare case) as a function of $T' \leq T$, relativistic case. The value for $T = 3L/2$ has been fixed.

rections. Therefore, the plateau level is gradually pushed downwards for decreasing values of T' . This behaviour changes for $T' \approx 1$ fm. Since contributions from vacuum excitations are independent of the particular choice of ω , the systematic shift in the plateau level is a direct measure how large the contamination from excited meson states still is.

Obviously, the proposed ω_{opt} has rather small contributions from excited meson states. To safely extract the decay constant, one could have used $T' \geq 18a$ at $\beta = 6.0$ and $T' \geq 20a$ at $\beta = 6.2$ for the present level of statistics.

6.5.2 The Static Case

Data are analysed along the line of reference [98]. The quantity $r_0^{3/2}\Phi_{\text{RGI}}$, as given in eq. (3.26), is computed with $Z_{\text{A}}^{\text{stat}}$ from ref. [73]. The improvement coefficient $c_{\text{A}}^{\text{stat}}$ is known to 1-loop, refs. [72, 66], and $b_{\text{A}}^{\text{stat}}$ has been set to its tree-level value $b_{\text{A}}^{\text{stat}} = 1/2$. The subtracted light quark masses m_{q} , which are necessary for $\text{O}(a)$ -improvement in the massive case, are computed with κ_{c} -values from ref. [47] and are listed in table 6.5. Unfortunately, the extraction of Φ_{RGI} was only possible at $\beta = 6.0$. In all other cases, the correlation matrices were too noisy. Plateau values are investigated for two

β	κ_c	κ	am_q	Z_A^{stat}
6.0	0.135196	0.133901	0.0358	0.6944
6.2	0.135795	0.134905	0.0243	0.6804
6.45	0.135701	0.13510	0.0164	0.6769

Table 6.5: Renormalisation constants to compute Φ_{RGI} from available data.

optimal wave functions ω_{opt} and ω'_{opt} that are given by

$$v^{(0)} = (0.2103, 0.4400, 0.5969, 0.6371), \quad v^{(0)'} = (0.3927, 0.5301, 0.5222, 0.5404),$$

and for the trial wave functions ω_3, ω_4 . The larger time extent, $T = 24a$, is fixed and the smaller one is varied. The results are summarised in table 6.6 and shown in figure 6.21.

Obviously, the plateau level decreases for $16 \geq T'/a \geq 10$ by $\sim 20\%$, from $16a$ down to $14a$ still by about 10% . These corrections are described by eq. (2.91).¹⁰ The decrease of the plateau level is caused by excited meson state contributions. The smallest variation of the plateau level in T' has been observed for ω'_{opt} . Therefore, the latter is taken for the plot in figure 6.21.

Since the plateau level for $T'/a = 8$ is above the one for $T'/a = 10$, one concludes that vacuum corrections are very strong for small time extents.

For the largest pair of time extents, $(T', T) = (16a, 24a)$, table 6.6 gives

$$r_0^{3/2} \Phi_{\text{RGI}} \Big|_{\beta=6.0} = 1.82(5) \longrightarrow r_0 F_{B_s}^{\text{stat}} = 0.60(2),$$

setting $r_0 = 0.5 \text{ fm}$. Since statistical noise prevents a simulation of Φ_{RGI} at $T' > 16a$, it has not been possible to check how large remaining corrections to the asymptotics are.

¹⁰whereas light-light correlators have to be replaced by static-light ones and the factor $x_0 - T'/2$ is used instead of $x_0 - T'/2 - 1/(2\tilde{E}_0^{(\text{PS})})$

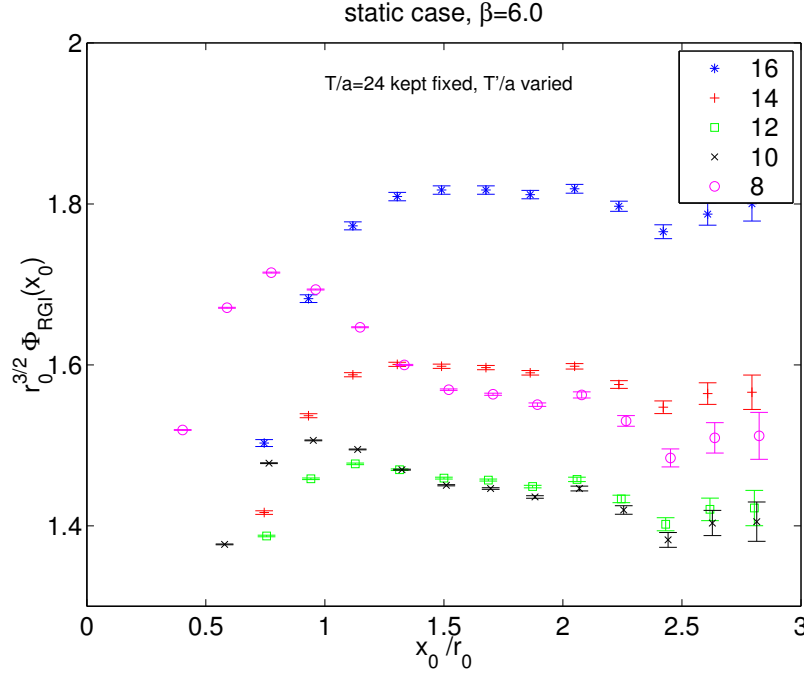


Figure 6.21: Change of $r_0^{3/2}\Phi_{\text{RGI}}$ for several time extents T' and ω'_{opt} at $\beta = 6.0$, $\kappa = \kappa_s$.

T'/a	$r_0^{3/2}\Phi_{\text{RGI}}$	ω'_{opt}	ω_3	ω_4
8	1.45(3)	1.56(3)	1.30(2)	1.31(4)
10	1.35(2)	1.44(2)	1.22(3)	1.22(3)
12	1.37(2)	1.45(2)	1.26(3)	1.26(3)
14	1.53(5)	1.59(3)	1.42(5)	1.42(4)
16	1.75(5)	1.82(5)	1.65(4)	1.65(4)

Table 6.6: The quantity $r_0^{3/2}\Phi_{\text{RGI}}$ at $\beta = 6.0$, $L = 16a$, $T = 24a$ fixed and various $T' < T$. The optimal wave functions are given in the text. Quoted plateau values are taken at $x_0 \approx 2r_0$.

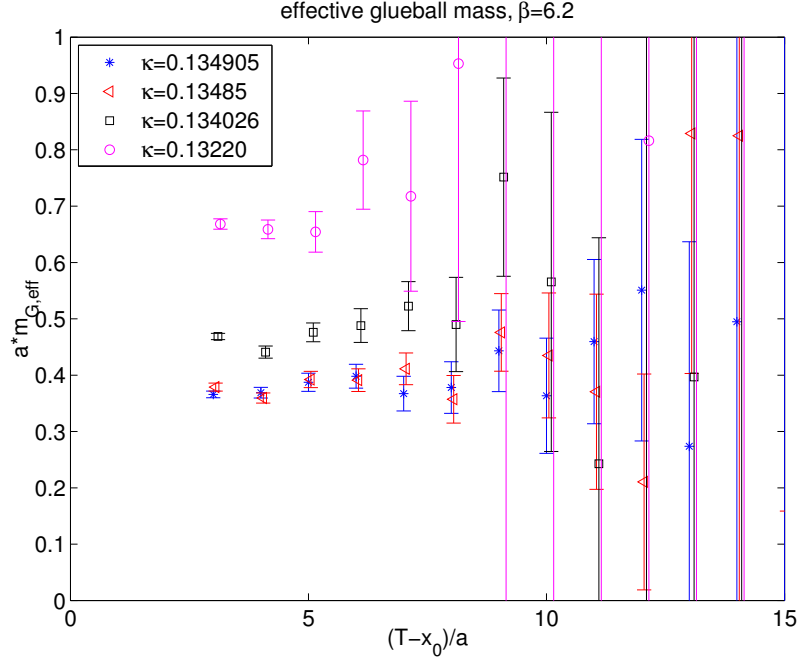
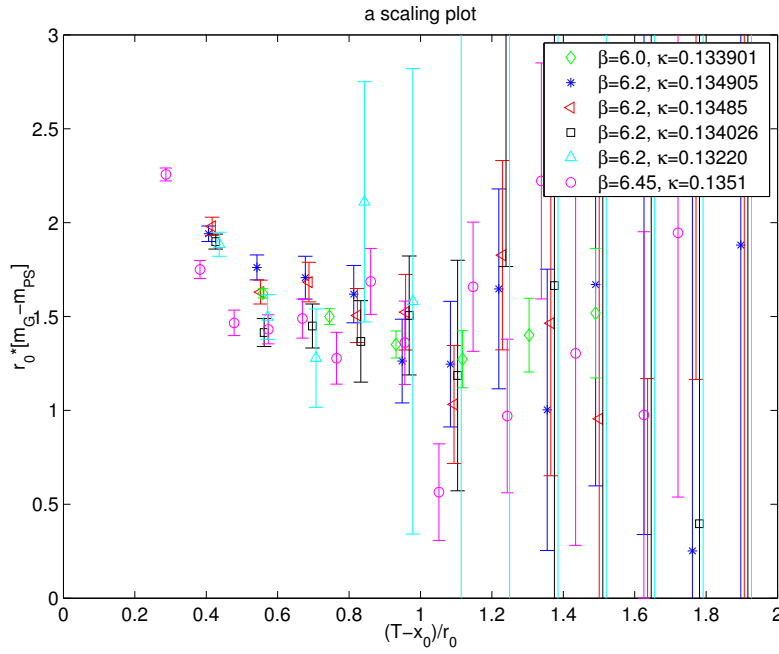
6.6 The Mass of the 0^{++} –Glueball

This section considers the practicality to extract the mass of the lowest-lying excitation in the vacuum channel from a combination of correlation functions, eq. (5.16). For instance, one may set $X = f_A^I(\omega_i)$ and $Y = f_P(\omega_j)$ for arbitrary wave functions. As a purely gluonic quantity, the extracted glueball mass m_G has to be independent of fermionic parameters,

1. c_A ,
2. meson wave functions ω ,
3. the quark mass (hopping parameter).

Point one has been checked by comparing m_G through setting c_A either to zero or to the fit value from its non-perturbative determination in ref. [40]. The second point is also confirmed provided that the time extent of the lattice will be large enough to suppress contributions from excited mesons. More than 2 fm are enough to get a long plateau of f_A^I/f_P in x_0 , thus separating excitations in the meson and vacuum channel well.

Point three, however, is *not* confirmed by the numerical findings of this work. At $\beta = 6.2$, the dependence on the quark mass (two sets have light quark masses at about the mass of the strange quark, m_s , another one at about $2m_s$, and a third one at roughly $4m_s$) is shown in figure 6.22. Extracted values of m_G , as they are given for four different quark masses, clearly depend on κ . The curves have moderate errors for $T - x_0 \leq 8a (\approx r_0/a)$, but for larger times statistical errors are very large. Even more surprising is that the difference $m_G - m_{PS}$ has a very weak dependency on the quark mass. This behaviour is not understood by the author of this thesis. The statistical errors are dominated by those of m_G .

Figure 6.22: Quark mass dependence of m_G (from eq. (5.16)) at $\beta = 6.2$.Figure 6.23: Plot of $m_G - m_{PS}$ for various quark masses and β -values.

6.7 Summary and Discussion of the Results

This section summarises the results for masses, the mass gap and decay constants as obtained by different extraction methods in the preceding sections and compares them to results of other works.

The variational principle is used to obtain estimates of the ground/first excited state mass and the gap between them. The optimal wave functions that come out are used to build up 'optimised' correlation functions f_A^I , f_P , f_1 , ... with a larger overlap to the particular energy level. In this work, masses of the ground and first excited state are given and their difference is an estimate of the gap. Alternatively, a suitable optimised wave function may be found for a pair of trial wave functions (combined with weight R_{ij}) such that the first excited state contribution is considerably reduced. And one more possibility to extract the gap has been explained.

6.7.1 The Relativistic Case

The results are listed in table 6.7. The ground state masses are statistically compatible. Results from the variational principle have a larger error but coincide with those extracted from f_A^I (or f_P) provided that (T', T) are large enough for the asymptotics to have set in. Results from reference [96] may be interpolated to the κ -values of the present work. This yields $am_{PS}^{\text{interpol}} = 0.3401(11)$ at $\beta = 6.0$ and $am_{PS}^{\text{interpol}} = 0.2493(6)$ at $\beta = 6.2$. They are in perfect agreement with the values quoted here.¹¹

However, it was not always possible to extract the mass of the first excited meson state unambiguously with available data sets. The variational principle requires a set of lattices. Estimates of am_{PS}^* at $\beta = 6.0$ are compatible. At $\beta = 6.2$, however, one should do runs with smaller time extents T' , and solve the GEVP there.

The results for the pseudoscalar gap seem to crucially depend on the methods. Its extraction from an effective mass plot of the axial current or pseudoscalar density strongly depends on the quality of $v^{(1)}$. Since this state decays fast, one still might have sizeable contributions from the second excited state at small values of x_0 where the signal is good. The indirect extraction of am_{PS}^* through the pseudoscalar gap has turned out to be a good alternative.

In reference [43], appendix A, one has estimated the size of the pseudoscalar

¹¹The decay constant aF_{PS} has also been checked and confirmed.

gap to be $r_0\Delta \approx 3.2$ ($a\Delta \approx 0.43$) at $\beta = 6.2, \kappa = 0.1345, L/a = 24$ and $T = 2L$. The value is reported to vary only little in the bare quark mass, so that it may be compared to the ones in table 6.7. They are about the same, but we are able to also give an error estimate.

β	method	am_{PS}	am_{PS}^*	$a\Delta$
6.0	GEVP, evals	0.341(4)	0.84(3)	0.49(3)
	ω_{opt} from GEVP	0.340(3)	0.83(5)	0.49(5)
	ω_{opt} from R_{ij}	0.340(3)	—	—
	Δ from $m_{\text{eff}}(f_{\text{P}})$	—	—	0.55(5)
6.2	GEVP, evals	0.250(5)	0.63(3)	0.38(3)?
	ω_{opt} from GEVP	0.250(5)	0.67(3)	0.42(3)
	ω_{opt} from R_{ij}	0.249(3)	—	—
	Δ from $m_{\text{eff}}(f_{\text{P}})$	—	—	0.41(5)

Table 6.7: Summary of pseudoscalar masses in the relativistic case, $\kappa \approx \kappa_s$.

There are two further data sets at $\beta = 6.2$ with quark masses of about twice and four times the strange quark mass available. The extraction of the gap, as explained in section 5.2, yields $r_0\Delta = 2.5(2)$ ($a\Delta = 0.34(3)$) for the former and $r_0\Delta = 2.0(1)$ ($a\Delta = 0.27(2)$) for the latter. Thus, the pseudoscalar gap decreases as the quark mass is increased.

6.7.2 The Static Case

As listed in table 6.8, the results of the ground state energy from the static axial current and those from the variational principle (only done at $\beta = 6.0$) differ significantly. Since the gap to the first excited state is rather small, one cannot expect to obtain a safe estimate for the true ground state energy, aE , from the GEVP within accessible values of $T' < T$. Since the variationally determined energy is larger than the one from a plateau in $E_{\text{eff}}(f_{\text{A}}^{\text{stat}})$, remaining contaminations of the former come from excited states in the meson channel.

As shown in figure 6.13, the plateau value of the subtracted ground state energy scales. Its continuum estimate is

$$L_0\Delta E_a = 0.420(14) \longleftrightarrow r_0\Delta E_a = 1.17(4).$$

This is a more precise result than the one given in ref. [76],

$$L_0\Delta E_a = 0.40(4).$$

The subtracted energy of the first excited state, however, shows sizeable scaling violations. Different methods to estimate the gap give consistent results. They all yield small values for this quantity. Equally precise estimates have been obtained by (1) the alternative determination of the gap, section 5.2, and (2) the energy difference, table 6.2. Their continuum estimates are

$$r_0\Delta = 1.38(13) \quad \text{and} \quad r_0\Delta = 1.58(12).$$

Using quenched data from ref. [99], table 2, one may extract $r_0\Delta \approx 1.10(5)$. A direct comparison is not possible since their β -value is far away from the continuum limit, hence their result should have large cutoff effects. But the order of magnitude is the same.

β	method	aE	aE^*	$a\Delta$
6.0	GEVP, evals	0.67(2)	0.88(5)	0.25(5)
	ω_{opt} from GEVP	0.630(6)	0.88(3)	0.25(4)
	ω_{opt} from R_{ij}	0.630(5)	–	–
	Δ from $E_{\text{eff}}(f_{\text{A}}^{\text{stat}})$	–	–	0.268(4)
6.2	GEVP, evals	–	–	–
	ω_{opt} from GEVP	0.541(6)	0.740(7)	0.199(9)
	ω_{opt} from R_{ij}	0.530(10)	–	–
	Δ from $E_{\text{eff}}(f_{\text{A}}^{\text{stat}})$	–	–	0.194(11)
6.45	GEVP, evals	–	–	–
	ω_{opt} from GEVP	0.465(6)	0.623(5)	0.158(8)
	ω_{opt} from R_{ij}	0.456(10)	–	–
	Δ from $E_{\text{eff}}(f_{\text{A}}^{\text{stat}})$	–	–	0.138(11)

Table 6.8: Summary of the results in the static case, $\kappa = \kappa_s$.

The extraction of the RGI matrix element of the static axial current was only successful at $\beta = 6.0$. For the best wave function and $(T', T) = (16a, 24a)$ it is

$$r_0^{3/2}\Phi_{\text{RGI}}|_{\beta=6.0} = 1.82(5) \quad \text{at } x_0 \approx 2r_0,$$

which is compatible to $r_0^{3/2}\Phi_{\text{RGI}} = 1.74(13)$ from ref. [98]. However, their result is an estimate of the continuum limit. Compared to the present work (where it is not possible to investigate still remaining systematic corrections of excited states to the asymptotics), their correlation functions have a much clearer signal at Euclidean time extents larger than 1.5 fm. In their case, decay constants may be computed for larger time extents and hence extracted more reliably.

Chapter 7

Conclusions and Outlook

In this work we have investigated how to construct improved meson interpolating fields from a basis of interpolating fields (here: a basis of hydrogen-like wave functions) at the Schrödinger functional boundaries by means of various procedures. These fields have been used to build up correlation functions with a suppressed contribution from the first excited state in the meson channel.

A procedure to construct these improved fields is the variational principle, as outlined in chapter 4. It has been applied to correlation matrices that have been built up from boundary-to-boundary correlators f_1 . Additionally, some alternative techniques to cancel contributions from the first excited meson state have been presented in chapter 5.

It has turned out that the variational principle provides suitable improved meson interpolating fields. The extraction of ground and first excited state masses of pseudoscalars, their gap as well as the decay constant of the ground state has been done in the light-light channel. The on-set of ground state dominance in the pseudoscalar mass and decay constant typically starts at Euclidean time separations as small as $x_0 \approx 0.7$ fm. This is a considerable improvement of the standard case, where the on-set starts after $x_0 \approx 1$ fm.

Regarding the static-light channel, improved meson interpolating fields have allowed to extract effective energies for all lattice spacings used, and estimating the continuum limit of $E - \Gamma^{\text{stat}}$ has been possible. The RGI matrix element Φ_{RGI} of the static axial current has been computed at $\beta = 6.0$ with small statistical errors. However, investigations at larger β -values have not been possible because of too much statistical noise. The matrix element

$\Phi_{\text{RGI}}|_{\beta=6.0}$ is in agreement with a recent (continuum) result of the ALPHA collaboration.

A disadvantage of the variational principle for f_1 -correlation matrices is a non-trivial systematic increase of generalised eigenvalues with meson quantum numbers due to contributions from vacuum excitations. The variationally determined energy does *not* yield an upper bound to the true ground state energy in the considered channel! Generalised eigenvectors, however, are not affected by these vacuum excitations.

We have shown how to extract information about the ground state and the gap between the ground and the first excited state on a single lattice. Compared to the variational principle, this may mean a large reduction of the computational effort.

Some investigations of the present work have been used in the computation of the B_s -meson decay constant [98] in the static approximation. Another example is a non-perturbative determination of the improvement coefficient c_A . First results may be found in ref. [100]. And it should be possible to carry these quenched simulations over to full QCD ($N_f = 2$) in the near future.

Some further potential applications are calculations of moments of structure functions [101] as well as nucleon masses [102].

Appendix A

Notation

Euclidean γ -matrices are listed here. They may be obtained from those in Minkowski space by

$$\gamma_0 = \gamma_0^{\text{Minkowski}}, \quad (\text{A.1})$$

$$\gamma_k = -i\gamma_k^{\text{Minkowski}}, \quad k = 1, 2, 3. \quad (\text{A.2})$$

Written in terms of the Pauli matrices σ_k ,

$$\sigma_1 = \begin{pmatrix} 0 & 1 \\ 1 & 0 \end{pmatrix}, \quad \sigma_2 = \begin{pmatrix} 0 & -i \\ i & 0 \end{pmatrix}, \quad \sigma_3 = \begin{pmatrix} 1 & 0 \\ 0 & -1 \end{pmatrix}, \quad (\text{A.3})$$

they are

$$\gamma_0 = \begin{pmatrix} 1 & 0 \\ 0 & -1 \end{pmatrix}, \quad \gamma_k = i \begin{pmatrix} 0 & -\sigma_k \\ \sigma_k & 0 \end{pmatrix}. \quad (\text{A.4})$$

Their product $\gamma_5 = \gamma_0\gamma_1\gamma_2\gamma_3$ reads

$$\gamma_5 = \begin{pmatrix} 0 & -1 \\ -1 & 0 \end{pmatrix}. \quad (\text{A.5})$$

The projectors $P_{\pm} = \frac{1}{2}(1 \pm \gamma_0)$ are diagonal in this representation,

$$P_+ = \begin{pmatrix} 1 & 0 \\ 0 & 0 \end{pmatrix}, \quad P_- = \begin{pmatrix} 0 & 0 \\ 0 & 1 \end{pmatrix}. \quad (\text{A.6})$$

The chiral representation of Dirac matrices [26] is used in the implementation of the APEmille code,

$$\gamma_\mu = \begin{pmatrix} 0 & \epsilon_\mu \\ \epsilon_\mu^\dagger & 0 \end{pmatrix} \quad (\text{A.7})$$

for $\mu = 0, 1, 2, 3$ and with

$$\epsilon_0 = -1, \quad \epsilon_k = -i\sigma_k, \quad k = 1, 2, 3. \quad (\text{A.8})$$

Again, the symbols σ_k are the Pauli matrices. For $\gamma_5 = \gamma_0\gamma_1\gamma_2\gamma_3$ one obtains

$$\gamma_5 = \begin{pmatrix} 1 & 0 \\ 0 & -1 \end{pmatrix}. \quad (\text{A.9})$$

All γ_μ are hermitean. The projectors $P_\pm = \frac{1}{2}(1 \pm \gamma_0)$ read

$$P_+ = \frac{1}{2} \begin{pmatrix} 1 & -1 \\ -1 & 1 \end{pmatrix}, \quad P_- = \frac{1}{2} \begin{pmatrix} 1 & 1 \\ 1 & 1 \end{pmatrix}. \quad (\text{A.10})$$

Appendix B

Program Implementation and related Issues

B.1 The Quark Propagator

In the improved theory [42], the quark propagator $S(x, y)$ is defined by

$$(D_I + m_0)S(x, y) = a^{-4}\delta_{x,y}, \quad 0 < x_0 < T, \quad (\text{B.1})$$

$$D_I = D + \delta D, \quad \delta D = \delta D_b + \delta D_v, \quad (\text{B.2})$$

with imposed boundary conditions,

$$P_+ S(x, y)|_{x_0=0} = 0, \quad P_- S(x, y)|_{x_0=T} = 0. \quad (\text{B.3})$$

In this notation, D is the standard Wilson-Dirac operator, eq. (2.34), and the correction term δD accounts for all $\mathcal{O}(a)$ improvements that are independent of the boundaries (v) or due to their presence (b). The relation to the $\mathcal{O}(a)$ improved fermionic part of the action $S_F^I = S_F + \delta S_F$, eqs. (2.33) and (2.42), is

$$\frac{\partial S_F^I}{\partial \psi(x)} = (D_I + m_0)\psi(x), \quad -\frac{\partial S_F^I}{\partial \bar{\psi}(x)} = \bar{\psi}(x)(\overleftarrow{D}_I^\dagger + m_0), \quad (\text{B.4})$$

for $0 < x_0 < T$. The quark propagator is γ_5 -hermitean,

$$S(x, y)^\dagger = \gamma_5 S(y, x) \gamma_5. \quad (\text{B.5})$$

This follows from the γ_5 -hermiticity of the improved Dirac operator. Therefore,

$$S(x, y)|_{y_0=0} P_- = 0, \quad S(x, y)|_{y_0=T} P_+ = 0. \quad (\text{B.6})$$

In general, the Dirac fields $\psi, \bar{\psi}$ may be decomposed into classical and fluctuation fields,

$$\psi(x) = \psi_{cl}(x) + \chi(x), \quad \bar{\psi}(x) = \bar{\psi}_{cl}(x) + \bar{\chi}(x), \quad (\text{B.7})$$

where the latter have zero boundary conditions. The classical quark field ψ_{cl} is defined such that it solves the homogeneous Dirac equation,

$$(D_I + m_0)\psi_{cl}(x) = 0, \quad 0 < x_0 < T. \quad (\text{B.8})$$

On the boundaries, it reproduces the classical boundary conditions,

$$P_+ \psi_{cl}(x)|_{x_0=0} = \rho(\mathbf{x}), \quad P_- \psi_{cl}(x)|_{x_0=T} = \rho'(\mathbf{x}). \quad (\text{B.9})$$

In the interior of the Schrödinger functional, the classical field is given by

$$\begin{aligned} \psi_{cl}(x) = a^3 \tilde{c}_t \sum_{\mathbf{y}} (S(x, y) U^\dagger(y - a\hat{0}, 0) \rho(\mathbf{y})|_{y_0=a} + \\ S(x, y) U(y, 0) \rho'(\mathbf{y})|_{y_0=T-a}). \end{aligned} \quad (\text{B.10})$$

Furthermore, using the adjoint Dirac equation one obtains

$$\bar{\psi}_{cl}(x) P_-|_{x_0=0} = \bar{\rho}(\mathbf{x}), \quad \bar{\psi}_{cl}(x) P_+|_{x_0=T} = \bar{\rho}'(\mathbf{x}), \quad (\text{B.11})$$

for the boundaries and

$$\begin{aligned} \bar{\psi}_{cl}(x) = a^3 \tilde{c}_t \sum_{\mathbf{y}} (\bar{\rho}(\mathbf{y}) U(y - a\hat{0}, 0) S(y, x)|_{y_0=a} + \\ \bar{\rho}'(\mathbf{y}) U^\dagger(y, 0) S(y, x)|_{y_0=T-a}) \end{aligned} \quad (\text{B.12})$$

in the interior $0 < x_0 < T$.

B.2 The Fermionic Generating Functional

To discuss fermionic correlation functions \mathcal{O} , it is suitable to write down the fermionic part of the generating functional and integrate quark fields out by hand in a gauge background average $\langle \dots \rangle_G$,

$$\langle \mathcal{O} \rangle = \langle |\mathcal{O}|_F \rangle_G, \quad (\text{B.13})$$

with a probability density proportional to

$$\exp(-S_{\text{eff}}[U]) = \det(D_I + m_0) \exp(-S_G^I[U]). \quad (\text{B.14})$$

In the quenched approximation, the fermion determinant in eq. (B.14) is set to a constant thus neglecting effects of sea quarks. As a rule of thumb, quenched quantities of interest usually differ by about 10% from unquenched ones. From the computational point of view, the quenched approximation represents a large reduction of the effort compared to the full, unquenched case, and is therefore useful for explorations of new fields and for testing of new ideas.

The fermionic generating functional is given by

$$\mathcal{Z}_F[\bar{\rho}', \rho', \bar{\rho}, \rho, \bar{\eta}, \eta, U] = \int D[\psi] D[\bar{\psi}] \exp(-S_F^I[U, \bar{\psi}, \psi] + S_S[\bar{\psi}, \psi]) \quad (\text{B.15})$$

with a source term for quark fields in the interior $0 < x_0 < T$,

$$S_S[\bar{\psi}, \psi] = a^4 \sum_{0 < x_0 < T} \sum_{\mathbf{x}} [\bar{\psi}(x) \eta(x) + \bar{\eta}(x) \psi(x)]. \quad (\text{B.16})$$

By substituting

$$\psi(x) = \frac{\delta}{\delta \bar{\eta}(x)}, \quad \bar{\psi}(x) = -\frac{\delta}{\delta \eta(x)}, \quad (\text{B.17})$$

in the polynomial \mathcal{O} , its quark field average is obtained through

$$[\mathcal{O}]_F = \left(\frac{1}{\mathcal{Z}_F} \mathcal{O} \mathcal{Z}_F \right)_{|\bar{\rho}' = \dots = \eta = 0}. \quad (\text{B.18})$$

In [42] it is shown, that Wick's theorem may be used such that eq. (B.18) reduces to algebraic expressions of quark two-point functions.

B.3 Quark Two-Point Functions

The complete list of non-zero contractions is taken from [42] and given here for later use,

$$\begin{aligned}
[\psi(x)\bar{\psi}(y)]_F &= S(x, y), \\
[\psi(x)\bar{\zeta}(\mathbf{y})]_F &= \tilde{c}_t S(x, y) U^\dagger(y - a\hat{0}, 0) P_+|_{y_0=a}, \\
[\psi(x)\bar{\zeta}'(\mathbf{y})]_F &= \tilde{c}_t S(x, y) U(y, 0) P_-|_{y_0=T-a}, \\
[\zeta(\mathbf{x})\bar{\psi}(y)]_F &= \tilde{c}_t P_- U(x - a\hat{0}, 0) S(x, y)|_{x_0=a}, \\
[\zeta'(\mathbf{x})\bar{\psi}(y)]_F &= \tilde{c}_t P_+ U^\dagger(x, 0) S(x, y)|_{x_0=T-a}, \\
[\zeta(\mathbf{x})\bar{\zeta}(\mathbf{y})]_F &= \tilde{c}_t^2 P_- U(x - a\hat{0}, 0) S(x, y) U^\dagger(y - a\hat{0}, 0) P_+|_{x_0=y_0=a} \\
&\quad - \frac{1}{2} \tilde{c}_s P_- \gamma_k (\nabla_k^* + \nabla_k) a^{-2} \delta_{\mathbf{x}, \mathbf{y}}, \\
[\zeta(\mathbf{x})\bar{\zeta}'(\mathbf{y})]_F &= \tilde{c}_t^2 P_- U(x - a\hat{0}, 0) S(x, y) U^\dagger(y, 0) P_-|_{x_0=a, y_0=T-a}, \\
[\zeta'(\mathbf{x})\bar{\zeta}(\mathbf{y})]_F &= \tilde{c}_t^2 P_+ U^\dagger(x, 0) S(x, y) U^\dagger(y - a\hat{0}, 0) P_+|_{x_0=T-a, y_0=a}, \\
[\zeta'(\mathbf{x})\bar{\zeta}'(\mathbf{y})]_F &= \tilde{c}_t^2 P_+ U^\dagger(x, 0) S(x, y) U(y, 0) P_-|_{x_0=y_0=T-a} \\
&\quad - \frac{1}{2} \tilde{c}_s P_+ \gamma_k (\nabla_k^* + \nabla_k) a^{-2} \delta_{\mathbf{x}, \mathbf{y}}.
\end{aligned}$$

For vanishing boundary conditions, contributions proportional to \tilde{c}_s will drop out.

B.4 Correlation Functions in terms of Two-point Functions

This will be considered on the example of f_A and f_1 . The generalisation to other cases is straightforward.

B.4.1 The Correlator f_A

Taking eqs. (2.51), (2.49) and (2.53) as definitions one finds for f_A ,

$$\begin{aligned}
f_A(x_0, \omega) &= -\frac{a^3}{2} \sum_{\mathbf{x}} \langle A_0^{ij}(x) \mathcal{O}^{ij}(\omega) \rangle \\
&= -\frac{a^9}{2L^3} \sum_{\mathbf{x}, \mathbf{y}, \mathbf{z}} \langle \bar{\psi}_{j\alpha A}(x) (\gamma_0 \gamma_5)_{AB} \psi_{i\alpha B}(x) \bar{\zeta}_{i\beta C}(\mathbf{y}) \omega(\mathbf{y} - \mathbf{z}) (\gamma_5)_{CD} \zeta_{j\beta D}(\mathbf{z}) \rangle.
\end{aligned}$$

Colour (α, β) and Dirac (A, B, \dots) indices that appear twice are summed over. Flavour indices i, j , however, are not contracted. Using the anti-commutation property of Grassmann variables, one obtains

$$f_A(x_0, \omega) = \frac{a^9}{2L^3} \sum_{\mathbf{x}, \mathbf{y}, \mathbf{z}} \langle (\gamma_5)_{CD} \zeta_{j\beta D}(\mathbf{z}) \bar{\psi}_{j\alpha A}(x) (\gamma_0 \gamma_5)_{AB} \psi_{i\alpha B}(x) \bar{\zeta}_{i\beta C}(\mathbf{y}) \omega(\mathbf{y} - \mathbf{z}) \rangle.$$

This amounts to a trace Tr' in Dirac and colour space,

$$f_A(x_0, \omega) = -\frac{a^9}{2L^3} \sum_{\mathbf{x}, \mathbf{y}, \mathbf{z}} \langle \text{Tr}' \left(\gamma_5 [\zeta_j(\mathbf{z}) \bar{\psi}_j(x)]_F \gamma_5 \gamma_0 [\psi_i(x) \bar{\zeta}_i(\mathbf{y})]_F \right) \rangle_G, \quad (\text{B.19})$$

where the anti-commutation property of γ_5 has been used and the fermionic part of the action has been integrated out. For that reason, the expectation value $\langle \dots \rangle_G$ is only taken with respect to the gauge action. Using the contractions given in the last section, f_A may be written as a product of two propagators. With

$$\gamma_5 [\zeta_j(\mathbf{z}) \bar{\psi}_j(x)]_F \gamma_5 = [\psi_j(x) \bar{\zeta}_j(\mathbf{z})]_F^\dagger \quad (\text{B.20})$$

one obtains

$$f_A(x_0, \omega) = -\frac{a^9}{2L^3} \sum_{\mathbf{x}, \mathbf{y}, \mathbf{z}} \langle \text{Tr}' \left([\psi_j(x) \bar{\zeta}_j(\mathbf{z})]_F^\dagger \gamma_0 [\psi_i(x) \bar{\zeta}_i(\mathbf{y})]_F \omega(\mathbf{y} - \mathbf{z}) \right) \rangle_G. \quad (\text{B.21})$$

A few comments are in order:

- the expression $[\]_F$ above is the quark propagator¹ for the flavour index i including the parallel transport from $y_0 = 0$ to a ,

$$S^i(x, \mathbf{y}) = [\psi_i(x) \bar{\zeta}_i(\mathbf{y})]_F. \quad (\text{B.22})$$

It solves the inhomogeneous Dirac equation

$$(D_I + m_0^i) S^i(x, \mathbf{y}) = a^{-4} \delta_{x_0, a} \delta_{\mathbf{x}, \mathbf{y}} \tilde{c}_t U^\dagger(x - a\hat{0}, 0) P_+. \quad (\text{B.23})$$

The static propagator is known explicitly,

$$S^h(x, \mathbf{y}) = a^{-3} \delta_{\mathbf{x}, \mathbf{y}} W(x) P_+, \quad a \leq x_0 \leq T - a, \quad (\text{B.24})$$

$$W(x) = U^\dagger(x - a\hat{0}, 0) \cdots U^\dagger((0, \mathbf{x}), 0), \quad a \leq x_0 \leq T. \quad (\text{B.25})$$

Thus, one has to compute the propagator from every point on the bottom to everywhere inside the Schrödinger functional box.

- for wave functions ω with the relative displacement $\mathbf{y} - \mathbf{z}$ of quark boundary fields as their argument, the summations over \mathbf{y} and \mathbf{z} cannot be performed independently.

The final formula for f_A is

$$f_A(x_0, \omega) = -\frac{a^9}{2L^3} \sum_{\mathbf{x}, \mathbf{y}, \mathbf{z}} \langle \text{Tr}' \left(S^j(x, \mathbf{z})^\dagger \gamma_0 S^i(x, \mathbf{y}) \omega(\mathbf{y} - \mathbf{z}) \right) \rangle_G. \quad (\text{B.26})$$

¹that is defined for $0 < x_0 < T$

B.4.2 The Correlator f_1

Starting with eq. (2.57) and applying Wick's theorem, one obtains

$$\begin{aligned}
f_1(\omega, \omega') &= -\frac{1}{2} \langle (\mathcal{O}^{ij})'(\omega') \mathcal{O}^{ij}(\omega) \rangle \\
&= -\frac{a^{12}}{2L^6} \sum_{\mathbf{y}, \mathbf{z}, \mathbf{u}, \mathbf{v}} \langle \text{Tr}' \left(\bar{\zeta}'_j(\mathbf{u}) \gamma_5 \omega'(\mathbf{v} - \mathbf{u})^* \zeta'_i(\mathbf{v}) \bar{\zeta}_i(\mathbf{y}) \gamma_5 \omega(\mathbf{y} - \mathbf{z}) \zeta_j(\mathbf{z}) \right) \rangle \\
&= \frac{a^{12}}{2L^6} \sum_{\mathbf{y}, \mathbf{z}, \mathbf{u}, \mathbf{v}} \langle \text{Tr}' \left(\gamma_5 [\zeta_j(\mathbf{z}) \bar{\zeta}'_j(\mathbf{u})]_{\text{F}} \gamma_5 \omega'(\mathbf{v} - \mathbf{u})^* [\zeta'_i(\mathbf{v}) \bar{\zeta}_i(\mathbf{y})]_{\text{F}} \omega(\mathbf{y} - \mathbf{z}) \right) \rangle_G \\
&= \frac{a^{12}}{2L^6} \sum_{\mathbf{y}, \mathbf{z}, \mathbf{u}, \mathbf{v}} \langle \text{Tr}' \left([\zeta'_j(\mathbf{u}) \bar{\zeta}_j(\mathbf{z})]_{\text{F}}^\dagger [\zeta'_i(\mathbf{v}) \bar{\zeta}_i(\mathbf{y})]_{\text{F}} \omega(\mathbf{y} - \mathbf{z}) \omega'(\mathbf{v} - \mathbf{u})^* \right) \rangle_G.
\end{aligned}$$

The term $[\]_{\text{F}}$ describes the propagation of a quark from $x_0 = 0$ to T including appropriate parallel transports from $x_0 = 0$ to a and $x_0 = T - a$ to T . To keep notation brief, one may introduce

$$S_T^i(\mathbf{x}, \mathbf{y}) = [\zeta'_i(\mathbf{x}) \bar{\zeta}_i(\mathbf{y})]_{\text{F}} = \tilde{c}_t P_+ U^\dagger(x, 0) S^i(x, \mathbf{y})|_{x_0=T-a}, \quad (\text{B.27})$$

and one finally obtains

$$f_1(\omega, \omega') = \frac{a^{12}}{2L^6} \sum_{\mathbf{y}, \mathbf{z}, \mathbf{u}, \mathbf{v}} \langle \text{Tr}' (S_T^j(\mathbf{u}, \mathbf{z})^\dagger S_T^i(\mathbf{v}, \mathbf{y}) \omega(\mathbf{y} - \mathbf{z}) \omega'(\mathbf{v} - \mathbf{u})^*) \rangle_G. \quad (\text{B.28})$$

Similar to the case of f_A , a knowledge of the propagator for all points from the bottom to the top of the Schrödinger functional is needed.

Appendix C

Numerical Results

C.1 Simulation Parameters

C.1.1 Wave functions

The trial basis consists of four hydrogen-like wave functions, as defined in eq. (4.32). This table lists the parameters n and r_H/r_0 .

WF#	1	2	3	4
n	0	0	1	0
r_H/r_0	0.1863	0.3726	0.3726	0.7457

Table C.1: The set of 4 hydrogen-like trial wave functions.

C.1.2 Data sets

All runs use the clover improved action for light quarks and the Eichten-Hill action for static ones. Table C.1 lists the $N_\omega = 4$ hydrogen-like wave functions. Data sets for smeared light and static quarks are summarised in tables C.2 and C.3. All runs use $\theta = 0$.

Hopping parameters in table C.3 correspond to those of the strange quark, $\kappa = \kappa_s$. Given κ -values in table C.2 are for quark masses at about the strange (written in roman), and those in *italic* roughly correspond to twice and four times the strange quark mass.

β	L/a	T/a	κ	N_{meas}
6.0	16	3	0.133901	1600
		6		4000
		8		4000
		10		4000
		12		4000
		14		3600
		16		2000
		18		5600
		20		1100
		22		1200
		24		4800
6.2	24	15	0.13485	580
		20		600
		24		590
		36		565
		36	<i>0.134026</i>	590
		36	<i>0.13220</i>	390

Table C.2: Relativistic case: List of several time extents of the Schrödinger functional box.

β	L/a	T/a	κ	N_{meas}
6.0	16	6	0.133901	9600
		8		4800
		10		19200
		12		8000
		14		4800
		16		12000
		24		4160
6.2	24	32	0.134905	900
		36		675
6.45	32	28	0.1351	275
		48		970

Table C.3: Static case: List of several time extents of the Schrödinger functional box.

C.2 The Variational Principle

C.2.1 The Relativistic Case

obs	T''/a	T'/a						
$m_{\text{PS}a}$ $m_{\text{PS}a}^*$ $a\Delta$	no	3	$T/a =$	6	8	10	12	14
				0.196(2)	0.201(1)	0.218(1)	0.248(1)	0.282(1)
				0.870(2)	0.824(1)	0.789(1)	0.765(3)	0.762(4)
				0.674(2)	0.623(2)	0.572(2)	0.518(2)	0.480(3)
			$T/a =$	16	18	20	22	24
				0.295(1)	0.305(1)	0.311(1)	0.312(1)	0.320(1)
$m_{\text{PS}a}$ $m_{\text{PS}a}^*$ $a\Delta$	no	6		0.758(10)	0.772(15)	0.87(13)	n.a.	n.a.
				0.463(9)	0.467(15)	0.56(11)	n.a.	n.a.
			$T/a =$	8	10	12	14	
				0.207(3)	0.232(2)	0.270(2)	0.308(2)	
				0.749(3)	0.727(3)	0.715(3)	0.728(5)	
				0.542(3)	0.495(2)	0.445(2)	0.420(5)	
$m_{\text{PS}a}$ $m_{\text{PS}a}^*$ $a\Delta$	no	6	$T/a =$	16	18	20	22	24
				0.321(2)	0.328(2)	0.332(2)	0.331(2)	0.335(2)
				0.744(14)	0.759(18)	0.81(8)	n.a.	n.a.
				0.423(14)	0.431(18)	0.48(8)	n.a.	n.a.
			$T/a =$	8	10	12	14	
				0.209(3)	0.234(2)	0.273(2)	0.314(2)	
$m_{\text{PS}a}$ $m_{\text{PS}a}^*$ $a\Delta$	3	6		0.756(3)	0.729(2)	0.713(3)	0.722(5)	
				0.547(3)	0.495(2)	0.440(3)	0.408(5)	
			$T/a =$	16	18	20	22	24
				0.329(2)	0.335(2)	0.338(2)	0.336(2)	0.338(2)
				0.737(13)	0.753(18)	0.88(14)	n.a.	n.a.
				0.409(13)	0.418(18)	0.54(14)	n.a.	n.a.
$m_{\text{PS}a}$ $m_{\text{PS}a}^*$ $a\Delta$	no	8	$T/a =$	10	12	14		
				0.255(3)	0.294(3)	0.326(2)		
				0.706(4)	0.704(4)	0.734(7)		
				0.451(3)	0.410(3)	0.408(3)		
			$T/a =$	16	18	20	22	24
				0.334(2)	0.338(2)	0.340(2)	0.351(2)	0.350(2)
$m_{\text{PS}a}$ $m_{\text{PS}a}^*$ $a\Delta$	no	8		0.758(16)	0.774(22)	0.77(8)	n.a.	n.a.
				0.424(16)	0.436(22)	0.44(8)	n.a.	n.a.
			$T/a =$	10	12	14		
				0.259(3)	0.306(2)	0.349(2)		
				0.703(4)	0.692(4)	0.711(7)		
				0.443(4)	0.387(4)	0.362(6)		
$m_{\text{PS}a}$ $m_{\text{PS}a}^*$ $a\Delta$	no	8	$T/a =$	16	18	20	22	24
				0.359(2)	0.360(2)	0.359(2)	0.354(2)	0.354(2)
				0.733(16)	0.752(22)	0.90(16)	n.a.	n.a.
				0.374(16)	0.392(22)	0.54(16)	n.a.	n.a.
			$T/a =$	10	12	14		
				0.258(3)	0.302(2)	0.341(2)		
$m_{\text{PS}a}$ $m_{\text{PS}a}^*$ $a\Delta$	no	8		0.704(4)	0.698(4)	0.720(7)		
				0.446(4)	0.396(4)	0.379(7)		
			$T/a =$	16	18	20	22	24
				0.350(2)	0.352(2)	0.352(2)	0.349(2)	0.348(2)
				0.743(16)	0.759(22)	0.82(9)	n.a.	n.a.
				0.393(16)	0.407(22)	0.47(9)	n.a.	n.a.

Table C.4: Effective masses directly from the Variational Principle, eq. (4.9), or à la Lüscher-Wolff, eq. (4.10), for the relativistic case, at $\beta = 6.0$ and $\kappa = 0.133901$.

obs	T''/a	T'/a					
	no	10	$T/a =$				
$m_{\text{PS}a}$					12		14
$m_{\text{PS}a}^*$					0.316(3)		0.331(3)
$m_{\text{PS}a}^{a\Delta}$					0.717(9)		0.776(11)
					0.401(9)		0.445(11)
$m_{\text{PS}a}$			$T/a =$				
$m_{\text{PS}a}^*$			16	18	20	22	24
$m_{\text{PS}a}^{a\Delta}$			0.333(3)	0.338(2)	0.339(2)	0.366(2)	0.364(2)
			0.799(25)	0.814(34)	0.74(10)	n.a.	n.a.
			0.466(23)	0.476(28)	0.40(10)	n.a.	n.a.
$m_{\text{PS}a}$	3	10	$T/a =$				
$m_{\text{PS}a}^*$					12		14
$m_{\text{PS}a}^{a\Delta}$					0.352(3)		0.394(3)
					0.682(8)		0.715(10)
					0.330(8)		0.321(9)
$m_{\text{PS}a}$			$T/a =$				
$m_{\text{PS}a}^*$			16	18	20	22	24
$m_{\text{PS}a}^{a\Delta}$			0.392(2)	0.385(2)	0.379(2)	0.370(2)	0.367(2)
			0.743(21)	0.764(28)	0.94(20)	n.a.	n.a.
			0.351(20)	0.379(28)	0.56(19)	n.a.	n.a.
$m_{\text{PS}a}$	6	10	$T/a =$				
$m_{\text{PS}a}^*$					12		14
$m_{\text{PS}a}^{a\Delta}$					0.346(3)		0.383(3)
					0.691(8)		0.729(10)
					0.346(8)		0.346(10)
$m_{\text{PS}a}$			$T/a =$				
$m_{\text{PS}a}^*$			16	18	20	22	24
$m_{\text{PS}a}^{a\Delta}$			0.380(2)	0.376(2)	0.371(2)	0.364(2)	0.361(2)
			0.756(21)	0.773(27)	0.85(10)	n.a.	n.a.
			0.376(21)	0.397(28)	0.47(10)	n.a.	n.a.
$m_{\text{PS}a}$	8	10	$T/a =$				
$m_{\text{PS}a}^*$					12		14
$m_{\text{PS}a}^{a\Delta}$					0.333(3)		0.361(2)
					0.702(8)		0.748(11)
					0.369(8)		0.387(10)
$m_{\text{PS}a}$			$T/a =$				
$m_{\text{PS}a}^*$			16	18	20	22	24
$m_{\text{PS}a}^{a\Delta}$			0.360(2)	0.359(2)	0.357(2)	0.353(2)	0.351(2)
			0.775(21)	0.780(28)	0.79(10)	n.a.	n.a.
			0.416(21)	0.421(28)	0.44(10)	n.a.	n.a.
$m_{\text{PS}a}$	no	12	$T/a =$				
$m_{\text{PS}a}^*$					14		
$m_{\text{PS}a}^{a\Delta}$					0.323(5)		
					0.861(25)		
					0.538(26)		
$m_{\text{PS}a}$			$T/a =$				
$m_{\text{PS}a}^*$			16	18	20	22	24
$m_{\text{PS}a}^{a\Delta}$			0.324(4)	0.334(3)	0.336(3)	0.371(2)	0.367(2)
			0.857(40)	0.858(45)	0.68(13)	n.a.	n.a.
			0.533(34)	0.523(36)	0.35(13)	n.a.	n.a.
$m_{\text{PS}a}$	3	12	$T/a =$				
$m_{\text{PS}a}^*$					14		
$m_{\text{PS}a}^{a\Delta}$					0.436(7)		
					0.747(20)		
					0.311(19)		
$m_{\text{PS}a}$			$T/a =$				
$m_{\text{PS}a}^*$			16	18	20	22	24
$m_{\text{PS}a}^{a\Delta}$			0.412(3)	0.396(2)	0.386(3)	0.374(3)	0.370(2)
			0.773(32)	0.792(37)	1.00(25)	n.a.	n.a.
			0.362(31)	0.395(37)	0.62(25)	n.a.	n.a.
$m_{\text{PS}a}$	6	12	$T/a =$				
$m_{\text{PS}a}^*$					14		
$m_{\text{PS}a}^{a\Delta}$					0.420(6)		
					0.765(21)		
					0.345(20)		
$m_{\text{PS}a}$			$T/a =$				
$m_{\text{PS}a}^*$			16	18	20	22	24
$m_{\text{PS}a}^{a\Delta}$			0.398(3)	0.386(2)	0.378(3)	0.368(3)	0.364(2)
			0.788(32)	0.800(36)	0.88(13)	n.a.	n.a.
			0.391(31)	0.414(36)	0.50(13)	n.a.	n.a.
$m_{\text{PS}a}$	8	12	$T/a =$				
$m_{\text{PS}a}^*$					14		
$m_{\text{PS}a}^{a\Delta}$					0.389(5)		
					0.794(22)		
					0.405(21)		
$m_{\text{PS}a}$			$T/a =$				
$m_{\text{PS}a}^*$			16	18	20	22	24
$m_{\text{PS}a}^{a\Delta}$			0.373(3)	0.368(2)	0.363(3)	0.357(3)	0.354(2)
			0.812(32)	0.806(37)	0.81(13)	n.a.	n.a.
			0.439(32)	0.438(37)	0.45(13)	n.a.	n.a.
$m_{\text{PS}a}$	10	12	$T/a =$				
$m_{\text{PS}a}^*$					14		
$m_{\text{PS}a}^{a\Delta}$					0.346(5)		
					0.835(23)		
					0.489(23)		
$m_{\text{PS}a}$			$T/a =$				
$m_{\text{PS}a}^*$			16	18	20	22	24
$m_{\text{PS}a}^{a\Delta}$			0.342(3)	0.346(2)	0.345(3)	0.344(3)	0.343(2)
			0.842(34)	0.843(37)	0.75(13)	n.a.	n.a.
			0.500(34)	0.497(37)	0.40(13)	n.a.	n.a.

Table C.5: Continuation of table C.4

obs	T''/a	T'/a						
m_{PS}^a m_{PS}^* $a\Delta$	no	14	$T/a =$	16	18	20	22	24
				0.319(13)	0.340(3)	0.342(3)	0.357(3)	0.355(2)
				0.85(10)	0.86(7)	n.a.	n.a.	n.a.
				0.53(8)	0.52(7)	n.a.	n.a.	n.a.
m_{PS}^a m_{PS}^* $a\Delta$	3	14	$T/a =$	16	18	20	22	24
				0.387(9)	0.376(4)	0.370(4)	0.358(3)	0.356(2)
				0.80(7)	0.81(6)	1.10(30)	n.a.	n.a.
				0.41(7)	0.44(6)	0.73(30)	n.a.	n.a.
m_{PS}^a m_{PS}^* $a\Delta$	6	14	$T/a =$	16	18	20	22	24
				0.375(7)	0.369(3)	0.364(4)	0.354(4)	0.353(2)
				0.81(7)	0.82(6)	0.92(17)	n.a.	n.a.
				0.44(7)	0.45(6)	0.56(17)	n.a.	n.a.
m_{PS}^a m_{PS}^* $a\Delta$	8	14	$T/a =$	16	18	20	22	24
				0.357(6)	0.357(3)	0.354(4)	0.349(4)	0.347(2)
				0.83(7)	0.81(6)	0.82(17)	n.a.	n.a.
				0.47(7)	0.45(6)	0.46(17)	n.a.	n.a.
m_{PS}^a m_{PS}^* $a\Delta$	10	14	$T/a =$	16	18	20	22	24
				0.338(6)	0.345(3)	0.345(4)	0.343(4)	0.342(2)
				0.85(7)	0.85(6)	0.72(17)	n.a.	n.a.
				0.51(7)	0.50(6)	0.37(17)	n.a.	n.a.
m_{PS}^a m_{PS}^* $a\Delta$	no	16	$T/a =$		18	20	22	24
					0.364(7)	0.360(5)	0.348(3)	0.348(3)
					n.a.	n.a.	n.a.	n.a.
					n.a.	n.a.	n.a.	n.a.
m_{PS}^a m_{PS}^* $a\Delta$	3	16	$T/a =$		18	20	22	24
					0.366(7)	0.361(5)	0.349(3)	0.349(2)
					0.86(12)	n.a.	n.a.	n.a.
					0.50(12)	n.a.	n.a.	n.a.
m_{PS}^a m_{PS}^* $a\Delta$	6	16	$T/a =$		18	20	22	24
					0.362(6)	0.358(5)	0.348(3)	0.347(2)
					0.83(12)	n.a.	n.a.	n.a.
					0.47(12)	n.a.	n.a.	n.a.
m_{PS}^a m_{PS}^* $a\Delta$	8	16	$T/a =$		18	20	22	24
					0.357(5)	0.353(4)	0.346(4)	0.345(2)
					0.79(12)	n.a.	n.a.	n.a.
					0.44(12)	n.a.	n.a.	n.a.
m_{PS}^a m_{PS}^* $a\Delta$	10	16	$T/a =$		18	20	22	24
					0.353(6)	0.350(5)	0.345(4)	0.343(2)
					0.84(12)	n.a.	n.a.	n.a.
					0.494(12)	n.a.	n.a.	n.a.
m_{PS}^a	no	18	$T/a =$			20	22	24
						0.355(9)	0.340(5)	0.343(3)
m_{PS}^a	3	18	$T/a =$			20	22	24
						0.356(9)	0.340(5)	0.343(2)
m_{PS}^a	6	18	$T/a =$			20	22	24
						0.353(8)	0.340(5)	0.342(2)
m_{PS}^a	8	18	$T/a =$			20	22	24
						0.349(8)	0.341(5)	0.341(2)
m_{PS}^a	10	18	$T/a =$			20	22	24
						0.348(8)	0.342(4)	0.340(2)
m_{PS}^a	no	20	$T/a =$				22	24
							0.326(11)	0.337(5)
m_{PS}^a	3	20	$T/a =$				22	24
							0.325(12)	0.337(5)
m_{PS}^a	6	20	$T/a =$				22	24
							0.327(10)	0.337(5)
m_{PS}^a	8	20	$T/a =$				22	24
							0.331(10)	0.337(5)
m_{PS}^a	10	20	$T/a =$				22	24
							0.336(11)	0.336(5)
m_{PS}^a	no	22	$T/a =$					24
								0.347(10)
m_{PS}^a	3	22	$T/a =$					24
								0.347(10)
m_{PS}^a	6	22	$T/a =$					24
								0.346(8)
m_{PS}^a	8	22	$T/a =$					24
								0.341(7)
m_{PS}^a	10	22	$T/a =$					24
								0.335(8)

Table C.6: Continuation of table C.4

T'/a	T/a	symbol				
8		b_1	0.1971	0.4345	0.6006	0.6416
		b_2	-0.7808	-0.4686	0.2254	0.3463
		b_3	0.4259	-0.4729	-0.4595	0.6195
		b_4	0.4124	-0.6065	0.6143	-0.2909
10	$v^{(0)}$		0.1419	-0.1156	0.9831	0
			0.7710	-0.6369	0	0
	$v^{(1)}$		0.0020	0.8020	0.5974	0
			0.0027	1.0000	0	0
12	$v^{(0)}$		0.1403	-0.4309	0.8914	0
			0.3096	-0.9509	0	0
	$v^{(1)}$		0.0100	0.9981	-0.0607	0
			0.0100	1.0000	0	0
14	$v^{(0)}$		0.0845	-0.5017	0.8609	0
			0.1662	-0.9861	0	0
	$v^{(1)}$		0.0181	0.9321	-0.3618	0
			0.0193	0.9998	0	0
16	$v^{(0)}$		0.0925	-0.6652	0.7409	0
			0.1378	-0.9905	0	0
	$v^{(1)}$		0.0210	0.8974	-0.4407	0
			0.0233	0.9997	0	0
18	$v^{(0)}$		0.0915	-0.6852	0.7225	0
			0.1324	-0.9912	0	0
	$v^{(1)}$		0.0065	0.2606	-0.9654	0
			0.0243	0.9997	0	0
20	$v^{(0)}$		0.1294	-0.9916	0	0
	$v^{(1)}$		0.0249	0.9997	0	0
22	$v^{(0)}$		0.1336	-0.9910	0	0
	$v^{(1)}$		0.0241	0.9997	0	0
24	$v^{(0)}$		0.1284	-0.9917	0	0
	$v^{(1)}$		0.0251	0.9997	0	0

Table C.7: Basis vectors b_i and state vectors $v^{(n)}$ in that basis, from the Variational Principle for the relativistic case, $\beta = 6.0$, $\kappa = 0.133901$.

T'/a	T/a	symbol				
10		b_1	0.1984	0.4352	0.6001	0.6411
		b_2	-0.7794	-0.4692	0.2256	0.3486
		b_3	0.4133	-0.4509	-0.4809	0.6283
		b_4	0.4271	-0.6222	0.5981	-0.2697
12	$v^{(0)}$		0.0736	-0.6785	0.7309	0
			0.1082	-0.9941	0	0
	$v^{(1)}$		0.0067	0.5452	-0.8383	0
			0.0121	0.9999	0	0
14	$v^{(0)}$		0.0300	-0.4548	0.8901	0
			0.0659	-0.9978	0	0
	$v^{(1)}$		0.0107	0.5247	-0.8512	0
			0.0200	0.9998	0	0
16	$v^{(0)}$		0.0379	-0.6518	0.7574	0
			0.0581	-0.9983	0	0
	$v^{(1)}$		0.0113	0.4925	-0.8702	0
			0.0227	0.9997	0	0
18	$v^{(0)}$		0.0371	-0.6479	0.7608	0
			0.0572	-0.9984	0	0
	$v^{(1)}$		0.0031	0.1300	-0.9915	0
			0.0231	0.9997	0	0
20	$v^{(0)}$		0.0567	-0.9984	0	0
	$v^{(1)}$		0.0232	0.9997	0	0
22	$v^{(0)}$		0.0586	-0.9983	0	0
	$v^{(1)}$		0.0225	0.9998	0	0
24	$v^{(0)}$		0.0562	-0.9984	0	0
	$v^{(1)}$		0.0235	0.9997	0	0

Table C.8: Continuation of table C.7

T'/a	T/a	symbol				
12		b_1	0.2034	0.4382	0.5987	0.6389
		b_2	-0.7794	-0.4649	0.2307	0.3509
		b_3	0.4014	-0.4384	-0.4933	0.6351
		b_4	0.4359	-0.6322	0.5874	-0.2556
14	$v^{(0)}$		0.0118	-0.2911	0.9566	0
			0.0407	-0.9992	0	0
	$v^{(1)}$		0.0110	0.6672	-0.7448	0
			0.0162	0.9999	0	0
16	$v^{(0)}$		0.0384	-0.9993	0	0
	$v^{(1)}$		0.0172	0.9999	0	0
18	$v^{(0)}$		0.0389	-0.9992	0	0
	$v^{(1)}$		0.0170	0.9999	0	0
20	$v^{(0)}$		0.0393	-0.9992	0	0
	$v^{(1)}$		0.0168	0.9999	0	0
22	$v^{(0)}$		0.0410	-0.9992	0	0
	$v^{(1)}$		0.0161	0.9999	0	0
24	$v^{(0)}$		0.0387	-0.9992	0	0
	$v^{(1)}$		0.0171	0.9999	0	0

Table C.9: Continuation of table C.7

obs	T''/a	T'/a	$T/a =$		
$m_{\text{PS}}a$ m_{PS}^*a $a\Delta$	no	15	20	24	36
			0.248(4)	0.249(3)	0.250(2)
			0.626(30)	0.550(35)	0.49(10)
			0.378(30)	0.301(36)	0.24(10)
$m_{\text{PS}}a$ m_{PS}^*a $a\Delta$	no	20	$T/a =$	24	36
				0.247(4)	0.250(2)
				0.46(8)	0.43(12)
				0.21(8)	0.18(12)
$m_{\text{PS}}a$ m_{PS}^*a $a\Delta$	15	20	$T/a =$	24	36
				0.249(6)	0.250(2)
				0.46(9)	0.43(13)
				0.21(9)	0.18(13)
$m_{\text{PS}}a$ m_{PS}^*a $a\Delta$	no	24	$T/a =$		36
					0.255(4)
					n.a.
					n.a.
$m_{\text{PS}}a$ m_{PS}^*a $a\Delta$	15	24	$T/a =$		36
					0.250(3)
					0.42(17)
					0.17(17)
$m_{\text{PS}}a$ m_{PS}^*a $a\Delta$	20	24	$T/a =$		36
					0.251(3)
					0.42(17)
					0.17(17)

Table C.10: Effective masses directly from the Variational Principle, eq. (4.9), or à la Lüscher-Wolff, eq. (4.10), for the relativistic case, at $\beta = 6.2$ and $\kappa = 0.13485$.

T'/a	T/a	symbol				
15		b_1	0.1779	0.4143	0.5963	0.6642
		b_2	-0.7137	-0.5337	0.0880	0.4451
		b_3	0.4887	-0.2725	-0.5969	0.5749
		b_4	0.4693	-0.6850	0.5295	-0.1738
	20	$v^{(0)}$	0.0290	-0.4651	0.8848	0
			0.0626	-0.9980	0	0
		$v^{(1)}$	0.0056	0.1731	-0.9849	0
			0.0296	0.9996	0	0
	24	$v^{(0)}$	0.0438	-0.6503	0.7584	0
			0.0669	-0.9978	0	0
		$v^{(1)}$	0.0018	0.0737	0.9973	0
			0.0277	0.9996	0	0
	36	$v^{(0)}$	0.0367	-0.5727	0.8189	0
			0.0637	-0.9980	0	0
		$v^{(1)}$	0.0005	0.0265	0.9997	0
			0.0291	0.9996	0	0
20		b_1	0.1948	0.4266	0.5939	0.6537
		b_2	-0.7167	-0.5189	0.1093	0.4530
		b_3	0.5035	-0.3164	-0.5662	0.5708
		b_4	0.4415	-0.6698	0.5611	-0.2042
	24	$v^{(0)}$	0.1729	-0.9849	0	0
		$v^{(1)}$	0.0030	1.0000	0	0
	36	$v^{(0)}$	0.0948	-0.9955	0	0
		$v^{(1)}$	0.0056	1.0000	0	0
24		b_1	0.1960	0.4275	0.5937	0.6529
		b_2	0.6844	0.5388	-0.0813	-0.4844
		b_3	0.5888	-0.3583	-0.5063	0.5182
		b_4	0.3827	-0.6313	0.6201	-0.2654
	36	$v^{(0)}$	0.0571	0.9984	0	0
		$v^{(1)}$	-0.0041	1.0000	0	0

Table C.11: Basis vectors b_i and state vectors $v^{(n)}$ in that basis, from the Variational Principle for the relativistic case, at $\beta = 6.2$ and $\kappa = 0.13485$.

C.2.2 The Static Case

obs	T''/a	T'/a						
	no	6	$T/a =$	8	10	12	14	16
aE				0.455(6)	0.504(3)	0.554(3)	0.600(4)	0.634(5)
aE^*				0.755(7)	0.776(4)	0.800(6)	0.835(19)	0.793(23)
$a\Delta$				0.299(2)	0.272(2)	0.246(6)	0.235(21)	0.159(25)
	no	8	$T/a =$		10	12	14	16
aE					0.552(3)	0.599(3)	0.637(6)	0.667(8)
aE^*					0.798(4)	0.826(8)	0.870(27)	0.803(30)
$a\Delta$					0.246(3)	0.227(9)	0.233(31)	0.135(35)
	6	8	$T/a =$		10	12	14	16
aE					0.553(3)	0.604(3)	0.648(5)	0.678(6)
aE^*					0.798(4)	0.823(8)	0.861(25)	0.801(28)
$a\Delta$					0.245(3)	0.219(8)	0.213(28)	0.123(31)
	no	10	$T/a =$			12	14	16
aE						0.632(6)	0.659(11)	0.684(12)
aE^*						0.866(16)	0.924(44)	0.820(41)
$a\Delta$						0.234(19)	0.266(51)	0.136(48)
	6	10	$T/a =$			12	14	16
aE						0.655(5)	0.696(7)	0.714(8)
aE^*						0.848(15)	0.893(37)	n.a.
$a\Delta$						0.193(17)	0.197(41)	n.a.
	8	10	$T/a =$			12	14	16
aE						0.646(5)	0.679(9)	0.714(8)
aE^*						0.854(15)	0.906(40)	n.a.
$a\Delta$						0.208(17)	0.227(46)	n.a.
	no	12	$T/a =$				14	16
aE							0.671(28)	0.687(21)
aE^*							0.99(9)	0.82(6)
$a\Delta$							0.32(10)	0.13(6)
	6	12	$T/a =$				14	16
aE							0.737(15)	0.749(11)
aE^*							0.94(8)	n.a.
$a\Delta$							0.20(8)	n.a.
	8	12	$T/a =$				14	16
aE							0.713(18)	0.750(11)
aE^*							0.96(8)	n.a.
$a\Delta$							0.24(9)	n.a.
	10	12	$T/a =$				14	16
aE							0.686(22)	0.749(11)
aE^*							0.98(9)	n.a.
$a\Delta$							0.30(11)	n.a.
	no	14	$T/a =$					16
aE								0.767(25)
	6	14	$T/a =$					16
aE								0.767(25)
	8	14	$T/a =$					16
aE								0.767(25)
	10	14	$T/a =$					16
aE								0.768(25)

Table C.12: Effective energies directly from the Variational Principle, eq. (4.9), or à la Lüscher-Wolff, eq. (4.10), for the static case, at $\beta = 6.0$ and $\kappa = 0.133901$.

T'/a	T/a	symbol				
8		b_1	0.23616	0.45554	0.58861	0.62470
		b_2	-0.80900	-0.39648	0.27626	0.33466
		b_3	0.42765	-0.60469	-0.32672	0.58713
		b_4	0.32689	-0.51927	0.68591	-0.39120
	10	$v^{(0)}$	0.2494	0.1714	0.9531	0
			0.8544	0.5196	0	0
		$v^{(1)}$	-0.0100	0.4519	0.8920	0
			-0.0159	0.9999	0	0
	12	$v^{(0)}$	0.5809	-0.1630	0.7975	0
			0.9587	-0.2846	0	0
		$v^{(1)}$	0.0033	0.5399	0.8417	0
			0.0077	1.0000	0	0
	14	$v^{(0)}$	0.5783	-0.8159	0	0
		$v^{(1)}$	0.0368	0.9993	0	0
	16	$v^{(0)}$	0.4659	-0.8849	0	0
		$v^{(1)}$	0.0495	0.9988	0	0
10		b_1	0.2314	0.4524	0.5899	0.6275
		b_2	-0.8035	-0.4092	0.2685	0.3388
		b_3	0.4312	-0.5862	-0.3482	0.5909
		b_4	0.3388	-0.5332	0.6772	-0.3771
	12	$v^{(0)}$	0.4554	-0.8903	0	0
		$v^{(1)}$	0.0307	0.9995	0	0
	14	$v^{(0)}$	0.2736	-0.9618	0	0
		$v^{(1)}$	0.0552	0.9985	0	0
	16	$v^{(0)}$	0.1906	-0.9817	0	0
		$v^{(1)}$	0.0807	0.9967	0	0
12		b_1	0.2402	0.4571	0.5869	0.6236
		b_2	-0.7998	-0.4055	0.2733	0.3481
		b_3	0.4243	-0.5695	-0.3679	0.6003
		b_4	0.3501	-0.5498	0.6675	-0.3600
	14	$v^{(0)}$	0.1826	-0.9832	0	0
		$v^{(1)}$	0.0552	0.9985	0	0
	16	$v^{(0)}$	0.0940	-0.9956	0	0
		$v^{(1)}$	0.1081	0.9941	0	0

Table C.13: Basis vectors b_i and state vectors $v^{(n)}$ in that basis, from the Variational Principle in the static approximation, $\beta = 6.0, \kappa = 0.133901$.

C.3 Alternative Extraction of the Ground State Mass

C.3.1 Relativistic case, $\beta = 6.2$

(i, j)	x_0/a	8	9	10	11	12	13	14
	7							
R_{ij} from F_{eff} , where $d_0(\omega_i)/d_0(\omega_j)$ is from f_1								
(1,2)	0.05(8)	0.19(6)	0.22(6)	0.27(7)	0.29(7)	0.30(6)	0.38(6)	0.28(19)
(1,3)	0.02(4)	0.10(4)	0.12(4)	0.15(5)	0.18(6)	0.18(5)	0.25(5)	0.16(14)
(1,4)	0.02(3)	0.08(3)	0.10(4)	0.13(5)	0.15(5)	0.16(5)	0.22(5)	0.14(13)
(2,3)	0.47(3)	0.53(3)	0.55(3)	0.58(4)	0.60(4)	0.61(4)	0.66(4)	0.58(11)
(2,4)	0.38(3)	0.44(3)	0.46(4)	0.49(4)	0.52(5)	0.52(4)	0.58(5)	0.50(12)
(3,4)	0.81(1)	0.83(1)	0.83(1)	0.85(2)	0.87(2)	0.86(2)	0.88(2)	0.85(4)
R_{ij} from $m_{\text{eff}}(f_A^I)$, where $d_0(\omega_i)/d_0(\omega_j)$ is from f_1								
(1,2)	0.10(4)	0.17(5)	0.24(5)	0.26(5)	0.29(5)	0.30(5)	0.33(5)	0.33(8)
(1,3)	0.05(2)	0.09(3)	0.13(3)	0.15(4)	0.17(4)	0.18(4)	0.21(5)	0.21(7)
(1,4)	0.04(2)	0.08(2)	0.11(3)	0.13(3)	0.15(4)	0.16(4)	0.18(4)	0.18(6)
(2,3)	0.50(2)	0.53(2)	0.57(3)	0.58(3)	0.60(3)	0.61(3)	0.63(3)	0.62(5)
(2,4)	0.42(2)	0.45(2)	0.48(3)	0.49(3)	0.52(4)	0.53(4)	0.55(4)	0.54(6)
(3,4)	0.83(1)	0.84(1)	0.85(1)	0.85(1)	0.86(1)	0.87(1)	0.87(2)	0.87(2)
R_{ij} from $m_{\text{eff}}(f_A^I)$, where $d_0(\omega_i)/d_0(\omega_j)$ is from f_A^I								
(1,2)	0.10(4)	0.17(4)	0.23(5)	0.26(5)	0.29(5)	0.30(5)	0.33(5)	0.33(8)
(1,3)	0.05(2)	0.09(3)	0.13(3)	0.15(4)	0.17(4)	0.18(4)	0.21(4)	0.20(7)
(1,4)	0.04(2)	0.08(2)	0.11(3)	0.13(3)	0.15(4)	0.16(4)	0.18(4)	0.18(6)
(2,3)	0.50(2)	0.53(2)	0.56(3)	0.58(3)	0.60(3)	0.61(3)	0.62(3)	0.62(5)
(2,4)	0.41(2)	0.44(2)	0.47(3)	0.49(3)	0.51(4)	0.53(4)	0.54(4)	0.54(6)
(3,4)	0.83(1)	0.84(1)	0.84(1)	0.85(1)	0.86(1)	0.87(1)	0.87(2)	0.87(2)
R_{ij} from $m_{\text{eff}}(f_P)$, where $d_0(\omega_i)/d_0(\omega_j)$ is from f_1								
(1,2)	-0.25(6)	-0.01(5)	0.11(4)	0.17(4)	0.21(5)	0.25(6)	0.29(6)	0.33(5)
(1,3)	-0.09(2)	-0.01(2)	0.05(2)	0.09(3)	0.12(3)	0.14(4)	0.17(5)	0.21(5)
(1,4)	-0.07(2)	-0.01(2)	0.04(2)	0.07(2)	0.10(3)	0.12(4)	0.15(4)	0.18(4)
(2,3)	0.37(2)	0.45(2)	0.50(2)	0.53(2)	0.55(3)	0.57(4)	0.59(4)	0.62(4)
(2,4)	0.29(2)	0.36(2)	0.41(2)	0.44(2)	0.46(3)	0.48(4)	0.51(4)	0.54(4)
(3,4)	0.78(1)	0.80(1)	0.82(1)	0.83(1)	0.84(1)	0.84(2)	0.85(2)	0.86(2)

Table C.14: Various determinations of R_{ij} to build up ω_{opt} from a linear combination of trial WFs ω_i and ω_j , $\beta = 6.2$, relativistic case.

x_0/a	WF#	1	2	3	4
5		0.005(13)	0.31(4)	0.13(1)	0.12(1)
6		-0.025(27)	0.18(2)	0.12(1)	0.11(1)
7		-0.13(12)	0.14(2)	0.11(1)	0.11(1)
8		-5(65)	0.14(3)	0.12(2)	0.11(1)
9		0.74(130)	0.14(3)	0.12(2)	0.12(2)
10		0.8(2.1)	0.17(4)	0.14(3)	0.13(3)
11		2(13)	0.23(11)	0.19(6)	0.18(6)
12		3(61)	0.31(28)	0.24(14)	0.22(12)
13		0.5(3.3)	0.21(26)	0.18(16)	0.17(14)

Table C.15: Values for $R_{f_{\Lambda}^I f_P}$ to build up f_{Λ}^I with an absent first excited pseudoscalar state, $\beta = 6.2$, $\kappa = 0.13485$, relativistic case.

β	6.0	6.2	6.2	6.2	6.45
L/a	16	24	24	24	32
κ	0.133901	0.13485	0.134026	0.13220	0.1351
$R_{f_{\Lambda}^I f_P}$	0.08(1)	0.12(2)	0.15(2)	0.26(2)	0.05(1)

Table C.16: Some more extracted R -values for the application of eq. (5.10).

C.3.2 Static Case, $\beta = 6.45$

(i, j)	x_0/a	7	8	9	10	11	12	13	14
(4,1)	0.63(51)	0.64(51)	0.65(50)	0.65(49)	0.65(49)	0.64(48)	0.67(48)	0.66(46)	
(4,2)	0.73(24)	0.71(23)	0.70(22)	0.69(21)	0.68(21)	0.66(21)	0.66(20)	0.65(19)	
(4,3)	1.07(13)	1.13(16)	1.16(19)	1.19(20)	1.21(22)	1.23(23)	1.22(22)	1.23(22)	
(3,1)	0.59(52)	0.57(50)	0.56(48)	0.55(46)	0.54(45)	0.52(44)	0.55(44)	0.54(43)	
(3,2)	0.68(27)	0.63(26)	0.60(25)	0.58(25)	0.56(25)	0.54(25)	0.55(24)	0.53(23)	
(2,1)	0.87(50)	0.90(50)	0.93(51)	0.95(51)	0.96(51)	0.97(51)	1.00(52)	1.02(51)	

Table C.17: Table of weights R_{ij} (E_{eff} and $d_0(\omega_i)/d_0(\omega_j)$ are extracted from $O(a)$ -improved $f_{\Lambda}^{\text{stat}}$) to build up ω_{opt} from ω_i and ω_j , $\beta = 6.45$, static case.

Bibliography

- [1] Weyl, H., Electron and gravitation, Z. Phys. 56 (1929) 330,
- [2] S.L. Glashow, Nucl. Phys. 22 (1961) 579.
- [3] J. Goldstone, A. Salam and S. Weinberg, Phys. Rev. 127 (1962) 965.
- [4] S. Weinberg, Phys. Rev. Lett. 19 (1967) 1264.
- [5] P. Franzini, Phys. Rep. C173 (1989) 1.
- [6] E.A. Paschos and U. Türke, Phys. Rep. C178 (1989) 145.
- [7] BaBar Coll., G. Raven, Measurements of Lifetimes, Mixing and CP Violation of B Mesons with the BaBar Detector, (2002), hep-ex/0205045,
- [8] Belle Coll., T. Higuchi et. al., Improved Measurement of CP Asymmetry in the Neutral B Meson System, hep-ex/0205020.
- [9] Belle Coll., K. Abe et. al., Observation of Mixing induced CP Violation in the neutral B Meson System, Phys.Rev. D66 (2002) 032007, hep-ex/0205027.
- [10] P.W. Higgs, Phys. Lett. 12 (1964) 132.
- [11] Fritzsche, H. and Gell-Mann, Murray and Leutwyler, H., Advantages of the Color Octet Gluon Picture, Phys. Lett. B47 (1973) 365,
- [12] Gell-Mann, Murray, A Schematic model of baryons and mesons, Phys. Lett. 8 (1964) 214,
- [13] Zweig, G., An SU(3) Model for Strong Interaction Symmetry and its Breaking. 2, CERN-TH-412.

- [14] 't Hooft, Gerard, The Birth of Asymptotic Freedom, unpublished .
- [15] Politzer, H. David, Reliable Perturbation Results for Strong Interactions?, Phys. Rev. Lett. 30 (1973) 1346,
- [16] F. J. Dyson, The S matrix in quantum electrodynamics, Phys. Rev. 75 (1949) 1736,
- [17] I. Monvay and G. Münster, Quantum Fields on a Lattice, Cambridge University Press (1994).
- [18] Martin Lüscher, Advanced lattice QCD, (1998), hep-lat/9802029,
- [19] R. Gupta, Introduction to Lattice QCD, (1997), hep-lat/9807028.
- [20] G. Münster, M. Walzl, Lattice Gauge Theory - A Short Primer, (2000), hep-lat/0012005.
- [21] K. G. Wilson, Quark Confinement. (TALK).
- [22] H.B. Nielsen and M. Ninomiya, Nucl. Phys. 185 (1981) 20.
- [23] Paul H. Ginsparg and Kenneth G. Wilson, A Remnant of Chiral Symmetry on the Lattice, Phys. Rev. D25 (1982) 2649.
- [24] K. Symanzik, Continuum Limit and improved Action in Lattice Theories. 1. Principles and ϕ^4 Theory, Nucl. Phys. B226 (1983) 187.
- [25] K. Symanzik, Some topics in quantum field theory, in Mathematical problems in theoretical physics, eds. R. Schrader et al., Lecture Notes in Physics Vol. 153 (Springer, New York, 1982).
- [26] Martin Lüscher and Stefan Sint and Rainer Sommer and Peter Weisz, Chiral symmetry and $O(a)$ improvement in lattice QCD, Nucl. Phys. B478 (1996) 365, hep-lat/9605038.
- [27] K. Symanzik, Nucl. Phys. B190 (1981) 1.
- [28] Martin Lüscher and Rajamani Narayanan and Peter Weisz and Ulli Wolff, The Schrödinger functional: A Renormalizable probe for non-Abelian gauge theories, Nucl. Phys. B384 (1992) 168, hep-lat/9207009.

- [29] Stefan Sint, On the Schrödinger functional in QCD, Nucl. Phys. B421 (1994) 135, hep-lat/9312079.
- [30] Rainer Sommer, Non-perturbative renormalization of QCD, (1997), hep-ph/9711243,
- [31] Martin Lüscher and Peter Weisz and Ulli Wolff, A Numerical method to compute the running coupling in asymptotically free theories, Nucl. Phys. B359 (1991) 221.
- [32] Stefan Sint, One loop renormalization of the QCD Schrödinger functional, Nucl. Phys. B451 (1995) 416, hep-lat/9504005.
- [33] A. Bode, Two loop expansion of the Schrödinger functional coupling α -SF in SU(3) lattice gauge theory, Nucl. Phys. Proc. Suppl. 63 (1998) 796, hep-lat/9710043.
- [34] Martin Lüscher and Rainer Sommer and Peter Weisz and Ulli Wolff, A Precise determination of the running coupling in the SU(3) Yang-Mills theory, Nucl. Phys. B413 (1994) 481, hep-lat/9309005.
- [35] ALPHA, Achim Bode and Peter Weisz and Ulli Wolff, Two loop computation of the Schroedinger functional in lattice QCD, Nucl. Phys. B600 (2000) 517, hep-lat/9911018, Erratum-ibid.B600:453,2001, Erratum-ibid.B608:481,2001,
- [36] Kenneth G. Wilson, Confinement of Quarks, Phys. Rev. D10 (1974) 2445.
- [37] ALPHA, Bernd Gehrman, Juri Rolf, Stefan Kurth, Ulli Wolff, Schrödinger functional at negative flavor number, Nucl. Phys. B612 (2001) 3, hep-lat/0106025,
- [38] ALPHA, M. Della Morte et. al., Recent results on the running coupling in QCD with two massless flavors, DESY 02-124 (Sep. 2002) 1, hep-lat/0209023,
- [39] B. Sheikholeslami and R. Wohlert, Improved Continuum Limit Lattice Action for QCD with Wilson Fermions, Nucl. Phys. B259 (1985) 572.

- [40] Martin Lüscher and Stefan Sint and Rainer Sommer and Peter Weisz and Ulli Wolff, Nonperturbative $O(a)$ improvement of lattice QCD, Nucl. Phys. B491 (1997) 323, hep-lat/9609035.
- [41] Karl Jansen and Rainer Sommer, The Nonperturbative $O(a)$ improved action for dynamical Wilson fermions, Nucl.Phys.Proc.Suppl. 63 (1998) 853, hep-lat/9709022.
- [42] M. Lüscher and P. Weisz, $O(a)$ improvement of the axial current in lattice QCD to one loop order of perturbation theory, Nucl. Phys. B479 (1996) 429, hep-lat/9606016.
- [43] ALPHA, Marco Guagnelli and Jochen Heitger and Rainer Sommer and Hartmut Wittig, Hadron masses and matrix elements from the QCD Schrödinger functional, Nucl. Phys. B560 (1999) 465, hep-lat/9903040,
- [44] M. Lüscher, Construction of a Selfadjoint, Strictly Positive Transfer Matrix for Euclidean Lattice Gauge Theories, Commun. math. Phys. 54 (1977) 283.
- [45] Osterwalder, K. and Seiler, E., Gauge Field Theories on the Lattice, Ann. Phys. 110 (1978) 440,
- [46] Michael J. Teper, Glueball masses and other physical properties of $SU(N)$ gauge theories in $D = (3+1)$: A Review of lattice results for theorists, (1998), hep-th/9812187,
- [47] Martin Lüscher and Stefan Sint and Rainer Sommer and Hartmut Wittig, Nonperturbative determination of the axial current normalization constant in $O(a)$ improved lattice QCD, Nucl. Phys. B491 (1997) 344, hep-lat/9611015.
- [48] Stefan Sint and Peter Weisz, Further results on $O(a)$ improved lattice QCD to one loop order of perturbation theory, Nucl. Phys. B502 (1997) 251, hep-lat/9704001.
- [49] ALPHA, Jochen Heitger, Scaling investigation of renormalized correlation functions in $O(a)$ improved quenched lattice QCD, Nucl.Phys. B557 (1999) 309, hep-lat/9903016.

- [50] ALPHA, Marco Guagnelli and others, Non-perturbative results for the coefficients $b(m)$ and $b(A)-b(P)$ in $O(a)$ improved lattice QCD, Nucl. Phys. B595 (2001) 44, hep-lat/0009021,
- [51] ALPHA, Stefano Capitani and Martin Lüscher and Rainer Sommer and Hartmut Wittig, Nonperturbative quark mass renormalization in quenched lattice QCD, Nucl. Phys. B544 (1999) 669, hep-lat/9810063,
- [52] ALPHA, F. Knechtli et al., Running quark mass in two flavour QCD, (2002), hep-lat/0209025.
- [53] F. Jegerlehner, Electroweak Theory and LEP Physics, Lausanne Lectures, (1994).
- [54] N. Cabibbo, Phys. Lett. 10 (1963) 513.
- [55] M. Kobayashi and K. Maskawa, Prog. Theor. Phys. 49 (1973) 652.
- [56] L. Wolfenstein, Phys. Rev. Lett. 51 (1983) 1945.
- [57] Particle Data Group, K. Hagiawara et. al., Phys. Rev. D66 (2002) 010001.
- [58] Belle Coll., B. Golob, Measurement of CKM Elements and the Unitarity Triangle, hep-ex/0308060.
- [59] M. Ciuchini et. al., JHEP 0107 (2001) 013.
- [60] A. Höcker et. al., Eur. Phys. J. C21 (2001) 225.
- [61] K. Abe, Measurement of the Angle $\phi_1(\beta)$ and $B\bar{B}$ Mixing (Recent Results from BaBar and Belle), hep-ex/0308072.
- [62] Matthias Neubert, Heavy quark masses, mixing angles, and spin flavor symmetry, CERN-TH. 7225 (1994), hep-ph/9404296, review of heavy quark effective theory.
- [63] Estia Eichten and Brian Hill, An effective Field Theory for the Calculation of Matrix Elements Involving Heavy Quarks, Phys. Lett. B234 (1990) 511,
- [64] ALPHA, Jochen Heitger and Rainer Sommer, Non-perturbative Heavy Quark Effective Theory, (2003), hep-lat/0310035.

- [65] Estia Eichten and Brian Hill, Renormalization of heavy - light Bilinears and $f(B)$ for Wilson Fermions, Phys. Lett. B240 (1990) 193,
- [66] ALPHA, Martin Kurth and Rainer Sommer, Renormalization and $O(a)$ -improvement of the static axial current, Nucl. Phys. B597 (2001) 488, hep-lat/0007002,
- [67] ALPHA, Jochen Heitger, Martin Kurth and Rainer Sommer, Non-perturbative renormalisation of the static axial current in quenched QCD, (2003), hep-lat/0302019.
- [68] ALPHA, A. Jüttner and J. Rolf, A precise determination of the decay constant of the D_s -meson in quenched QCD, Phys.Lett. B560 (2003) 59, hep-lat/0302016.
- [69] Nathan Isgur and Mark B. Wise, Weak decays in the static quark approximation, Phys. Lett. B232 (1989) 113.
- [70] Nathan Isgur and Mark B. Wise, Weak transition form factors between heavy mesons, Phys. Lett. B237 (1990) 527.
- [71] Howard Georgi, An effective field theory for heavy quarks at low energies, Phys. Lett. B240 (1990) 447.
- [72] C. Morningstar and J. Shigemitsu, One loop matching of lattice and continuum heavy light axial vector currents using NRQCD, Phys. Rev. D57 (1998), hep-lat/9712015.
- [73] ALPHA, Jochen Heitger, Martin Kurth and Rainer Sommer, Non-perturbative determination of Z_A^{stat} in quenched QCD, (2002), hep-lat/0209078.
- [74] Ph. Boucaud, O. Pene and V.J. Hill, C.T. Sachrajda and G. Martinelli, Phys. Lett. 220B (1989) 219.
- [75] ALPHA, J. Heitger and R. Sommer, A strategy to compute the b-quark mass with non-perturbative accuracy, Nucl.Phys.Proc.Suppl. 106 (2002) 358, hep-lat/0110016.
- [76] ALPHA, R. Sommer, Non-perturbative renormalisation of HQET and QCD, (2002), hep-lat/0209162.

- [77] Estia Eichten, Field Theory on the Lattice, Nucl. Phys. (Proc. Suppl.) B4 (1988) 147.
- [78] C. Alexandrou, S. Güsken, F. Jegerlehner and K. Schilling and R. Sommer, Phys. Lett. B256 (1991) 60.
- [79] A. Duncan and others, Properties of B mesons in lattice QCD, Phys. Rev. D51 (1995) 5101, hep-lat/9407025,
- [80] C.R. Allton et. al., Nucl.Phys. B349 (1991) 598.
- [81] C. Alexandrou, S. Güsken, F. Jegerlehner and K. Schilling and R. Sommer, The static approximation of heavy-light quark systems. A detailed lattice study, Nucl.Phys. B414 (1994) 815.
- [82] Anthony Duncan and others, Properties of low lying heavy - light mesons, Nucl. Phys. Proc. Suppl. 30 (1993) 433, hep-ph/9211263,
- [83] ALPHA, Marco Guagnelli and Rainer Sommer and Hartmut Wittig, Precision computation of a low-energy reference scale in quenched lattice QCD, Nucl. Phys. B535 (1998) 389, hep-lat/9806005,
- [84] C. Michael and I. Teasdale, Extracting Glueball Masses from Lattice QCD, Nucl. Phys. B215 (1983) 433,
- [85] Martin Lüscher and Ulli Wolff, How to Calculate the Elastic Scattering Matrix in two- dimensional Quantum Field Theories by numerical Simulation, Nucl. Phys. B339 (1990) 222.
- [86] K. Ishikawa, M. Teper and G. Schierholz, . B110 (1982) 399.
- [87] UKQCD, McNeile, Craig and Michael, Chris, Mixing of scalar glueballs and flavour-singlet scalar mesons, Phys. Rev. D63 (2001) 114503, hep-lat/0010019,
- [88] Niedermayer, Ferenc and Rufenacht, Philipp and Wenger, Urs, Fixed point gauge actions with fat links: Scaling and glueballs, Nucl. Phys. B597 (2001) 413, hep-lat/0007007,
- [89] J. Balog et. al., Comparison of the O(3) Bootstrap sigma-Model with the Lattice Regularization at Low Energies, Phys. Rev. D60 (1999) 094508, hep-lat/9903036.

-
- [90] M. Lüscher, A portable high-quality random number generator for lattice field theory simulations, *Comp. Phys. Comm.* 79 (1994) 100, hep-lat/9309020.
 - [91] Stephen L. Adler, An overrelaxation method for the Monte Carlo evaluation of the partition function for multiquadratic actions, *Phys. Rev. D* 23 (1981) 2901.
 - [92] N. Cabibbo and E. Marinari, *Phys. Lett.* 119B (1982) 387.
 - [93] H. van der Vorst, *SIAM J. Sci. Stat. Comput.* 13 (1992) 631.
 - [94] S. Fischer, A. Frommer, U. Glaessner, Th. Lippert, G. Ritzenhoefer, K. Schilling, A Parallel SSOR Preconditioner for Lattice QCD, *Comput. Phys. Commun.* 98 (1996) 20.
 - [95] UKQCD, C. Michael and J. Peisa, Maximal variance reduction for stochastic propagators with applications to the static quark spectrum, *Phys.Rev. D* 58 (1998) 034506, hep-lat/9802015.
 - [96] ALPHA, Joyce Garden and Jochen Heitger and Rainer Sommer and Hartmut Wittig, Precision computation of the strange quark's mass in quenched QCD, *Nucl. Phys. B* 571 (2000) 237, hep-lat/9906013,
 - [97] H. Leutwyler, *Phys. Lett. B* 378 (1996) 313, hep-ph/9602366.
 - [98] ALPHA, M. Della Morte et al., Lattice HQET with exponentially improved statistical precision, *Phys.Lett. B* 581 (2004) 93, hep-lat/0307021.
 - [99] A.M. Green, J. Koponen, C. McNeile, C. Michael and G. Thompson, Excited B mesons from the lattice, (2003), hep-lat/0313007.
 - [100] ALPHA, S. Dürr and M. Della Morte, Exploring two non-perturbative definitions of c_A , hep-lat/0309169.
 - [101] M. Göckeler et al., Polarized and Unpolarized Nucleon Structure Functions from Lattice QCD, *Phys.Rev. D* 53 (1996), hep-lat/9508004.
 - [102] CP-PACS, S. Aoki et al., Light Hadron Spectrum and Quark Masses from Quenched Lattice QCD, *Phys.Rev. D* 67 (2003), hep-lat/0206009.

Acknowledgements

There are many people that deserve some words of thanks for contributing to this thesis.

In the first place, I would like to thank my supervisor Rainer Sommer for his guidance and advices, answering questions and his encouragements to look from different viewpoints onto the work.

Many thanks to my collaborator Stephan Dürr for discussions, sharing ideas and for doing some cross-checks of results. His collaboration was also invaluable.

I am also indebted to Juri Rolf and Michele Della Morte for their willingness to help me when I needed it.

Profs. Ulli Wolff and Fred Jegerlehner gave me various opportunities to join to discussion seminars on lattice gauge theory and phenomenology, respectively, for which I want to thank them.

Special thanks to Bernd Gehrman. His critical reading of large parts of the manuscript was invaluable.

I will miss the good working atmosphere that has been created by my colleagues I shared the room with. In particular, I would like to thank Cipollino, Alejandro, Silvia, Carsten and Niels. We have had a good time together with Axel, Janusz, Ines, Andrea, Gosia, James, Michael and many others.

It was an enjoyable stay in Zeuthen's Theory Group of DESY/NIC. I would like to thank the members of the Theory and NIC group, the secretaries as well as the computing staff, and DESY/NIC for providing me the opportunity to use the APE machines for my work.

Selbständigkeitserklärung

Hiermit erkläre ich, die vorliegende Arbeit selbständig ohne fremde Hilfe verfasst zu haben und nur die angegebene Literatur verwendet zu haben.

Heiko Molke
16. Januar 2004

Lebenslauf

Name: Heiko Molke
geboren am: 01.02.1976 in Frankfurt/Oder
Nationalität: Deutsch

9/1982–7/1986 Besuch der Polytechnischen Teiloberschule, Kietz
9/1986–7/1990 Besuch der Polytechnischen Oberschule, Manschnow
9/1990–7/1995 Besuch des Gymnasiums Seelow, Abitur
10/1995–5/2000 Studium an der Humboldt-Universität zu Berlin
in der Fachrichtung Physik
10/2000–12/2003 Doktorand im Deutschen Elektronensynchrotron
(DESY) Zeuthen

Auszeichnungen

01/2001 Förderpreis der Wilhelm & Else-Heraeus-Stiftung
zur Verkürzung der Studiendauer im Fach Physik

Publikationsliste

1. H. Molke, *Renormierte Kopplungen im $O(3) - \sigma$ -Modell*,
Diploma-Thesis (in German), Humboldt-University Berlin, 2000,
<http://dochoost.rz.hu-berlin.de/diplom/physik/molke-heiko-2000-05-02/PS/Molke.ps>
2. *Helicity modulus as renormalized coupling in the $O(3)$ sigma model*.
By ALPHA Collaboration (Heiko Molke and Ulli Wolff),
Nucl.Phys.B603:180-194,2001. hep-lat/0012027
3. *Lattice HQET with exponentially improved statistical precision*.
By ALPHA Collaboration (M. Della Morte et al.),
to appear in Phys.Lett.B, hep-lat/0307021

4. *Towards a precision computation of F_{B_s} in quenched QCD.*
By ALPHA Collaboration,
hep-lat/0309072
5. *Static quarks and improved statistical precision.*
By ALPHA Collaboration (M. Della Morte et al.),
hep-lat/0309080